Tunable three-body interactions between superconducting flux qubits for quantum annealing

by

Denis Melanson

A thesis
presented to the University of Waterloo
in fulfillment of the
thesis requirement for the degree of
Master of Science
in
Physics (Quantum Information)

Waterloo, Ontario, Canada, 2019

Abstract

The field of quantum information has been a fast growing field of research in the last few decades. The reason for this development is the potentially immense power of quantum computers, capable of solving hard problems in a fraction of the time it would take a classical computer. Quantum annealers are a type of quantum computer that seek to solve computational problems by finding the ground state of a quantum system. This type of quantum computer has been implemented on a large scale using superconducting flux quantum bits, but the computational power is limited. One potential improvement to help in this context is the implementation of multi-body interactions between quantum bits. Many-body interactions would be useful in allowing quantum annealers to solve more complex problems that are relevant in various areas of quantum information and science and implementing quantum error correction.

We present a superconducting device that implements a strong and tunable in sign and magnitude three-body interaction between superconducting flux quantum bits. The circuit design proposed has vanishing two-body interactions and robustness against noise and parameter variations. This circuit behaves as an ideal computational basis ZZZ coupler in a simulated three-qubit quantum annealing experiment. These properties are confirmed by calculations based on the Born-Oppenheimer approximation, a two-level spin model for the coupling circuit, and full numerical diagonalization.

The proposed circuit is based on already available technology and therefore could be readily implemented in the next generation of quantum annealing hardware. This work will be relevant for advanced quantum annealing protocols and future developments of high-order many-body interactions in quantum computers and simulators.

Acknowledgments

I would like to first thank Dr. Adrian Lupascu for, without his guidance, knowledge, experience and patience, this thesis would not have been possible. I have learned immensely from his encyclopedic knowledge of physics and invaluable lessons on conducting research during my time in his group. I wold also like to thank all the members of Dr. Lupascu's Superconducting Quantum Devices research group for countless discussions and priceless help with the simulations and calculations. In particular, I would like to highlight the help of Antonio J. Martinez with the many circuit simulations necessary for this thesis, Dr. Salil Bedkihal for his contribution to the spin model calculations in this thesis and the help of Dr. M. Ali Yurtalan with the various design projects, electromagnetic simulations and fabrications encountered throughout my program.

Finally, I would like to thank my friends on and off campus and my family for their love and constant support that made this thesis possible.

This material is based upon work supported by the Intelligence Advanced Research Projects Activity (IARPA) and the Army Research Office (ARO) under Contract No. W911NF-17-C-0050

Dedication

This is dedicated to my friends and family.

Table of Contents

List of Tables viii

List of Figures ix

1 Introduction 1

1.1 The Quest for a Quantum Computer 1

1.2 Quantum annealing 3

2 Superconducting Quantum Circuits 7

2.1 Superconductivity 7

2.2 Superconducting circuits 11

2.2.1 Josephson Effect 12

2.2.2 Circuit quantization 14

2.3 Superconducting Interferometers 16

2.3.1 RF-SQUID 16

2.3.2 DC-SQUID 18

2.4 Superconducting Flux Qubits 20

2.5 Quantum Coherence and Decoherence 23

2.5.1 Sources of Decoherence 25

3 Mediated Inductive Coupling 27
3.1 Direct and indirect interactions 27
3.2 Two-qubit Tunable Inductive Coupler 28
    3.2.1 rf-SQUID Coupler 28
    3.2.2 Split-Junction rf-SQUID Coupler 35
3.3 Born-Oppenheimer Inversion Method for Extracting Coupling Strength . . 39

4 Three-body Inductive Coupler for Quantum Annealing 42
4.1 Coupling circuit 43
4.2 Born-Oppenheimer approximation analysis 48
4.3 Spin model analysis 49
4.4 Full numerical analysis 54
4.5 Robustness of the coupler to noise and fabrication variations 56
4.6 Quantum annealing simulations 58
4.7 Extension to more qubits 60

5 Conclusion 62

References 64

APPENDICES 78

A Numerical Diagonalization 79
A.1 Non-periodic potential 79
A.2 Periodic potential 81

B Derivation of tunable rf-SQUID Hamiltonian 82
B.1 Symmetric case 82
B.2 Asymmetric case 85

List of Tables

4.1 Annealing parameter standard deviations due to uncorrelated flux noise in all coupler loops. 57

List of Figures

2.1 Superconducting ring threaded by an external flux. The dashed line at the center of the ring cross-section is the integrating path, as in the text. . . . 10

2.2 Josephson junction circuit schematics. (a) Boxed cross circuit schematic symbol of a Josephson junction. (b) The circuit schematic representation of the RCSJ model of a Josephson junction, that is a resistively and capacitively shunted ideal junction. 13

2.3 Circuit schematic of an RF-SQUID, with loop inductance. The circulating current, junction phase and external flux positive directions are indicated. . 17

2.4 Potential of the RF-SQUID from Eq. (2.32) with $E_{\mathrm{L}} = 300.0$ GHz and $f_{\mathrm{x}} = 0.5$. Changing the Josephson energy to be in the (a) bi-stable and (b) mono-stable regimes. The dashed lines in both plots represent the first two energy levels of the RF-SQUID. 19

2.5 Circuit schematic of a DC-SQUID with symmetric junctions and no geometric or self-inductance. The current, junction phases and bias flux positive directions are indicated. 19

2.6 Capacitively shunted flux qubit circuit, comprised of a superconducting loop interrupted by three Josephson junctions. The third junction is drawn smaller than the other two (which are identical) to indicate its physically smaller size, this also results in a smaller capacitance. The positive direction of the circulating current and the external flux bias are indicated. The arrows next to the phases indicate the direction of positive phase drop. . . 21

3.1 Three rf-SQUIDs inductively coupled to each other through mutual inductances. The middle RF-SQUID is operated as a mediator or coupler while rf-SQUIDs 1 and 3 are operated as qubits. 29

3.2 The expectation value of the circulating current in the loop of an RF-SQUID coupler with respect to the external flux threading its loop with $E_{\mathrm{L}} = 467.0$ GHz and $E_{\mathrm{C}} = 18.4$ GHz, at various values of the Josephson energy or β. 35

3.3 The potential energy of an RF-SQUID with respect to the superconducting phase with $E_{\mathrm{L}} = 297.2$ GHz and $E_{\mathrm{C}} = 38.7$ GHz and $f_x = 0.5$. 36

3.4 Compound-junction RF-SQUID coupler circuit representation. The current, junction phases and bias flux positive directions are indicated. 37

3.5 The expectation value of the circulating current in the loop of a compound-junction RF-SQUID-type coupler with respect to the external flux threading its large loop, at various values of the external flux threading its small loop. The parameters of the SQUID are $E_{\mathrm{L}} = 467.0$ GHz, $E_{\mathrm{J}} = 208.6$ GHz and $E_{\mathrm{C}} = 18.4$ GHz; the change in the flux in the small loop effectively changes the non-linearity parameter β. 39

3.6 The 2-qubit coupling strength mediated by a compound-junction RF-SQUID coupler, with $E_{\mathrm{L}} = 467.0$ GHz, $E_{\mathrm{J}} = 208.6$ GHz and $E_{\mathrm{C}} = 18.4$ GHz, versus the flux threading the large loop, at various values of the flux threading the small loop. 41

4.1 Circuit schematic of the coupler - qubits system. The two tunable rf-SQUID circuits forming the coupler ("c1" and "c2") are coupled to the three tunable capacitively shunted flux qubits ("q1", "q2", and "q3") by mutual inductances. Each loop of these circuits is subjected to a flux bias, as indicated. Josephson junctions are indicated by crosses; arrows indicate the orientation of the relative phase. Capacitances and inductances of the secondary loops of the qubits are not shown. See text for additional details. 44

4.2 Three-body coupling strength extracted by Born-Oppenheimer method in the circuit model (solid line), perturbation theory in the spin model (dashed line), and numerical calculations of the full circuit (dotted line) versus the external magnetic flux threading loop $c1\,s$. The inset shows a wider scan of the magnetic flux, where the three-body coupling is extracted by the Born-Oppenheimer method only. The flux biases are $f^{\mathrm{m}}_{\mathrm{c}\,1} = f^{\mathrm{m}}_{\mathrm{c}\,2} = 1/2$, $f^{\mathrm{s}}_{\mathrm{c}\,1} = -f^{\mathrm{s}}_{\mathrm{c}\,2}$, $f^{\mathrm{m}}_{\mathrm{q}\,i} = 1/2$ and $f^{\mathrm{s}}_{\mathrm{q}\,i} = 0$ for $i \in \{1, 2, 3\}$. 50

4.3 Spin-model schematic of the coupler plus qubits system. The circles and squares represent the qubit and coupler spins, respectively. The dashed lines represent bare two-body interactions. 51

4.4 Energy spectrum of the complete circuit Hamiltonian, relative to the ground state energy. (a) When the three-body coupling is turned on, an avoided level crossing between level 4 and 5 corresponding to $2\,|J_{123}|$ appears around $\Delta_{\mathrm{Q3}} \approx \Delta_{\mathrm{Q1}}+\Delta_{\mathrm{Q2}}$ (dotted line and circle). (b) When the three-body coupling is turned off, levels 4 and 5 simply cross each other around $\Delta_{\mathrm{Q3}} \approx \Delta_{\mathrm{Q1}}+\Delta_{\mathrm{Q2}}$ (dotted line and circle). The conditions of $\Delta_{\mathrm{Q3}} \approx \Delta_{\mathrm{Q1}} + \Delta_{\mathrm{Q2}}$ happen at different flux values with and without coupling because of a re-normalization of the qubit energy levels due to the coupling. 55

4.5 Low-energy spectrum versus annealing parameter s. (a) Spectrum of the 8 levels of an ideal 3-spin Hamiltonian implementing Eq. (4.45). (b) Spectrum of the lowest 8 qubit-like levels of the circuit Hamiltonian (4.15) when biased to implement a linear annealing schedule as in (4.45). 58

4.6 (a) Simplified coupler schematic. The circles represent the qubits ("q1", "q2", "q3"), the rectangular boxes represent the couplers ("C1", "C2") and the straight lines indicate the direct inductive coupling. (b) Extension of proposed three-body coupler to many qubits. The introduction of circular tree-couplers ("tc") make the connection and switching between other qubits possible. 61

Chapter 1

Introduction

1.1 The Quest for a Quantum Computer

The era of digital computing revolutionized modern science. While the scientists of the pre-digital period did push the boundaries of science, they were limited by the sheer difficulty of the theoretical calculations when investigating increasingly complex systems. The development of the first computing infrastructure permitted the scientific community to explore problems that did not have analytical solutions and required immense numerical calculations to solve. Because of this, the progress in all fields of science grew by leaps and bounds, and with it the power of the computers also grew in turn [1]. With this increase of computational power, along with the development of communication technology, came the development of the Internet. The Internet represented an important opportunity for the scientific community through enabling global instant communication and knowledge sharing. However, some hard problems with many real-world applications, remain extremely difficult to solve on computers because of the immense computational resources required [2]. A few examples of such hard problems are: prime factorization, the traveling salesman, graph coloring, the knapsack and satisfiability problems [3] and matrix permanent calculation [4]. Additionally, the constant progression in computer performance that was experienced from the 1960's to the 2010's has begun to show signs of slowing down and saturation in recent years [5]. The main reason for this slow-down is the physical limitations of the electrical circuitry making the miniaturization of these components increasingly difficult. The curiosity of the scientific community and the complexity of the problems posed by this community are, however, not slowing down but growing. The natural tendency of humanity to seek an understanding and mastery of nature has led us to this point and we are beginning to see this tendency push against the current computational paradigm, push to go beyond the paradigm of classical computing.

The first stirrings of a new computation paradigm were felt in the early 1980's, when the first proposals to use quantum effects to improve classical computation were made by Feynman [6] and Benioff [7]. Feynman's proposal sought to solve a persistent problem in modern science, the intractability of simulating even moderately sized quantum systems such as atoms and molecules. This important problem is due to the exponential growth, with the size of the system, of the classical computational resources required to accurately simulate the quantum system. Feynman proposed to use controllable quantum systems onto which would be encoded the quantum systems of interest. This would circumvent the exponential growth in computational resources by substituting classical computational resources with quantum systems that can naturally encode the quantum variables. These types of quantum simulators are capable of simulating large and complex many-body quantum systems with ease and thus would have wide ranging applications in the fields of physics, chemistry and biology [8, 9].On the other hand, Benioff and others proposed to build quantum Turing machines and therefore to use quantum properties in a more conventional computing architecture based on quantum logical circuits and quantum bits (qubits). With the development of the standard circuit model of quantum computing by Deutsch in 1989 [10], the circuit model would become the main avenue explored by quantum computation scientists. In the following decades, powerful quantum algorithms were developed, capable of solving provably hard problems for classical computers, like prime factorization [11] and the unstructured database search [12], with an huge increase in efficiency over classical algorithms. The physical requirements for the implementation of a quantum computer were consolidated by DiVincenzo into criteria on the scalability, coherence lifetimes, ability to initialize and measure the physical qubits, ability to transfer quantum information between qubits at different locations and requirements on the set of universal quantum gates to implement [13]. There were also important developments in the field of quantum communication and cryptography, where scientist build communication protocols that are safe from any potential eavesdropper [14].

A distinct quantum computation model developed in parallel to the circuit model. This model of quantum computation was based on encoding the solution to combinatorial problems to the lowest energy state of a quantum system [15, 16, 17]. This approach to solve combinatorial problems was adapted from a classical algorithm called simulated annealing where one optimizes a cost function using random simulated thermal fluctuations and hopping over barriers in the cost function. In the quantum counterpart called simulated quantum annealing, one uses simulated quantum fluctuations and tunneling, as opposed to thermal fluctuations and hopping, to overcome barriers in the optimization of the cost function. The quantum computation model that evolved from this work is called adiabatic quantum computation. In adiabatic quantum computation, the goal is to find the solution to a computational problem by finding the ground state of a quantum system. In order to do so, one initializes the computational qubits in the trivial ground state of an initial Hamiltonian and slowly transforms this Hamiltonian to the final Hamiltonian, the ground state of which encodes the solution. This method of computation employs the adiabatic theorem of quantum mechanics [18]. This theorem states that if a system is in an eigenstate of a Hamiltonian and the Hamiltonian is changed slowly compared to the energy gap between eigenstates, the system will stay in the eigenstate of the instantaneous Hamiltonian of the system at every point in time. This model of quantum computation has been proven to be computationally equivalent to the circuit model of quantum computation [19] and therefore can solve all the problems and run all the algorithms that a circuit model quantum computer can. However, to be equivalent, the design of the adiabatic quantum computer needs to follow important requirements. These requirements include exotic interactions between qubits such as multi-body interactions (see subsection below), but are otherwise beyond the scope of this thesis, see Refs. [19, 18] for details.

Physical implementation of quantum bits, in the context of the circuit model, has been achieved using nuclear and electron spin resonance, photons, trapped ions, cold atoms, quantum dots and superconducting electronic circuits. Early experiments were focused on isolating the quantum behavior of these systems from the environment. All the experimental efforts lead to the implementation of small scale quantum algorithms and simulations [20]. Circuit model quantum computers have gone through the embryonic prototypical stage of development and are now being implemented with a few tens of qubits. Superconducting circuits have been the main thrust in the field of quantum computing implementations largely due to the large knowledge pool acquired in the field of classical microwave integrated electronics [21, 22, 23, 24], to the fact that they can easily be manufactured and designed into a large variety fo devices and their good prospects for building large scale machines [25]. In this present thesis, we will focus on superconducting electronic circuits for quantum computing, in the context of quantum annealing.

1.2 Quantum annealing

Quantum annealing is a model of quantum computation that is based on the adiabatic quantum computation model. These two models are distinct in that, in quantum annealing, one deals with open quantum systems and thus the condition of adiabaticity is not strictly held. In quantum annealing, as in adiabatic quantum computation, one initializes a physical system in the trivial ground state of the so-called initial Hamiltonian, then one slowly transforms the initial Hamiltonian to the final problem Hamiltonian. The quantum annealing protocol follows the time dependent Hamiltonian

$$H_{\text{anneal}}\left(s\right) = A\left(s\right) H_{\text{initial}} + B\left(s\right) H_{\text{problem}}, \tag{1.1}$$

where H_{initial} and H_{problem} are the time-independent initial and problem Hamiltonians, respectively, and where $A\left(s\right)$ and $B\left(s\right)$ are time-dependent parameters that are varied during the schedule such that $B\left(0\right) = 0$ and $A\left(1\right) = 0$, where $s = t/T$ is the dimensionless annealing parameter that goes from 0 at the beginning of the annealing and to 1 at the end, with T the total annealing time.

The current paradigm being investigated for quantum annealing is the transverse field Ising Hamiltonian [18]. The Ising problem Hamiltonian in Eq. (1.2) that encodes the computational problem belongs to the complexity class StoqMA [18] and can encode NP-complete problems such as satisfiability problems[1] (SAT) [134] in the form of quadratic unconstrained binary optimization problems [26]. The transverse field Ising Hamiltonian is written for a system of N spins as

$$H_{\text{anneal}}\left(s\right) = A\left(s\right)\sum_{i=1}^{N} \Delta_i\, \sigma_i^{\text{x}} + B\left(s\right)\left(\sum_{i=1}^{N} h_i\, \sigma_i^{\text{z}} + \sum_{\substack{i,j=1 \\ i\neq j}}^{N} J_{ij}\, \sigma_i^{\text{z}}\sigma_j^{\text{z}}\right), \tag{1.2}$$

where Δ_i, h_i and J_{ij} are the transverse field on each spin, the energy bias on each spin and the spin-spin coupling strength, respectively, and where $\sigma_i^{\text{z,x}}$ are the Pauli matrices for spin i. The Pauli matrices are used throughout the field of quantum information and are defined as follows

$$\sigma^{\text{x}} = \begin{bmatrix} 0 & 1 \\ 1 & 0 \end{bmatrix}, \sigma^{\text{y}} = \begin{bmatrix} 0 & -\text{i} \\ \text{i} & 0 \end{bmatrix}, \sigma^{\text{z}} = \begin{bmatrix} 1 & 0 \\ 0 & -1 \end{bmatrix}. \tag{1.3}$$

Along with the identity operator

$$\sigma^{\text{I}} = \begin{bmatrix} 1 & 0 \\ 0 & 1 \end{bmatrix}, \tag{1.4}$$

---

[1] The computational question being asked in a SAT problem is whether an expression of Boolean variables can be made to evaluate to True with a certain assignment of Boolean variables. The NP-completeness of these problems means that any computational problem that is in the computational class NP can be solved by an algorithm that solves the SAT problem.

the Pauli matrices form a complete basis in the space of 2 × 2 matrices.

As discussed above, there exist many physical implementations of qubits or quantum spins. The transverse field model of quantum annealing has been physically implemented using a system of superconducting flux qubits by the D-Wave company. The progress of the D-Wave company on implementing a quantum annealer on chip, started in the early 2000's with a single qubit and few qubit experiments [27, 28, 29, 30, 31], has now reached the large scale. The most recent device developed by the company has around 2000 flux qubits playing the role of the spins in the Ising problem and 6000 tunable two-qubit couplers mediating the desired spin-spin interactions [32].

Solving various combinatorial problems and simulating exotic quantum systems with this machine as well as benchmarking the quantum annealer against the best classical solvers has evolved into a thriving field of research [33, 34]. The consensus on whether quantum annealing has a general computational advantage versus the best classical computers is still an open question. However, the D-Wave machine has been found to perform well and even outperform classical solvers at very specific problems [35, 32, 36]. The research does point to some factors that are currently limiting the computational power of the D-Wave quantum annealer, one of which is the embedding overhead incurred due to the limited connectivity between qubits and due to the lack of multi-qubit interactions. Embedding here refers to the encoding of the computational problem, constructed on an arbitrary graph with arbitrary connections, to the physical device graph. Embedding arbitrary problems on a quantum annealer requires first a reduction of the problem to the fundamental problem and graph of the annealer. The fundamental problem and graph of the annealer is defined by H_{problem} and is limited by the physical connectivity of the qubits in the device. For example, the D-Wave machine has a problem Hamiltonian of the Ising type as in Eq. 1.2, but more importantly this machine has a physical connectivity of 6, that means, each physical qubit is directly connected and interacts with at most 5 of it's nearest neighbors (in the physical device, the sum over the two-qubit interactions J_{ij} in Eq. 1.2 is limited by the device's connectivity.) [32]. The problems that require larger connectivity can be mapped onto the quantum annealer by using chains of physical qubits to encode one logical qubit (a qubit that encodes a problem variable) [37, 38]. This method of encoding arbitrary problems on the annealer comes at the cost of a significant decrease of the number of possible logical qubits in the problem. Therefore, when one encounters a large discrepancy between the connectivity of the problem one wants to solve and the physical connectivity of the annealer, embedding this problem engenders large computational costs and limits the problem size that can be solved on the machine.

Related to the problem of connectivity is multi-body interactions. A quantum annealer with multi-body interactions could lead to improvements in implementing error correction codes [39, 40] and in implementing quantum simulations of complex systems [41, 42]. Embedding these types of problems in a quantum annealer with only two-qubit interactions also presents significant computational cost in the form of ancillary qubit gadgets in order to be simulated [43, 44].

The field of quantum annealing is at an exploratory point, work around the first large scale machines has shown promise and has shown a potential path forward to increase the computational value of quantum annealing. The avenues being explored for improved quantum annealing include increasing the connectivity between the qubits [**?** 45], implementing non-stoquastic interactions between qubits (interactions such as XX) [46, 47, 48, 49], implementing error correction codes [50], using qubits with longer coherence times [51, 52], controlled cooling [53], adaptive annealing schedules [54, 55, 56] and implementing multi-qubit interactions [43, 57]. In the present thesis, we will focus on implementing multi-qubit interactions with superconducting flux qubits for quantum annealing.

This thesis is organized as follows. Chapter 2 is an introduction to superconductivity and superconducting circuits. We will discuss the properties of superconductivity that make quantum bits possible, the basic circuit elements that form the building blocks superconducting quantum bits and we will discuss how to isolate the qubits from their environments. In chapter 3 we will discuss the concept of mediated tunable interactions between superconducting flux qubits. We will study how two-qubit interactions are implemented in the current state of the art quantum annealers by analyzing two superconducting coupling circuits and introducing the methods to characterize such circuits. In chapter 4 we will discuss the main proposal of this thesis: a superconducting circuit capable of mediating three-qubit interactions between flux qubits. The proposed circuit is analyzed using the Born-Oppenheimer approximation, a spin model and full numerical calculations. Chapter 5 includes a summary of the work and concluding remarks.

Chapter 2

Superconducting Quantum Circuits

2.1 Superconductivity

Ever since the discovery of superconductivity by Kamerlingh Onnes in 1911 [58], superconductivity has been an active area of physics research. Shortly after the discovery, the early development of the phenomenological understanding of superconductivity laid the ground work for the more complete theories that were developed in the later half of the 20^{th} century. The first developments were made by the London brothers in 1935. They proposed a phenomenological electromagnetic explanation of the resistance-less propagation of current and the magnetic field expulsion in a superconductor [59]. This was later followed by the work of Ginzburg and Landau on a theory of phase transitions in the 1950s. The work of Ginzburg and Landau culminated in their explanation of superconductivity as a phase transition with a complex order parameter, which we call the Ginzburg-Landau (GL) theory of superconductivity [60]. The next developments were the microscopic theory of superconductivity developed by Bardeen, Cooper and Schrieffer (BCS) in 1957 [61] and the discovery of the Josephson effect in 1962 [62], which we will discuss below. All these important developments have enabled scientists and engineers today to construct novel superconducting electronic devices as well as to develop new theories.

In the last century, scientists and engineers have developed the theory and technique of superconductivity for building strong superconducting magnets for various applications from particle accelerators to magnetic resonance imagery, as well as low-loss wires and transmission lines, to name a few large scale applications. On the smaller scale, researchers and designers have built various superconducting electronic components such as amplifiers, sensors and detectors. Finally, through the development of superconducting electronics design and fabrication, scientists have studied various types of superconducting resonators and superconducting qubits. These superconducting circuits are built using Josephson junctions along with regular circuit elements (capacitances and inductances) and, as we will see below, these circuits have a strongly anharmonic energy spectrum that enables specific levels to be isolated and addressed for computational tasks. When two energy levels are well-isolated we can encode in them bits of information. We assign the value “0” to one of the levels and the value “1” to the other, as in classical bits. However, these quantum bits (qubits) correspond to quantum states and these states have useful quantum properties such as the ability to exist in coherent superposition between the state “0” and “1”, the ability to be entangled (perfectly correlated) with other states and the ability to tunnel through energy barriers. Superconducting qubits have been shown to be a promising candidate for the implementation of quantum computing because of their inherent versatility in design and well developed fabrication methods.

We must begin by outlining the fundamental concepts of superconducting devices. The scope of this thesis does not permit us to do an exhaustive review of this field, however, one can read a more complete review of superconducting devices here [63, 25].

What distinguishes most commonly a superconductor from a regular conductor is the fact that electrons inside the former propagate as current without dissipation, that is, without resistance. To give an intuitive picture of this, let us consider two metal rings, one a normal conductor and one a superconductor. If one induced circulating current in the normal conductor ring, the current will quickly be dissipated due to collisions of electrons with atoms. Astonishingly, if one induces the same circulating current in the superconducting ring, this current will keep circulating effectively indefinitely without being attenuated by collisions. This fascinating property of superconductivity can be understood with the help of the BSC theory [61], or microscopic theory of superconductivity.

Superconductivity is a phase of matter which appears when the temperature of a solid and the strength of an imposed external magnetic field are below a certain critical point. Below this critical point, the solid undergoes a phase transition from normal conductor to superconductor. In the superconducting phase, the conducting electrons inside a solid interact with the lattice vibrations, or phonons, of the solid in such a way as to make two electrons with opposing momenta mutually attract. These now paired electrons are called Cooper pairs and they have fundamentally different properties than solitary electron. The Cooper pairs act as bosons while the solitary electrons are fermions. This distinction is important because identical fermions cannot occupy the same quantum state while bosons have a tendency to condense together at low temperature and form a collective ground state; it is this property of the bosonic Cooper pairs that makes superconductivity possible. The group of Cooper pairs behaves as a collective and because of this the breaking of one pair does not change the behavior of the collective. This has the result of leaving the collective of Cooper pairs protected from small energy fluctuations such as electron-atom collisions, thus the collective of pairs flows through the material unobstructed and without dissipation as a super-current. This super-current is sustained as long as the temperature and magnetic field are below their critical points.

The behavior of a superconductor in a magnetic field is also very different from that of a normal conductor. Consider the following situation of an external magnetic field on a conductor. If the conductor is in its normal state the magnetic field will completely penetrate inside the solid. If this conductor is then cooled such that it enters the superconducting phase, the magnetic field will be completely expelled from the solid. More accurately, the external magnetic field will penetrate the surface of the solid, but be exponentially suppressed with a characteristic depth called the London penetration depth λ_{L}, and this depth is material specific. This magnetic field suppression will occur regardless of whether the magnetic field is applied before or after the superconducting transition or of the time-dependence of the field, if the magnitude of the external field is lower than the critical field of the superconductor. This phenomena is called the Meissner effect [64]. This expulsion of the magnetic field is caused by the formation of super-currents at the surface of the superconductor inducing a self magnetic field to cancel the external field. The free energy of the superconductor is minimized when the magnetic field in the bulk of the solid is zero, this is in sharp contrast to a simple “perfect conductor” for which the free energy is minimized for a constant internal field and thus only a time-varying magnetic field would be expelled due to induction. The above description of superconductors is appropriate for conventional superconductors of so-called type-I. There exists other types of superconductors, such as conventional type-II and non-conventional superconductors that behave in a similar manner, but with important distinctions [65].

The collective nature of the Cooper pairs lends itself to a collective description of the immense number of electrons involved. The group of Cooper pairs can be described by one collective wave function written as

$$\Psi_{\mathrm{col}}\left(\boldsymbol{r}\right) = \left|\Psi_{\mathrm{col}}\left(\boldsymbol{r}\right)\right| \mathrm{e}^{\mathrm{i}\varphi(\boldsymbol{r})}, \tag{2.1}$$

where $\left|\Psi_{\mathrm{col}}\left(\boldsymbol{r}\right)\right|$ and $\varphi\left(\boldsymbol{r}\right)$ are the amplitude and the phase of the collective wave function for the Cooper pairs, respectively. These two quantities are, in general, dependent on the position vector $\boldsymbol{r}$ in the superconductor. The amplitude of the wave-function $\left|\Psi_{\mathrm{col}}\left(\boldsymbol{r}\right)\right|$ corresponds to the density of superconducting Cooper pairs at the position $\boldsymbol{r}$ in the solid [65]. The above wave function is also related to the complex order parameter describing the phase transition in the GL theory of superconductivity [60]. Indeed, one can show that the

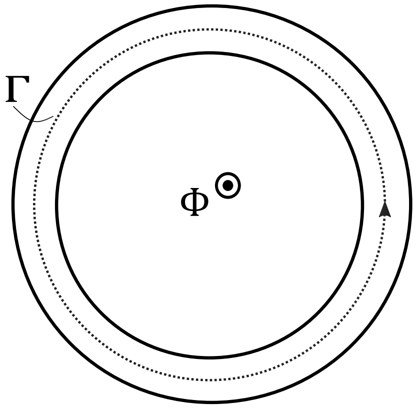

Figure 2.1: Superconducting ring threaded by an external flux. The dashed line at the center of the ring cross-section is the integrating path, as in the text.

GL theory predicts that the current $\boldsymbol{I}_{\text{sc}}\left(\boldsymbol{r}\right)$ inside the superconductor is constrained by

$$\boldsymbol{I}_{\text{sc}}\left(\boldsymbol{r}\right) = \frac{e}{m_{\text{e}}}\left|\Psi_{\text{col}}\left(\boldsymbol{r}\right)\right|^2\left[\hbar\boldsymbol{\nabla}\varphi\left(\boldsymbol{r}\right) - 2e\mathbf{A}\left(\boldsymbol{r}\right)\right], \tag{2.2}$$

where e and m_{e} are the electron charge and mass, respectively, where $\hbar = h/2\pi$ with h the Plank constant, and where $\mathbf{A}\left(\boldsymbol{r}\right)$ is the magnetic vector potential.

An other important consequence of this collective wave-function is the quantization of the flux in a superconductor. Consider a superconducting ring as in figure 2.1 with a contour Γ going around the ring and deep inside the bulk of the superconductor, such that the magnetic field and circulating currents vanish. If we integrate Eq. (2.2) along this contour, we get

$$\oint_{\Gamma}\boldsymbol{I}_{\text{sc}}\left(\boldsymbol{r}\right)\cdot\mathrm{d}\boldsymbol{r} = \frac{2e^2}{m_{\text{e}}}\left|\Psi_{\text{col}}\right|^2\left[\frac{\hbar}{2e}\oint_{\Gamma}\boldsymbol{\nabla}\varphi\left(\boldsymbol{r}\right)\cdot\mathrm{d}\boldsymbol{r} - \oint_{\Gamma}\mathbf{A}\left(\boldsymbol{r}\right)\cdot\mathrm{d}\boldsymbol{r}\right], \tag{2.3}$$

Where we have assumed that $\left|\Psi_{\text{col}}\left(\boldsymbol{r}\right)\right|^2 \approx \left|\Psi_{\text{col}}\right|^2$, which is justified because the integration path is deep in the bulk of the solid, where the variation in the density of Cooper pairs is negligible [65]. In order for the wave function to have a uniquely defined value of its phase all along the contour, the first integral on the right-hand-side of Eq. (2.3) must be integer valued, thus

$$n_{\text{fluxoid}} = \frac{1}{2\pi}\oint_{\Gamma}\boldsymbol{\nabla}\varphi\left(\boldsymbol{r}\right)\cdot\mathrm{d}\boldsymbol{r}, \tag{2.4}$$

where n_{fluxoid} is called the fluxoid number. The second integral on the right-hand-side of Eq.(2.3) is simply the definition of the magnetic flux threading the contour Γ. The integral on the left-hand-side of Eq.(2.3) is negligible because Γ is deep inside the superconductor where the current is vanishing. Finally, This leads to the quantization of the total flux threading the contour to an integer number of flux quanta

$$\Phi_\Gamma = n_{\text{fluxoid}}\, \Phi_0, \tag{2.5}$$

where Φ_Γ is the total flux threading the contour Γ and $\Phi_0 = h/2|e|$ is the flux quantum.

2.2 Superconducting circuits

We now briefly introduce the electronics concepts that we will need in the rest of the thesis. The Kirchoff circuit laws for the current, that the sum of currents entering a node of the circuit is equal to the sum of currents exiting that node, and voltage, that the sum of all voltage drop along a loop in the circuit must be equal to zero, are just as important in the context of superconducting circuits as in normal-conductor electronics [66]. The electronic components most important to superconducting electronics are the inductor and the capacitor and the Josephson junction. The latter is not used in normal-conductor electronics and will be introduced in the next subsection. The capacitor and the inductor are readily found in normal-conductor electronics, but here their behavior can be understood in terms of the phase of superconducting collective of Cooper pairs and or the number of Cooper pairs on the superconductor.

To see this, let us consider a generalization of the concept of magnetic flux through a loop to a magnetic flux on a branch of the circuit as the integral of the voltage difference across this branch in time [67, 68, 66]

$$\Phi_{\mathrm{B}}(t) = \int_{-\infty}^{t} V_{\mathrm{B}}(t')\, \mathrm{d}t', \tag{2.6}$$

where $\Phi_{\mathrm{B}}(t)$ is the branch flux and $V_{\mathrm{B}}(t')$ is the branch voltage drop, defined by the space integral of the electric field along the branch. We can equivalently write this relation in terms of the magnetic flux quantum as

$$\phi_0\, \gamma_{\mathrm{B}}(t) = \int_{-\infty}^{t} V_{\mathrm{B}}(t')\, \mathrm{d}t', \tag{2.7}$$

where γ_{B} is the superconducting phase difference across the branch and where $\phi_0 = \Phi_0/2\pi$ is the reduced flux quantum. If we consider an inductive branch of total inductance L, the current flowing through L is then

$$I_{\mathrm{L}}\left(t\right) = \frac{\phi_0}{L}\,\gamma_{\mathrm{L}}\left(t\right), \tag{2.8}$$

where I_{L} is the current flowing through the branch. Now, for a capacitive branch, the current flowing through a branch of total capacitance C is found by differentiating Eq. (2.6) twice

$$I_{\mathrm{C}}\left(t\right) = C\,\frac{\mathrm{d}V_{\mathrm{C}}\left(t\right)}{\mathrm{d}t} = C\phi_0\,\frac{\mathrm{d}^2\gamma_{\mathrm{C}}\left(t\right)}{\mathrm{d}t^2}, \tag{2.9}$$

where γ_{C} is the superconducting phase across the branch. Next, let us observe that we can just as well write the current flowing through a branch in terms of the total charge $q_{\mathrm{B}}\left(t\right)$ on the branch

$$I_{\mathrm{B}}\left(t\right) = \frac{\mathrm{d}q_{\mathrm{B}}\left(t\right)}{\mathrm{d}t}, \tag{2.10}$$

and from this, we re-write Eq. (2.8) in terms of the charge as

$$\frac{\mathrm{d}\gamma_{\mathrm{L}}\left(t\right)}{\mathrm{d}t} = \frac{\phi_0}{L}\,\gamma_{\mathrm{L}}\left(t\right), \tag{2.11}$$

and we re-write Eq. (2.9) in terms of the charge as

$$q_{\mathrm{C}}\left(t\right) = C\phi_0\,\frac{\mathrm{d}\gamma_{\mathrm{C}}\left(t\right)}{\mathrm{d}t}. \tag{2.12}$$

We have seen that the phase and the charge can both be used to represent capacitances and inductances in electronic circuits. In what follows we will omit the explicit dependence on time of the charge and phase. Let us now discuss third component, the Josephson junction.

2.2.1 Josephson Effect

In 1962, Josephson predicted that if two superconductors were separated by a thin barrier, there would be a current flowing through this barrier without dissipation due to quantum tunneling of Cooper pairs [62]. Josephson's predictions were experimentally proven in 1963 [69] in a superconducting-insulator-superconducting junction (where the insulator plays the role of thin barrier). This element is typically known as a Josephson junction (JJ) and can be fabricated in various ways.

The JJ can be understood by two simple current-to-phase and voltage-to-phase relations, the Josephson relations [70]. The Josephson tunneling current flowing through a JJ is related to the difference between the phases of the two superconductors as

$$I_{\mathrm{J}} = I_{\mathrm{c}}\,\sin\gamma, \tag{2.13}$$

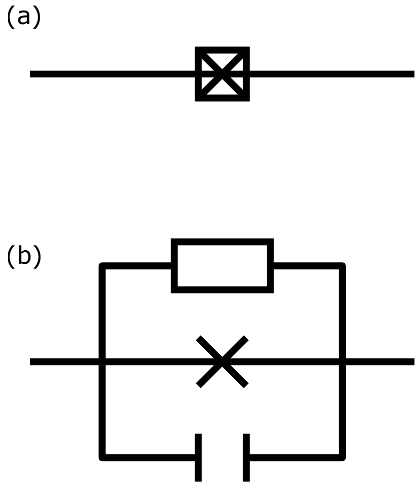

Figure 2.2: Josephson junction circuit schematics. (a) Boxed cross circuit schematic symbol of a Josephson junction. (b) The circuit schematic representation of the RCSJ model of a Josephson junction, that is a resistively and capacitively shunted ideal junction.

where $\gamma = \varphi_2 - \varphi_1$ is the phase difference between the two superconductors across the junction and I_c is the critical current of the junction. The critical current is a device-specific constant that dictates the magnitude under which the current flowing through the JJ creates zero voltage drop across the junction.

The voltage across the junction is related to the rate of change of the phase difference as

$$V_\mathrm{J} = \phi_0 \frac{\mathrm{d}\gamma}{\mathrm{d}t}. \tag{2.14}$$

From Eq. (2.13), we see that the JJ can be treated as a non-linear inductance circuit element when compared to Eq. (2.8). The JJ circuit element is represented by a cross or a boxed cross in circuit schematics, as in panel (a) of figure 2.2. A useful model for this circuit element is the resistively and capacitively shunted ideal JJ model (the RCSJ model)[1], as in panel (b) of figure 2.2. We can write the total current flowing through the JJ as a sum of three contributions, the first from the Josephson tunnel current, the second from the charging current of the capacitor and finally from the dissipative current of the resistance, the last two given by the standard current-voltage relations for the capacitor

---

[1] The simple cross circuit symbol typically represents an ideal Josephson junction, while the boxed cross symbol represents a shorthand for the RCSJ description of the junction.

and the resistance. The total current flowing through a RCSJ is

$$I_{\mathrm{b}} = I_{\mathrm{c}} \sin\gamma + C \frac{\mathrm{d}V_{\mathrm{J}}}{\mathrm{d}t} + \frac{V_{\mathrm{J}}}{R}, \tag{2.15}$$

where C and R are the capacitance and resistance shunting the JJ, respectively, V_{J} is the voltage across the junction and I_{b} is the external bias current through the junction.

For the operation regime discussed in this thesis (both in the low-current and low-temperature limit), the JJ can be considered a dissipationless circuit element and thus the $1/R$ contribution to the current is negligible. The current flowing through the junction can thus be re-written, by using (2.14), as

$$I_{\mathrm{b}} = I_{\mathrm{c}} \sin\gamma + C\phi_0\,\ddot{\gamma}, \tag{2.16}$$

where we have used the shorthand $\ddot{\gamma} \equiv \mathrm{d}^2\gamma/\mathrm{d}t^2$.

2.2.2 Circuit quantization

We now introduce the main concepts of circuit quantization. Circuit quantization is a method that describes electrical circuits in terms of quantum operators and energy scales [66]. With this description, one can determine the extent to which a certain circuit will have its behavior dominated by quantum fluctuations. With the quantization of a circuit, one can analyze the energy spectrum of the circuit and if this spectrum is sufficiently anharmonic, one can define a qubit subspace to encode the quantum information. The quantum properties of these superconducting circuits can be analyzed straightforwardly by first going to the Hamiltonian description of these circuits.

Let us determine the Hamiltonian description of the Josephson junction with zero current bias using the capacitively shunted junction model. We start from the current equation (2.16) and write the Lagrangian of the JJ as

$$\begin{aligned}\mathcal{L}_{\mathrm{J}} &= T - U \\ &= \frac{C\phi_0^2}{2}\,\dot{\gamma}^2 + I_{\mathrm{c}}\phi_0 \cos\gamma,\end{aligned} \tag{2.17}$$

where the kinetic energy is the energy stored in the capacitance which is given by $T = CV^2/2$ and the potential is the energy stored in the junction [68, 66] given by $U = \int I_{\mathrm{J}} V_{\mathrm{J}} \mathrm{d}t$. We can verify that Lagrangian (2.17) properly describes the dynamics of the JJ by noting that the Euler-Lagrange equation for this Lagrangian in terms of the coordinate γ and its velocity $\dot{\gamma}$

$$\frac{\mathrm{d}}{\mathrm{d}t}\left(\frac{\partial \mathcal{L}_{\mathrm{J}}}{\partial \dot{\gamma}}\right) = \frac{\partial \mathcal{L}_{\mathrm{J}}}{\partial \gamma} \;\rightarrow\; C\phi_0^2\,\ddot{\gamma} = -I_{\mathrm{c}}\phi_0 \sin\gamma \tag{2.18}$$

is equivalent to the current equation (2.16).

The Hamiltonian of the JJ is then related to the Lagrangian by a Legendre transform as

$$H_{\mathrm{J}} = \dot{\gamma}\,p - \mathcal{L}_{\mathrm{J}}, \tag{2.19}$$

where we have defined the conjugate momentum as

$$p = \frac{\partial\,\mathcal{L}_{\mathrm{J}}}{\partial \dot{\gamma}} = C\phi_0^2\,\dot{\gamma}. \tag{2.20}$$

Using Eqs. (2.17–2.20), the Hamiltonian for the unbiased JJ is then written as

$$H_{\mathrm{J}} = \frac{E_{\mathrm{C}}}{2\hbar^2}\,p^2 - E_{\mathrm{J}}\,\cos\gamma, \tag{2.21}$$

where we have defined new energy scales: the charging energy $E_{\mathrm{C}} = 4e^2/C$ and the Josephson energy $E_{\mathrm{J}} = I_{\mathrm{c}}\phi_0$.

The quantization of the Hamiltonian is done by replacing the phase γ and conjugate momentum p with quantum operators that obey the standard commutation relation $[\hat{\gamma}, \hat{p}] = \mathrm{i}\hbar$. From Eqs. (2.12) and (2.20), the momentum operator $\hat{p}$ can also be viewed as the charge operator $\hat{q}$. The charge operator represents the number of charges, which in the case of superconductors is the number of Cooper pairs, that have gone through the branch, this can be written as $\hat{q} = \hbar\hat{n}$, where $\hat{n}$ is the Cooper pair number operator. The Cooper pair number operator has the following representation in the basis of charge (Cooper pairs) states

$$\hat{n} = \sum_n n \left|n\right\rangle_{\mathrm{ch}} \left\langle n\right|_{\mathrm{ch}}, \tag{2.22}$$

where $|n\rangle$ are charge states and n is the number of charges in that state. It can be shown that the charge basis and the phase basis are related by the following transformations

$$\left|\gamma\right\rangle_{\mathrm{ph}} = \frac{1}{\sqrt{2\pi}} \sum_n \mathrm{e}^{-\mathrm{i}n\gamma} \left|n\right\rangle_{\mathrm{ch}} \tag{2.23}$$

and

$$\left|n\right\rangle_{\mathrm{ch}} = \frac{1}{\sqrt{2\pi}} \int_0^{2\pi} \mathrm{d}\gamma\, \mathrm{e}^{\mathrm{i}n\gamma} \left|\gamma\right\rangle_{\mathrm{ph}}, \tag{2.24}$$

where $|\gamma\rangle_{\mathrm{ph}}$ and $|n\rangle_{\mathrm{ch}}$ are phase and charge states, respectively. This can be understood by recognizing that both the charge and phase states are eigenstates of $\hat{H}_{\mathrm{J}}$. Furthermore, we can see that the effect of the charge operator in the phase basis is equivalent to the derivative with respect to the phase

$$\hat{n} = -\mathrm{i}\,\widehat{\frac{\partial}{\partial\gamma}}. \tag{2.25}$$

We can then conveniently write the JJ Hamiltonian in the phase basis with this definition as

$$\hat{H}_{\mathrm{J}} = -\frac{E_{\mathrm{C}}}{2}\left(\widehat{\frac{\partial}{\partial\gamma}}\right)^{2} - E_{\mathrm{J}}\cos\hat{\gamma}. \tag{2.26}$$

2.3 Superconducting Interferometers

An important circuit to introduce at this stage is the superconducting quantum interferometry device (SQUID). The phase of the quantum collective wave-function of the Cooper pairs inside such a superconducting interferometer is found to be the basis of the interference. These devices produce interference patterns in the electrical current similar to the patterns that appear in the single electron double slit experiment [70], which can only be explained by the quantum mechanical wave-particle duality of the electron (the electron behaves both a wave and a particle). This implies that the SQUIDs are indeed quantum. The quantum world is typically limited to the smallest systems such as single atoms, electrons or photons. At larger scales, the quantum effects are dominated by classical effects. The fact that a macroscopic number of electrons (all the electrons in the superconducting phase of the device) can behave as one effective quantum dual wave-particle and that its quantum nature can be experimentally observed is a remarkable feature of superconducting quantum devices. These SQUIDs are most often used as ultra-sensitive magnetometers and flux-based measurement of qubits. In this thesis we will focus on the qubit-like behavior of these circuits and their ability to act as flux transformers.

2.3.1 RF-SQUID

The radio frequency SQUID or rf-SQUID is made up of a superconducting ring interrupted by a single JJ, as pictured in figure 2.3.

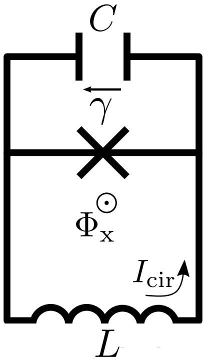

Figure 2.3: Circuit schematic of an RF-SQUID, with loop inductance. The circulating current, junction phase and external flux positive directions are indicated.

We start the circuit analysis by looking at the total flux threading the loop of the SQUID. The total flux is

$$\Phi_\mathrm{tot} = L^\mathrm{g} I_\mathrm{cir} + \Phi_\mathrm{x}, \tag{2.27}$$

with L^g the geometric inductance of the loop, I_cir the circulating current in the loop and Φ_x the external flux threading the loop.

The quantization of the fluxoid in a superconducting loop results in the following constraint on the phase across the junction

$$\begin{aligned}
\gamma + \gamma_\mathrm{k} &= -2\pi \frac{\Phi_\mathrm{tot}}{\Phi_0} \\
\gamma &= -\frac{\left(L^\mathrm{g} + L^\mathrm{k}\right) I_\mathrm{cir}}{\phi_0} - 2\pi \frac{\Phi_\mathrm{x}}{\Phi_0} \\
\gamma &= -\frac{L I_\mathrm{cir}}{\phi_0} - 2\pi f_\mathrm{x},
\end{aligned} \tag{2.28}$$

where $\gamma^\mathrm{k} = L^\mathrm{k} I_\mathrm{cir}$ is the superconducting phase difference along the loop due to the kinetic inductance of the superconductor, $L = L^\mathrm{g} + L^\mathrm{k}$ is the total inductance of the loop and where $f_\mathrm{x} = \Phi_\mathrm{x}/\Phi_0$.

Replacing the circulating current with the current flowing through the junction, we have that the equation of motion for the circuit is

$$I_\mathrm{c} \sin\gamma + C\phi_0 \, \ddot{\gamma} = -\frac{\phi_0}{L}\left(\gamma + 2\pi f_\mathrm{x}\right) \tag{2.29}$$

One can readily see that this equation of motion corresponds to the Euler-Lagrange equation for the following Lagrangian

$$\mathcal{L}_{\mathrm{rfSQUID}} = \frac{C\phi_0^2}{2}\,\dot{\gamma}^2 + I_{\mathrm{c}}\phi_0\,\cos\gamma - \frac{\phi_0^2}{2L}\,(\gamma - 2\pi f_{\mathrm{x}})^2\,. \tag{2.30}$$

The Hamiltonian is then

$$\hat{H}_{\mathrm{rfSQUID}} = \frac{E_{\mathrm{C}}}{2\hbar^2}\,\hat{p}^2 - E_{\mathrm{J}}\,\cos\hat{\gamma} + \frac{E_{\mathrm{L}}}{2}\,(\hat{\gamma} - 2\pi f_{\mathrm{x}})^2\ , \tag{2.31}$$

where we have introduced a third energy scale, $E_{\mathrm{L}} = \phi_0^2/L$ – the inductive energy.

We can thus understand the RF-SQUID as a hypothetical particle of mass E_{C}^{-1} moving on the potential

$$\hat{U}_{\mathrm{rf}} = -E_{\mathrm{J}}\,\cos\hat{\gamma} + \frac{E_{\mathrm{L}}}{2}\,(\hat{\gamma} - 2\pi f_{\mathrm{x}})^2\ . \tag{2.32}$$

It is important to discuss briefly two operating regimes of the rf-SQUID. The first operating regime is when the ratio $\beta = E_{\mathrm{J}}/E_{\mathrm{L}} \ll 1$. Here, the rf-SQUID potential is mono-stable resembles that of a harmonic oscillator (a parabolic potential). The low-energy states of the rf-SQUID, which are the smallest eigenvalues of the Hamiltonian Eq. (2.31), are also harmonic oscillator-like states centered on the minimum point of the potential at a specific value of the phase or circulating current, as in panel (b) of figure 2.4. By changing the external flux threading the loop, one can change the value of the circulating current corresponding to the low-energy states and even make it zero near $f_{\mathrm{x}} = 0.5$. The second operating regime is when $\beta \gg 1$. In this case, the potential is multi-stable and near $f_{\mathrm{x}} = 0.5$ the potential has a bi-stable double-well shape where the low-energy states are now harmonic oscillator-like states in the two wells, as in panel (a) of figure 2.4. In the double-well potential regime, the two lowest energy states in each well of the rf-SQUID are coupled by the tunneling through the barrier. These two states are also localized on two values of circulating current in the ring $\pm I_{\mathrm{p}}$ know as the persistent current states. Thus, the two lowest energy states of the rf-SQUID can be used as a type of flux qubit when operated in the regime where $\beta \gg 1$.

2.3.2 DC-SQUID

The direct current SQUID or DC-SQUID is composed of two JJs connected in parallel as in figure 2.5.

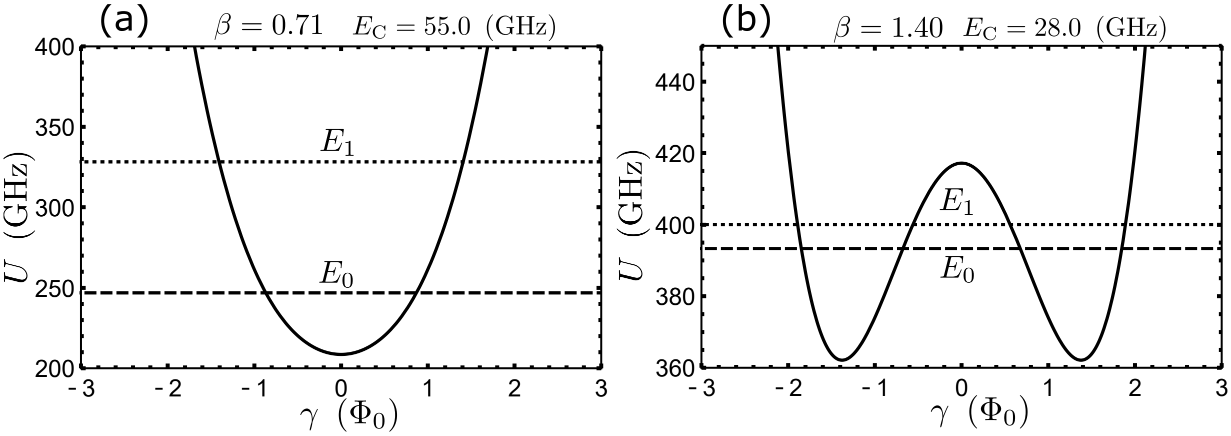

Figure 2.4: Potential of the RF-SQUID from Eq. (2.32) with $E_{\mathrm{L}} = 300.0$ GHz and $f_{\mathrm{x}} = 0.5$. Changing the Josephson energy to be in the (a) bi-stable and (b) mono-stable regimes. The dashed lines in both plots represent the first two energy levels of the RF-SQUID.

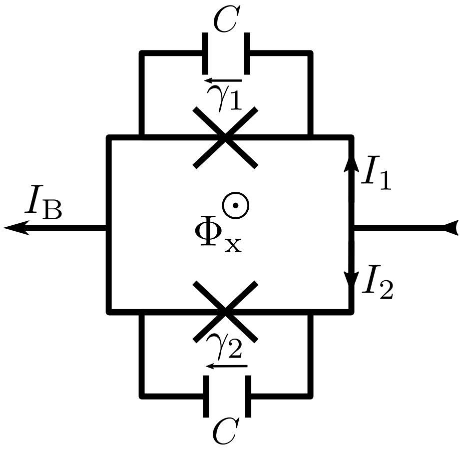

Figure 2.5: Circuit schematic of a DC-SQUID with symmetric junctions and no geometric or self-inductance. The current, junction phases and bias flux positive directions are indicated.

Let us consider the circuit equations of a DC-SQUID with negligible self-inductance. The fluxoid quantization condition along the loop imposes

$$\begin{aligned}\gamma_1 - \gamma_2 &= -2\,\pi \frac{\Phi_{\mathrm{DC}}}{\Phi_0} \\ &= -2\pi\left(f_{\mathrm{x}} + L I_{\mathrm{cir}}\right) \\ &\approx -2\pi f_{\mathrm{x}},\end{aligned} \tag{2.33}$$

where Φ_{DC} is the total flux threading the loop and where we have taken the assumption of negligible self flux. This last equation enables us to eliminate one of the phases as a degree of freedom of the problem, thus reducing the complexity of the problem from two to one variable.

The bias current flowing through the junctions is

$$\begin{aligned}I_{\mathrm{B}} &= I_1 + I_2 \\ &= I_{\mathrm{c1}}\,\sin\gamma_1 + C_1\phi_0\,\ddot{\gamma}_1 + I_{\mathrm{c2}}\,\sin\gamma_2 + C_2\phi_0\,\ddot{\gamma}_2,\end{aligned} \tag{2.34}$$

where I_i is the current flowing in arm i of the SQUID.

Now, taking for simplicity a symmetric DC-SQUID where $I_{\mathrm{c1}} = I_{\mathrm{c2}} = I_{\mathrm{c}}$ and $C_1 = C_2 = C$, the equation of motion is

$$\begin{aligned}I_{\mathrm{B}} &= I_{\mathrm{c}}\,\sin\gamma_1 + I_{\mathrm{c}}\,\sin\left(\gamma_1 + 2\pi f_{\mathrm{x}}\right) + 2C\phi_0\,\ddot{\gamma}_1 \\ &= 2I_{\mathrm{c}}\cos\left(\pi f_{\mathrm{x}}\right)\sin\left(\gamma_1 + \pi f_{\mathrm{x}}\right) + 2C\phi_0\,\ddot{\gamma}_1\,.\end{aligned} \tag{2.35}$$

We now see an important feature of the DC-SQUID (in the simplest case studied here, for the symmetric and small inductance DC-SQUID), it can be understood as a tunable JJ with a critical current dependent on the external flux threading its loop, this current can be varied from zero to $\tilde{I}_{\mathrm{c}} = 2I_{\mathrm{c}}|\cos\left(\pi f_{\mathrm{x}}\right)|$.

We have now introduced sufficient concepts to understand that these SQUIDs act as flux-current transformers. By threading flux through these loops the circulating or critical current is varied which is going to be important for analysis in the coming chapters.

2.4 Superconducting Flux Qubits

Superconducting flux qubits can be made in a few variants such as the RF-SQUID type [71, 29] that we discussed above, the persistent current qubit [72, 73] or the capacitively

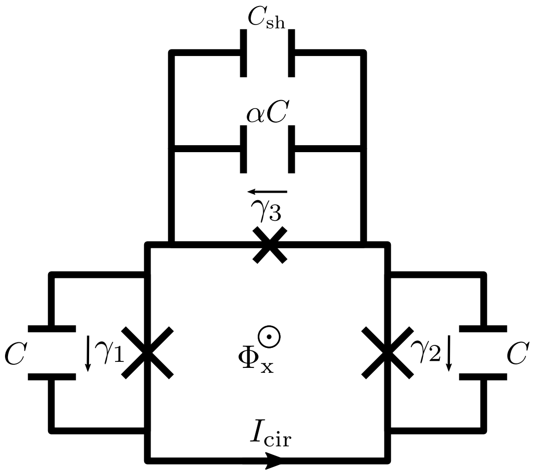

Figure 2.6: Capacitively shunted flux qubit circuit, comprised of a superconducting loop interrupted by three Josephson junctions. The third junction is drawn smaller than the other two (which are identical) to indicate its physically smaller size, this also results in a smaller capacitance. The positive direction of the circulating current and the external flux bias are indicated. The arrows next to the phases indicate the direction of positive phase drop.

shunted flux qubit [74]. These all have their qubit subspace (two quantum states used for computation) made of distinct circulating current or flux states in their loop. The circulating current in the loop of the qubit is distinct, often of opposite sign, when the qubit is in the ground or first excited states, or combinations of the energy eigenvalues. The distinct magnetic flux generated by these two states enables the measurement of these qubits. In this thesis, we will be focusing on the capacitively shunted flux qubit (CSFQ) because of the state of the art coherence times [74] and the recent efforts in coherent quantum annealing [51].

The circuit of the CSFQ is shown in figure 2.6, it is composed of a single superconducting loop of negligible self inductance interrupted by 3 JJs. Two of the JJs are nominally identical, with critical current I_{c} and capacitance C, while the third is smaller by a factor α, thus the critical current is αI_{c} and the junction capacitance is similarly αC. The smaller junction is also shunted by a large capacitor[2] of capacitance C_{sh}.

Following the steps laid out above to quantize the circuit, we write the current equations

---

[2] The large shunting capacitor is included to minimize the sensitivity of the circuit to charge fluctuations [74].

of this circuit as

$$\begin{aligned} I_{\mathrm{cir}} &= I_{\mathrm{c}}\,\sin\gamma_1 + C\phi_0\,\ddot{\gamma}_1, \\ I_{\mathrm{cir}} &= I_{\mathrm{c}}\,\sin\gamma_2 + C\phi_0\,\ddot{\gamma}_2 \end{aligned} \tag{2.36}$$

and

$$I_{\mathrm{cir}} = \alpha I_{\mathrm{c}}\,\sin\gamma_3 + \left(\alpha C + C_{\mathrm{sh}}\right)\phi_0\,\ddot{\gamma}_3. \tag{2.37}$$

The fluxoid quantization condition, with negligible self flux contribution, is written as

$$\gamma_1 - \gamma_2 + \gamma_3 \approx -2\pi f_{\mathrm{x}}\,. \tag{2.38}$$

We can eliminate one variable from the problem and write the Lagrangian as

$$\begin{aligned} \mathcal{L}_{\mathrm{csfq}} &= T - U \\ &= \frac{C\phi_0^2}{2}\,\dot{\gamma}_1^2 + \frac{C\phi_0^2}{2}\,\dot{\gamma}_2^2 + \frac{C_3\phi_0^2}{2}\,\left(\dot{\gamma}_2 - \dot{\gamma}_1\right)^2 \\ &\quad + I_{\mathrm{c}}\phi_0\,\cos\gamma_1 + I_{\mathrm{c}}\phi_0\,\cos\gamma_2 + \alpha I_{\mathrm{c}}\phi_0\,\cos\left(\gamma_2 - \gamma_1 - 2\pi f_{\mathrm{x}}\right), \end{aligned} \tag{2.39}$$

with $C_3 = \alpha C + C_{\mathrm{sh}}$.

The Hamiltonian can now be written in terms of new variables $\gamma_+ = \frac{1}{2}\left(\gamma_1 + \gamma_2\right)$ and $\gamma_- = \frac{1}{2}\left(\gamma_1 - \gamma_2\right)$ as

$$\hat{H}_{\mathrm{csfq}} = \frac{1}{2\hbar^2}\left(E_{\mathrm{C+}}\,\hat{p}_+^2 + E_{\mathrm{C-}}\,\hat{p}_-^2\right) + E_{\mathrm{J}}\left[-2\,\cos\hat{\gamma}_+\,\cos\hat{\gamma}_- - \alpha\,\cos\left(2\,\hat{\gamma}_- - 2\pi f_{\mathrm{x}}\right)\right]\,, \tag{2.40}$$

where the $\hat{p}_\delta = -\mathrm{i}\hbar\,\widehat{\frac{\partial}{\partial\gamma_\delta}}$ for $\delta \in \{+,-\}$ are the conjugate momenta associated with the new phase variables. The charging energies are renormalized to

$$\begin{aligned} E_{\mathrm{C+}} &= \frac{2\mathrm{e}^2}{C}\,, \\ E_{\mathrm{C-}} &= \frac{\mathrm{e}^2}{\left(C + \alpha + \frac{1}{2}\right)}\,. \end{aligned} \tag{2.41}$$

This Hamiltonian can be reduced to a qubit Hamiltonian by noticing that the two lowest energy levels, the ground and first excited state, have distinct values of circulating currents and are well separated from the higher energy states due to the large anharmonicity of the spectrum [74]. Taking the two persistent current states as the qubit basis, the qubit Hamiltonian is

$$\hat{H}_{\mathrm{csfq}} \approx -\frac{\hbar}{2}\left[\epsilon\left(f_{\mathrm{x}}\right)\,\hat{\sigma}_{\mathrm{z}} + \Delta\left(f_{\mathrm{x}}\right)\,\hat{\sigma}_{\mathrm{x}}\right]\,. \tag{2.42}$$

In the above Hamiltonian, $\hbar\epsilon\left(f_{\mathrm{x}}\right)/2 = \Phi_0\left(2\pi f_{\mathrm{x}} - 1/2\right)\left[I_{\mathrm{p}1}\left(f_{\mathrm{x}}\right) - I_{\mathrm{p}0}\left(f_{\mathrm{x}}\right)\right]/2$ is the flux dependent energy bias related to the persistent current in the 1 state, $I_{\mathrm{p}1}\left(f_{\mathrm{x}}\right)$, and in the 0 state, $I_{\mathrm{p}0}\left(f_{\mathrm{x}}\right)$, of the qubit and $\Delta\left(f_{\mathrm{x}}\right)$ is the flux-dependent tunneling between the two qubit states. The fact that these quantities are, in general, dependent on the external flux threading the loop means that there is significant contribution to the low-energy spectrum by the higher states (second excited state and above) of the circuit. Because of this, the complete Hamiltonian should be diagonalized at every flux bias point to extract the parameters of the two-level Hamiltonian [74].

Superconducting qubits can also be designed with different circuits and in different regimes such that one has other quantum operators, such as the charge or the phase, being a well-defined basis of computation. The most used other qubit types are the charge qubit and the phase qubit, more information can be found here [25].

2.5 Quantum Coherence and Decoherence

One of the most important distinctions between classical and quantum systems is that the state of a quantum system can be in a coherent superposition of many states [75].

To describe quantum states and their coherence in a more general manner, it is instructive to briefly introduce here the concept of the density matrix. The state $|\Psi_i\rangle$ of a two-level system can be described by the following density matrix

$$\begin{aligned} \rho &\equiv |\Psi_i\rangle\langle\Psi_i| \\ &= \begin{bmatrix} \rho_{00} & \rho_{01} \\ \rho_{10} & \rho_{11} \end{bmatrix}. \end{aligned} \tag{2.43}$$

The diagonal matrix elements ρ_{00} and ρ_{11} of (2.43) represent the probability of finding the system in state $|0\rangle$ or $|1\rangle$, respectively, while the off-diagonal elements represent the phase relation between the two quantum states. Thus these off-diagonal elements characterize the coherent superposition between the states [14].

The concept of coherence in quantum systems is a deep and fundamental question rooted in the interpretation one has of quantum mechanics itself. However, in the scope of this present thesis, it can be summarized as the phase correlations between the different parts of the wave function corresponding to the different superposed states of the quantum system. In the language of density matrices, this means that the density matrix describing the system has non-vanishing off-diagonal elements. When this phase relation is lost, the off-diagonal matrix elements decay and the state is no longer in superposition and is essentially reduced to a statistical mixture of states [75]. Quantum coherence is needed for the implementation of quantum computing and furthermore, needs to be long lived in the physical implementation. Unfortunately, real quantum systems and including superconducting qubits interact with their environment uncontrollably creating irreversible loss of information and of coherence. This undesirable process is called decoherence and it manifests itself on a time scale referred to as the (de)coherence time. This time scale is directly related to the available time one has to use the system in a quantum computation.

The concept of noise can be described in the following way: considering a system coupled to the environment, the uncontrollable degrees of freedom of the environment interact in a random way with the degrees of freedom of the system resulting in the appearance of random components in the degrees of freedom of the system. In a flux qubit for example, this can manifest itself as a random component in the bias and tunneling terms in the qubit Hamiltonian [76]. We can write the noisy qubit Hamiltonian as

$$\hat{H}_{\mathrm{qb}'} = -\frac{\hbar}{2}\left[\left(\epsilon + \delta\epsilon\right)\hat{\sigma}_{\mathrm{z}} + \left(\Delta + \delta\Delta\right)\hat{\sigma}_{\mathrm{x}}\right], \tag{2.44}$$

where $\hbar\epsilon/2 = I_{\mathrm{p}}\left(2\pi f_{\mathrm{x}} - \pi\right)$ with I_{p} the persistent current of the qubit and Δ is the tunneling between the two qubit states. In the above, the $\delta\epsilon$ and $\delta\Delta$ are uncontrollable time-dependent quantum operators of the environment that couple to the bias and tunneling energy of the qubit, coming from the interaction with the environment.

Taking the Block-Redfield model to understand the effect of noise on the dynamics of a system leads to two important decay rates (or time scales), the energy relaxation rate Γ_1 and the decoherence rate $\Gamma_2 = \frac{1}{2}\Gamma_1 + \Gamma_\phi$, where Γ_ϕ is the pure dephasing rate. The first rate describes how the diagonal matrix elements of the system's density matrix decay. These matrix elements decay through the energy exchange between the environment and the system either by spontaneous excitation or relaxation of the two level system: $\Gamma_1 = \Gamma_{1\to0} + \Gamma_{0\to1}$. The decoherence rate describes how the quantum information held by the off-diagonal matrix elements of the system's density matrix decays [77]. This decay is a combination of the energy relaxation rate and the pure dephasing rate. The latter is the rate at which the phase relation between the two states of the system in a superposition state is lost. The pure dephasing rate can be calculated in the following way: consider the qubit Hamiltonian written in the energy eigen basis

$$\hat{H}_{\mathrm{qb}} = -\frac{\hbar}{2}\left[\omega_{01} + \zeta\left(t\right)\right]\hat{\sigma}_{\mathrm{z}}, \tag{2.45}$$

where $\omega_{01} = \sqrt{\epsilon^2 + \Delta^2}$ is the qubit energy gap and $\zeta\left(t\right)$ is a time-dependent noisy parameter.

When the qubit is initialized in a superposition state, free evolution induces an added phase of the form $\phi(t) = \langle\omega_{01}\rangle\, t + \delta\phi\,(t)$, where we see the contribution from the static, $\langle\omega_{01}\rangle$, and noisy, $\delta\phi\,(t) = \frac{\partial\omega_{01}}{\partial\zeta}\int_0^t \zeta\,(t')\,\mathrm{d}t'$, part of the Hamiltonian. Here, $\delta\phi\,(t)$ is the phase diffusion coming from the fluctuations of the transition frequency due to the ζ noise [76]. It is relevant to consider the rate at which this accumulated phase decays during a typical evolution or experiment, the dephasing rate:

$$\left\langle \mathrm{e}^{\mathrm{i}\delta\phi(t)} \right\rangle = \exp\left[-\tau^2 \sum_{\zeta} \left(\frac{\partial\omega_{01}}{\partial\zeta}\right)^2 \int_0^\infty \mathrm{d}\omega\, S_\zeta\,(\omega)\, g\,(\omega,\tau)\right]. \tag{2.46}$$

Here we have assumed Gaussian noise processes. In the above, $S_\zeta\,(\omega)$, τ and $g\,(\omega,\tau)$ are the power spectral density (PSD) of the noisy environment, the free evolution time of the quantum state and the filter function of the particular experiment[3], respectively [76]. In the Bloch-Redfield picture, the noise has a short correlation time and is taken to be weak. This assumption holds when, for example, the dominant noise process has a constant PSD $S\,(\omega) = S(0)$, which is the case for white noise. White noise gives an exponential dephasing rate dependent on the PSD at zero frequency [77],

$$\left\langle \mathrm{e}^{\mathrm{i}\delta\phi(t)} \right\rangle = \mathrm{e}^{-\frac{1}{2}S_\zeta(0)\tau}\,, \tag{2.47}$$

This rate drifts from exponential decay when the noise correlation time increases, while staying singular at zero frequency. Such is the case of low frequency $\frac{1}{\omega}$ noise. The integral in (2.46) is not well behaved around $\omega \approx 0$ for $S_\zeta(\omega) = \frac{A}{|\omega|}$. One can include proper low and high frequency cutoffs to this integral (taken from the experimental time scales) to get a Gaussian decay rate (up to a small logarithmic correction) for the dephasing [77]. Thus, one can uncover significant information on the nature of the noise from the general shapes of these decays.

2.5.1 Sources of Decoherence

Since the quantum behavior of these circuits is brought on by the collective behavior of a macroscopic number of Cooper pairs, decoupling the environment degrees of freedom from this macroscopic system is inherently difficult. It is then relevant to discuss the various sources of noise fluctuations and energy loss in superconducting qubits.

---

[3] The dependence on the experimental protocol of (2.46) is a useful property used in noise spectroscopy experiments to uncover important details on the nature of the noisy environment. By choosing the experimental protocol and thus the filter function, one can probe specific frequency ranges of the noise spectrum [76].

One source of decoherence comes from the thermal fluctuations of the electronic equipment that is at room temperature that comes in contact with the circuits at cryogenic temperatures. This electronic equipment is required for manipulation and readout of the devices, but the signals they send to them carry with them a noise component from thermal fluctuations [25]. This noise affects the device by varying the voltage, current or magnetic flux driving it causing charge (variations in the number of charges on a superconducting island) and flux noise (variations in the amount of magnetic flux threading a superconducting loop) and potentially inducing transitions in the levels and loss of coherence. Through the use of proper filters and attenuators, this source of noise can be maintained at negligible levels [76, 74, 51].

General energy loss to the environment, be it by dielectric loss or quasi-particle (unpaired electrons) tunneling or general dissipative processes, during the operation of the device can also lead to loss of quantum information [78, 79]. The device itself can have sources of noise ubiquitously present in the form of clandestine defects trapped in the oxides on the surface of the superconducting circuits. These trapped two-level systems are charged and thus have a dipole moment capable of interacting with qubit electromagnetic fields. When these impurities fluctuate randomly, they create charge fluctuations [80] and magnetic flux variations, which in turn induce fluctuations [81, 82, 23] in the qubits degrees of freedom. The latter has been found to have significant effect on superconducting flux qubits and SQUIDs [83, 84, 85]. It is believed that this noise is intrinsic to the device, that it is coming from impurities spins and clusters of spins on the fabricated sample randomly reversing their orientation and cause flux variations, that it is dependent on the geometry of the device and dependent on temperature [81, 86, 87, 88].

Chapter 3

Mediated Inductive Coupling

3.1 Direct and indirect interactions

In nature, everything is interconnected and interdependent, there are countless interactions between the smallest sub-atomic particles and between the largest clusters of galaxies. This interaction, interconnectedness or interdependence between systems can also be called the coupling of these systems together. As scientists seeking to understand nature, we are often pushed by the complexity of these interconnections to study the component parts of nature in their isolation. However, to draw the most accurate conclusions, especially in the context of quantum systems, we must consider these component parts in their interconnectedness. As discussed in section 2.5, the interaction between a quantum system and uncontrollable quantum systems in the environment is very important for the implementation of physical quantum computers. Additionally, in interacting systems we can see emergent phenomena that are not present in the component parts. A particularly relevant example of this is superconductivity. As we discussed in section 2.1, superconductivity is governed by the attractive interaction between pairs of conducting electrons, something that is not observed in a pair of isolated electrons. It is only through considering the inter-electron interactions and the electron-phonon interactions that this attraction appears. We can refer to this important physical concept as an indirect or mediated interaction, i.e. in this case the attractive electron-electron interaction is mediated by the phonons.

Some of the earliest mediated interactions to be investigated were magnetic spin coupling between nuclei mediated by the hyperfine interaction between the nuclear magnetic moment and the magnetic field created by the surrounding electrons; these mediated interactions explained broadening observed in nuclear magnetic resonances [89, 90]. These mediated spin couplings are now being used to couple quantum dot and nuclear spin qubits for quantum computing [14, 20]. In fact, mediated interactions are a fundamental part of quantum computing implementations, where we have photon-photon coupling mediated by photon-atom interactions for photonic qubits and ion-ion coupling mediated by ion-phonon interactions in ion trap quantum computers [14, 20]. The coupling of qubits has also been investigated when mediated by a spin or chain of spins [91, 92, 93].

In the context of superconducting qubits, in both the circuit model and quantum annealing, qubit-qubit interactions have also been investigated through various mediators, such as distributed microwave resonators in the context of circuit quantum electrodynamics [94, 95], lumped LC-oscillators [96, 97], Josephson junctions [98, 99, 100], flux qubits [101, 102] and SQUID-type loops [103, 104, 105, 106, 28, 107, 108, 51]. In general, the mediator in these types of interactions is designed to have a large excitation energy (or otherwise a much higher oscillation frequency) than the coupled qubits such that the mediator does not change energy state during the qubit dynamics. When the mediators can be designed such that they have sufficient non-linear properties and that these properties are controllable by an external parameter (such as flux, current or voltage), then the mediated interaction strength can also controlled, in both sign and magnitude.

In the rest of the chapter, we will be discussing mediated controllable interactions in the context of quantum annealing with flux qubits. The standard circuit being used to mediate qubit-qubit coupling in the D-Wave annealers is based on the rf-SQUID [105, 28, 109]. These coupling circuits are capable of mediating positive and negative qubit-qubit inductive interactions in the computational basis (ZZ coupling) of flux qubits and are also capable of turning the coupling to zero. This tunability is done by threading a static control flux through the SQUID loop(s).

3.2 Two-qubit Tunable Inductive Coupler

3.2.1 rf-SQUID Coupler

One of the first study of tunable inductive coupling was done using the rf-SQUID circuit as the mediator [105]. The type of interaction mediated by the rf-SQUID is fundamental to the implementation of tunable qubit-qubit coupling in quantum annealing.

Let us analyze a basic coupled system using this circuit as the mediator and extract the mediated interaction. Consider the circuit in figure 3.1 of two rf-SQUID flux qubits coupled to a third rf-SQUID coupler through a mutual inductance M. For simplicity, we restrict

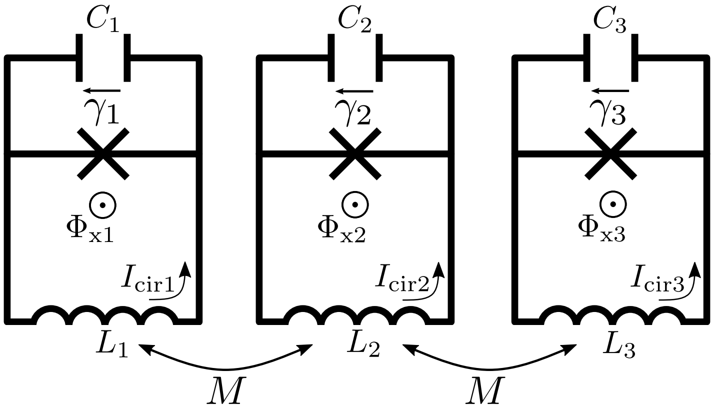

Figure 3.1: Three rf-SQUIDs inductively coupled to each other through mutual inductances. The middle RF-SQUID is operated as a mediator or coupler while rf-SQUIDs 1 and 3 are operated as qubits.

ourselves to rf-SQUID 1 and 2 as the qubits, but these could be swapped with CSFQs or other flux qubit types and the derivation below would be unchanged. The Hamiltonian for these three coupled rf-SQUIDs can be written as

$$\hat{H}_{3\mathrm{rf}} = \sum_{i=1}^{3} \frac{E_{\mathrm{C}\,i}}{2}\,\hat{p}_i^2 - \sum_{i=1}^{3} E_{\mathrm{J}\,i}\,\cos\hat{\gamma}_i + \frac{\phi_0^2}{2}\,\vec{\gamma}^{\mathrm{T}}\,\mathbf{L}^{-1}\,\vec{\gamma}\,. \tag{3.1}$$

In Eq. (3.1), $\vec{\gamma} = [\hat{\gamma}_1 - 2\pi f_{\mathrm{x}\,1}, \hat{\gamma}_2 - 2\pi f_{\mathrm{x}\,2}, \hat{\gamma}_3 - 2\pi f_{\mathrm{x}\,3}]$ is a vector of the three RF-SQUID phases and

$$\mathbf{L} = \begin{bmatrix} L_1 & -M & 0 \\ -M & L_2 & -M \\ 0 & -M & L_3 \end{bmatrix} \tag{3.2}$$

is the inductive matrix of the system containing the coupling through the mutual inductance[1] M and the self inductance of each rf-SQUID L_i. The direct inductive coupling between L_1 and L_3 has been taken to be zero.

The Hamiltonian of the coupled system can be re-written in a more suggestive form

$$\hat{H}_{\mathrm{coupled}} = \hat{H}_{\mathrm{rf}\,1} + \hat{H}_{\mathrm{rf}\,3} + \hat{H}_{\mathrm{c}}, \tag{3.3}$$

---

[1] The direct coupling between two inductive loops in this configuration is anti-ferromagnetic, the magnetic moment of each neighboring loop tends to anti-align, hence the negative sign for M.

with

$$\hat{H}_{\mathrm{c}} = \frac{E_{\mathrm{C}\,2}}{2\hbar^2}\,\hat{p}_2^2 - E_{\mathrm{J}\,2}\,\cos\hat{\gamma}_2 + \frac{E_{\mathrm{L}\,\mathrm{c}}}{2}\left(\hat{\gamma}_2 - \hat{f}_{\mathrm{c}}\right)^2. \tag{3.4}$$

In Eq. (3.3), we have renamed the Hamiltonian of rf-SQUID 2 as the coupler Hamiltonian, have renormalized the inductive energy as

$$E_{\mathrm{L}\,\mathrm{c}} = \phi_0^2\left(L_2 - \frac{M^2}{L_1} - \frac{M^2}{L_3}\right)^{-1} \tag{3.5}$$

and have included the inductive interactions in the qubit-dependent flux threading the coupler loop

$$\hat{f}_{\mathrm{c}} = 2\pi f_{\mathrm{x}2} - \delta\hat{\phi}_{\mathrm{q}}, \tag{3.6}$$

$$\delta\hat{\phi}_{\mathrm{q}} = \frac{M}{L_1}\left(\hat{\gamma}_1 - 2\pi f_{\mathrm{x}1}\right) + \frac{M}{L_3}\left(\hat{\gamma}_3 - 2\pi f_{\mathrm{x}3}\right). \tag{3.7}$$

Finally, the rf-SQUID qubits are treated as isolated and their Hamiltonians are as in Eq. (2.31).

With the form of Hamiltonian in Eq. (3.3), the effective interaction mediated by the coupler circuit can be readily determined by taking the Born-Oppenheimer (BO) approximation [110, 111, 105, 108]. In the context of superconducting circuits, this is done by taking the assumption that the coupler has a much higher excitation energy (energy gap between ground and first excited state) than the qubits, and thus the coupler degree of freedom evolves on a faster time-scale. One can then separate the fast coupler degree of freedom from the slow qubit degrees of freedom. The large difference in time-scales means that the fast coupler degree of freedom only "sees" the qubit degrees of freedom as slowly varying or quasi-static parameters. The fast coupler degree of freedom is then said to evolve adiabatically with respect to the qubits. This enables us to write the full system wave-function of state i in the following product form

$$\Psi^i_{\mathrm{coupled}}\left(\hat{\gamma}_{\mathrm{c}}, \hat{\gamma}_{\mathrm{q}}\right) = \psi^i_{\mathrm{c}}\left(\hat{\gamma}_{\mathrm{c}}; \gamma_{\mathrm{q}}\right)\,\chi^i_{\mathrm{q}}\left(\hat{\gamma}_{\mathrm{q}}\right), \tag{3.8}$$

where $\psi^i_{\mathrm{c}}\left(\hat{\gamma}_{\mathrm{c}}; \gamma_{\mathrm{q}}\right)$ is a coupler wave-function that depends parametrically on the qubit variables γ_{q}, and $\chi^i_{\mathrm{q}}\left(\hat{\gamma}_{\mathrm{q}}\right)$ is a qubit wave-function associated with the coupler wave-function.

Let us take the following definition for the coupler wave-function

$$\left[\hat{H}_{\mathrm{c}}\left(\hat{\gamma}_{\mathrm{c}}; \gamma_{\mathrm{q}}\right) - E^{(n)}_{\mathrm{c}}\left(\gamma_{\mathrm{q}}\right)\right]\psi^{(n)i}_{\mathrm{c}}\left(\hat{\gamma}_{\mathrm{c}}; \gamma_{\mathrm{q}}\right) = 0, \tag{3.9}$$

where $E_{\mathrm{c}}^{(n)}\left(\gamma_{\mathrm{q}}\right)$ is the quantum eigen-energy of the n^{th} coupler eigenstate. We can thus write the full wave-function as an expansion in terms of the coupler eigenstates (which form a complete basis)

$$\Psi_{\text{coupled}}^{i}\left(\hat{\gamma}_{\mathrm{c}},\hat{\gamma}_{\mathrm{q}}\right)=\sum_{n}\psi_{\mathrm{c}}^{(n)\,i}\left(\hat{\gamma}_{\mathrm{c}};\gamma_{\mathrm{q}}\right)\,\chi_{\mathrm{q}}^{(n)\,i}\left(\hat{\gamma}_{\mathrm{q}}\right). \tag{3.10}$$

The simplest form of the Born-Oppenheimer approximation is based on the assumption that, because of the large excitation energy difference between the coupler and the qubits, the coupler will stay in its ground state and will not get excited by the qubit dynamics [105, 108, 51]. This means that the sum in Eq. (3.10) can be truncated to $n=0$, the ground state. With this, the complete wave-function becomes

$$\Psi_{\text{coupled}}^{i}\left(\hat{\gamma}_{\mathrm{c}},\hat{\gamma}_{\mathrm{q}}\right)\approx\psi_{\mathrm{c}}^{(0)\,i}\left(\hat{\gamma}_{\mathrm{c}};\gamma_{\mathrm{q}}\right)\,\chi_{\mathrm{q}}^{(0)\,i}\left(\hat{\gamma}_{\mathrm{q}}\right). \tag{3.11}$$

We need to solve the time-independent Schrödinger equation for this system to find the energy eigenstates. We thus write

$$\begin{aligned}\left(\hat{H}_{\text{coupled}}-E_{\text{coupled}}^{i}\right)\Psi_{\text{coupled}}^{i}\left(\hat{\gamma}_{\mathrm{c}},\hat{\gamma}_{\mathrm{q}}\right)&=0\\ \left(\hat{H}_{\mathrm{rf}\,1}+\hat{H}_{\mathrm{rf}\,3}+\hat{H}_{\mathrm{c}}-E_{\text{coupled}}^{i}\right)\psi_{\mathrm{c}}^{(0)\,i}\left(\hat{\gamma}_{\mathrm{c}};\gamma_{\mathrm{q}}\right)\,\chi_{\mathrm{q}}^{(0)\,i}\left(\hat{\gamma}_{\mathrm{q}}\right)&=0.\end{aligned} \tag{3.12}$$

Now, if we multiply each side of Eq. (3.12) by $\psi_{\mathrm{c}}^{(0)\,i}\left(\hat{\gamma}_{\mathrm{c}};\gamma_{\mathrm{q}}\right)^{*}$ and integrate over the coupler variable while treating the qubit operators as parameters, we get

$$\begin{aligned}\int\mathrm{d}\gamma_{\mathrm{c}}\,\psi_{\mathrm{c}}^{(0)\,i}\left(\gamma_{\mathrm{c}};\gamma_{\mathrm{q}}\right)^{*}\left(\hat{H}_{\mathrm{rf}\,1}+\hat{H}_{\mathrm{rf}\,3}+\hat{H}_{\mathrm{c}}-E_{\text{coupled}}^{i}\right)\psi_{\mathrm{c}}^{(0)\,i}\left(\gamma_{\mathrm{c}};\gamma_{\mathrm{q}}\right)\,\chi_{\mathrm{q}}^{(0)\,i}\left(\gamma_{\mathrm{q}}\right)&=0\\ \left\langle\psi_{\mathrm{c}}^{(0)\,i}\middle|\left(\hat{H}_{\mathrm{rf}\,1}+\hat{H}_{\mathrm{rf}\,3}+\hat{H}_{\mathrm{c}}-E_{\text{coupled}}^{i}\right)\middle|\psi_{\mathrm{c}}^{(0)\,i}\right\rangle\,\chi_{\mathrm{q}}^{(0)\,i}\left(\gamma_{\mathrm{q}}\right)&=0,\end{aligned} \tag{3.13}$$

where we have defined $\int\mathrm{d}\gamma_{\mathrm{c}}\,\psi_{\mathrm{c}}^{(0)\,i}\left(\gamma_{\mathrm{c}};\gamma_{\mathrm{q}}\right)^{*}\,\psi_{\mathrm{c}}^{(0)\,i}\left(\gamma_{\mathrm{c}};\gamma_{\mathrm{q}}\right)=\left\langle\psi_{\mathrm{c}}^{(0)\,i}\middle|\psi_{\mathrm{c}}^{(0)\,i}\right\rangle$. The terms in Eq. (3.13) can be simplified due to our assumption that the qubits evolve adiabatically with respect to the coupler ground state. The integral of the Hamiltonian for qubit $j\in\{1,3\}$

on the coupler ground state becomes

$$\begin{aligned}\left\langle \psi_{\mathrm{c}}^{(0)\,i} \middle| \hat{H}_{\mathrm{rf}\,j} \middle| \psi_{\mathrm{c}}^{(0)\,i} \right\rangle &= \left\langle \psi_{\mathrm{c}}^{(0)\,i} \middle| \left(-\frac{E_{\mathrm{C}\,j}}{2}\,\hat{\partial}_{\gamma_j}^2 + \hat{U}_{\mathrm{rf}\,j} \right) \middle| \psi_{\mathrm{c}}^{(0)\,i} \right\rangle \\ &= -\frac{E_{\mathrm{C}\,j}}{2} \left\langle \psi_{\mathrm{c}}^{(0)\,i} \middle| \hat{\partial}_{\gamma_j}^2 \middle| \psi_{\mathrm{c}}^{(0)\,i} \right\rangle + \left\langle \psi_{\mathrm{c}}^{(0)\,i} \middle| \hat{U}_{\mathrm{rf}\,j} \middle| \psi_{\mathrm{c}}^{(0)\,i} \right\rangle \\ &= -\frac{E_{\mathrm{C}\,j}}{2} \Bigg(\left\langle \psi_{\mathrm{c}}^{(0)\,i} \middle| \partial_{\gamma_j}^2 \psi_{\mathrm{c}}^{(0)\,i} \right\rangle + \left\langle \psi_{\mathrm{c}}^{(0)\,i} \middle| \partial_{\gamma_j} \psi_{\mathrm{c}}^{(0)\,i} \right\rangle \hat{\partial}_{\gamma_j} \\ &\qquad + \left\langle \psi_{\mathrm{c}}^{(0)\,i} \middle| \psi_{\mathrm{c}}^{(0)\,i} \right\rangle \hat{\partial}_{\gamma_j}^2 \Bigg) + \left\langle \psi_{\mathrm{c}}^{(0)\,i} \middle| \psi_{\mathrm{c}}^{(0)\,i} \right\rangle \hat{U}_{\mathrm{rf}\,j} \\ &\approx -\frac{E_{\mathrm{C}\,j}}{2}\,\hat{\partial}_{\gamma_j}^2 + \hat{U}_{\mathrm{rf}\,j}, \end{aligned} \tag{3.14}$$

where we used the product rule on the momentum operator $\hat{\partial}_{\gamma_j}^2 = \left(\hat{\partial}/\partial\gamma_j\right)^2$, we defined $\left|\partial_{\gamma_j}^2 \psi_{\mathrm{c}}^{(0)\,i}\right\rangle = \hat{\partial}_{\gamma_j}^2 \psi_{\mathrm{c}}^{(0)\,i}\left(\gamma_{\mathrm{c}};\gamma_{\mathrm{q}}\right)$, similarly for the first derivative case, and where we used $\left\langle \psi_{\mathrm{c}}^{(0)\,i} \middle| \psi_{\mathrm{c}}^{(0)\,i} \right\rangle = 1$ and $\left\langle \psi_{\mathrm{c}}^{(0)\,i} \middle| \partial_{\gamma_j} \psi_{\mathrm{c}}^{(0)\,i} \right\rangle = 0$, which comes from the wave-function being a real eigenfunction of the coupler Hamiltonian. The assumption on the integral taken in Eq. (3.14), that $\left\langle \psi_{\mathrm{c}}^{(0)\,i} \middle| \partial_{\gamma_j}^2 \psi_{\mathrm{c}}^{(0)\,i} \right\rangle \approx 0$, is related to the assumption of adiabatic evolution of the qubits with respect to the coupler ground state. This assumption is valid in the limit regime where the coupler energy gap is much larger than the qubit energy gaps. If the coupler energy gap is comparable to the qubit gap or if the coupler is highly non-linear, however, this integral, which is related to the effect of the momentum operator on the ground state of the coupler, becomes important. With the parameters considered in this thesis, we are within the regime of applicability of the assumptions taken in Eq. (3.14).

Finally, by definition, we have

$$\left\langle \psi_{\mathrm{c}}^{(0)\,i}\left(\gamma_{\mathrm{c}};\gamma_{\mathrm{q}}\right) \right| \hat{H}_{\mathrm{c}} \left| \psi_{\mathrm{c}}^{(0)\,i}\left(\gamma_{\mathrm{c}};\gamma_{\mathrm{q}}\right) \right\rangle = E_{\mathrm{c}}^{(0)}\left(\gamma_{\mathrm{q}}\right). \tag{3.15}$$

Thus, because the coupler Hamiltonian in Eq. (3.3) is qubit-dependent, the coupler ground state energy forms the potential energy surface along which the qubits evolve. Now, replacing the qubit parameters with their operators again, the total effective Hamiltonian, now only dependent on qubit variables, can be written as

$$\hat{H}_{\mathrm{eff}} \approx \hat{H}_{\mathrm{rf}\,1} + \hat{H}_{\mathrm{rf}\,3} + \hat{E}_{\mathrm{c}}^{*}\left(\hat{f}_{\mathrm{c}}\right), \tag{3.16}$$

where $\hat{E}_{\mathrm{c}}^{*}\left(\hat{f}_{\mathrm{c}}\right)$ is the qubit-dependent ground state energy surface of H_{c} with the qubit treated as operators.

The effective interactions can then be calculated by perturbatively expanding the qubit-dependent coupler ground state up to second order in the qubit dependent flux offset $\delta\hat{\phi}_{\mathrm{q}}$, around the point $f_{\mathrm{c}} = 2\pi f_{\mathrm{x2}}$. Here we assume that we are in the weak coupling regime. The expansion is written up to second order as

$$\begin{aligned}\hat{E}_{\mathrm{c}}^{*}\left(\hat{f}_{\mathrm{c}}\right) \approx & E_{\mathrm{c}}^{(0)}\left(2\pi f_{\mathrm{x}\,2}\right) + \left(\hat{f}_{\mathrm{c}} - 2\pi f_{\mathrm{x}\,2}\right)\frac{\mathrm{d}}{\mathrm{d}f_{\mathrm{x}\,2}}E_{\mathrm{c}}^{(0)}\left(2\pi f_{\mathrm{x}\,2}\right) \\ & + \frac{1}{2}\left(\hat{f}_{\mathrm{c}} - 2\pi f_{\mathrm{x}\,2}\right)^{2}\frac{\mathrm{d}^{2}}{\mathrm{d}f_{\mathrm{x}\,2}^{2}}E_{\mathrm{c}}^{(0)}\left(2\pi f_{\mathrm{x}\,2}\right).\end{aligned} \tag{3.17}$$

This expansion can then be written, with new definitions, as

$$\begin{aligned}\hat{E}_{\mathrm{c}}^{*}\left(\hat{f}_{\mathrm{c}}\right) \approx & \, E_{\mathrm{c}}^{(0)}\left(2\pi f_{\mathrm{x}\,2}\right) - \frac{M\phi_0\langle\hat{I}_{\mathrm{c}}\rangle}{L_1}\left(\hat{\gamma}_1 - 2\pi f_{\mathrm{x1}}\right) - \frac{M\phi_0\langle\hat{I}_{\mathrm{c}}\rangle}{L_3}\left(\hat{\gamma}_3 - 2\pi f_{\mathrm{x3}}\right) \\ & + \frac{M^2\phi_0^2}{2L_1^2\,L_{\mathrm{eff}}}\left(\hat{\gamma}_1 - 2\pi f_{\mathrm{x1}}\right)^2 + \frac{M^2\phi_0^2}{2L_3^2\,L_{\mathrm{eff}}}\left(\hat{\gamma}_3 - 2\pi f_{\mathrm{x3}}\right)^2 \\ & - \frac{M^2\phi_0^2}{L_1L_3\,L_{\mathrm{eff}}}\left(\hat{\gamma}_1 - 2\pi f_{\mathrm{x1}}\right)\left(\hat{\gamma}_3 - 2\pi f_{\mathrm{x3}}\right).\end{aligned} \tag{3.18}$$

In the above, we have defined

$$L_{\mathrm{eff}}^{-1} \equiv \frac{1}{\phi_0^2}\frac{\mathrm{d}^2}{\mathrm{d}f_{\mathrm{x}\,2}^2}E_{\mathrm{c}}^{(0)}\left(2\pi f_{\mathrm{x}\,2}\right) \tag{3.19}$$

and

$$\left\langle\hat{I}_{\mathrm{c}}\right\rangle \equiv \frac{1}{\phi_0}\frac{\mathrm{d}}{\mathrm{d}f_{\mathrm{x}\,2}}E_{\mathrm{c}}^{(0)}\left(2\pi f_{\mathrm{x}\,2}\right), \tag{3.20}$$

as the effective quantum inductance of the coupler and the ground state expectation value of the coupler circulating current, respectively [51]. Due to the non-linearity of the RF-SQUID current-flux response, this effective quantum inductance can be either positive or negative depending on the flux threading the coupler circuit. The quantum inductance is similar to the quantum capacitance defined for capacitive coupling circuits [112] and is a typical metric to define the mediated coupling of a circuit. In passing, we note that we have the following relation between the expectation of the current and the effective quantum inductance

$$L_{\mathrm{eff}}^{-1} = \frac{1}{\phi_0}\frac{\mathrm{d}\left\langle\hat{I}_{\mathrm{c}}\right\rangle}{\mathrm{d}f_{\mathrm{x}\,2}}. \tag{3.21}$$

The effective 2-qubit interaction is thus given by the last term in Eq. (3.18). It is important to note that the other terms in this expansion also affect the effective Hamiltonian. They represent a coupler-dependent renormalization of the qubit Hamiltonians. The first order term represents an offset flux in the qubit loop dependent on the coupler circulating current and the second order term represents a renormalization of the qubit inductance dependent on the coupler effective inductance.

We now replace Eq. (3.18) and Eq. (3.14) into Eq. (3.16) as, we omit the first constant term in Eq. (3.18) because it has a trivial effect on the qubit dynamics and finally write the effective qubit Hamiltonian as

$$\begin{aligned} H_{\text{eff}} \approx \sum_{i\in\{1,3\}} \Bigg[& \frac{E_{\text{C}i}}{2}\,\hat{p}_i^2 - E_{\text{J}i}\,\cos\hat{\gamma}_i + \frac{E_{\text{L}i}}{2}\,(\hat{\gamma}_i - 2\pi f_{\text{x}i})^2 - \frac{M\phi_0\langle\hat{I}_{\text{c}}\rangle}{L_i}\,(\hat{\gamma}_i - 2\pi f_{\text{x}i}) \\ & + \frac{M^2\phi_0^2}{2L_i^2\,L_{\text{eff}}}\,(\hat{\gamma}_i - 2\pi f_{\text{x}i})^2 \Bigg] - \frac{M^2\phi_0^2}{L_1 L_3\,L_{\text{eff}}}\,(\hat{\gamma}_1 - 2\pi f_{\text{x}1})\,(\hat{\gamma}_3 - 2\pi f_{\text{x}3})\,. \end{aligned} \tag{3.22}$$

The tunable interactions mediated by an rf-SQUID is directly related to the fact that the flux-current response of the RF-SQUID is non-linear. In figure 3.2, we see that the expectation value of the current in the coupler, the derivative of which is proportional to the coupling strength, has regions where a negative, positive and a zero slope are possible. Thus, an important parameter to consider for these types of couplers is the degree of non-linearity. The degree of non-linearity can be defined as

$$\beta \equiv \frac{E_{\text{J}2}}{E_{\text{Lc}}} = \frac{I_{\text{c}2}\tilde{L}_2}{\phi_0}, \tag{3.23}$$

where $\tilde{L}_2 = L_2 - \frac{M^2}{L_1} - \frac{M^2}{L_3}$.

This parameter can be understood as the ratio of Josephson-to-linear inductance in the Hamiltonian (2.32) and when $\beta > 1$, the potential becomes by-stable, there appears two localized flux states. Thus, when this parameter is much larger than unity, the coupler becomes qubit-like and the excitation energy decreases rapidly, and thus cannot be considered as a passive mediator anymore because the coupler will be excited to its higher energy states. Furthermore, the tunability of the coupler is negatively affected by a larger β. Figure 3.2 compares the current expectation values for couplers with $\beta \approx 1$ and couplers with larger β. It is clear from figure 3.2 that large β "inearizes" the current-flux relation and affects tunability negatively. This makes turning off the interaction ($J_{12} = 0$) impossible for large β (the point of zero slope of the current-flux relation vanishes). This

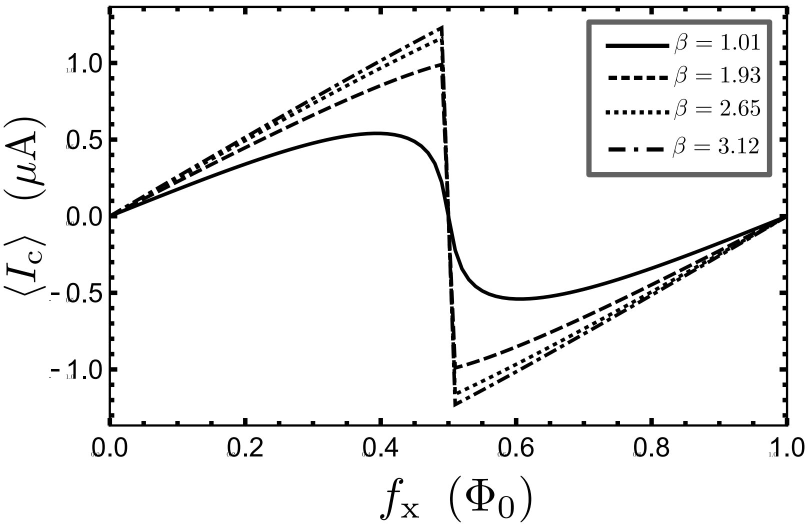

Figure 3.2: The expectation value of the circulating current in the loop of an RF-SQUID coupler with respect to the external flux threading its loop with $E_L = 467.0$ GHz and $E_C = 18.4$ GHz, at various values of the Josephson energy or β.

point makes the coupler very sensitive to fabrication variations in the junction size (the junction size controls the critical current), if one wants to have optimal tunability. The operating regime typically used to get strong mediated interactions while having no or very small by-stability is $1 \gtrsim \beta$. Figure 3.3 shows the potential energy of an rf-SQUID in this ideal regime of $\beta \approx 1$, that is of quartic shape (we can see the beginning of a double well shape). This shape of potential gives rise to appreciable quantum fluctuations in the phase degree of freedom [113] which contribute to the coupling. Experimental demonstration of this circuit as a two-qubit coupler has been made in the monostable regime of $\beta < 1$ [28] and in the quartic regime or the regime of small bi-stability where $\beta \approx 1$ [51].

3.2.2 Split-Junction rf-SQUID Coupler

We have seen that the rf-SQUID circuit can be used as a tunable coupler. Next, we will introduce a slight modification to the rf-SQUID circuit to improve the coupling properties. This circuit is shown in figure 3.4 and is typically called a split-junction rf-SQUID, tunable rf-SQUID [113] or compound-Josephson-junction rf-SQUID [109]. This modification can

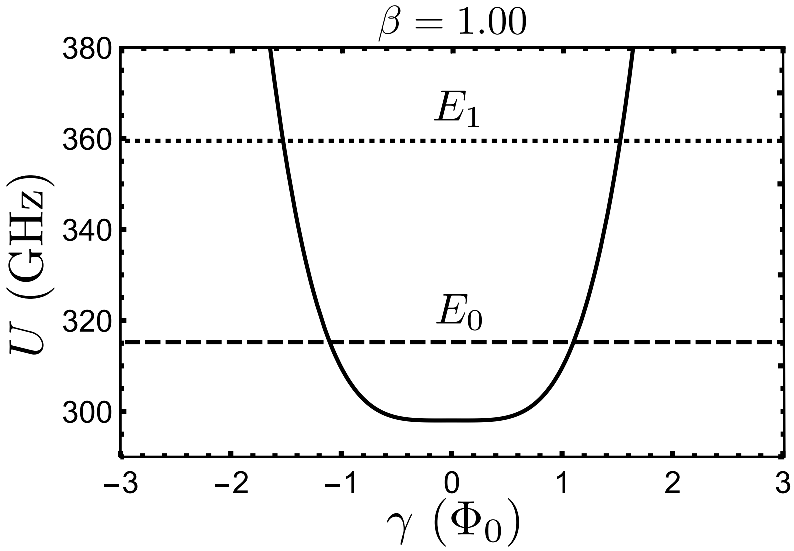

Figure 3.3: The potential energy of an RF-SQUID with respect to the superconducting phase with $E_{\mathrm{L}} = 297.2$ GHz and $E_{\mathrm{C}} = 38.7$ GHz and $f_x = 0.5$.

be understood as simply replacing the single junction in the rf-SQUID by a DC-SQUID[2], which we have determined to act as a tunable junction. Thus, this circuit is simply an rf-SQUID with a tunable critical current.

If we consider a symmetric DC-SQUID with negligible self inductance replacing the single junction in the rf-SQUID, we have the flux threading the main loop and the top part of the secondary loop

$$\Phi_{\mathrm{ms1}} = I_{\mathrm{m}} L_{\mathrm{m}} + \Phi_{\mathrm{x\,m}} + \Phi_{\mathrm{x\,s}} \tag{3.24}$$

and the flux threading the main loop and the bottom part of the secondary loop

$$\Phi_{\mathrm{ms2}} = I_{\mathrm{m}} L_{\mathrm{m}} + \Phi_{\mathrm{x\,m}} \tag{3.25}$$

with I_{m} the circulating current in the main loop and $\Phi_{\mathrm{x\,m}}$ ($\Phi_{\mathrm{x\,s}}$) the external flux in the main (secondary DC-SQUID loop) loop and L_{m} is the total inductance of the main loop; the subscripts identifying the loops are defined as “m” for the main loop and “s” for the secondary loop.

---

[2] It is interesting to note here that the DC-SQUID itself can act as a tunable inductive 2-qubit coupler, see [103, 105, 114] for details.

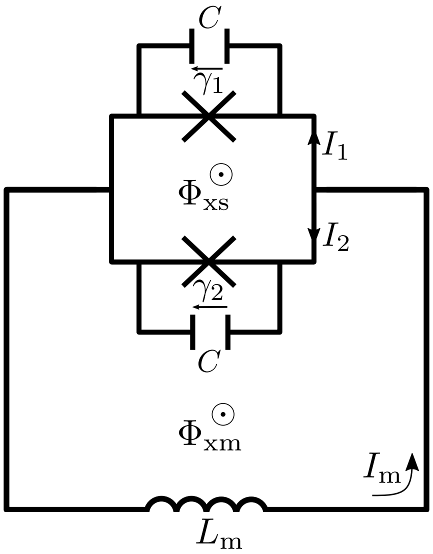

Figure 3.4: Compound-junction RF-SQUID coupler circuit representation. The current, junction phases and bias flux positive directions are indicated.

The fluxoid quantization along the main loop and the top part of the secondary loop imposes

$$\begin{aligned} \gamma_1 &= -2\,\pi \frac{\Phi_{\mathrm{ms1}}}{\Phi_0} \\ &= -\frac{I_{\mathrm{m}} L_{\mathrm{m}}}{\phi_0} - 2\,\pi f_{\mathrm{x\,m}} - 2\,\pi f_{\mathrm{x\,s}} \end{aligned} \tag{3.26}$$

while along the main loop and the bottom part of the secondary loop we have

$$\begin{aligned} \gamma_2 &= -2\,\pi \frac{\Phi_{\mathrm{ms2}}}{\Phi_0} \\ &= -\frac{I_{\mathrm{m}} L_{\mathrm{m}}}{\phi_0} - 2\,\pi f_{\mathrm{x\,m}}. \end{aligned} \tag{3.27}$$

From these fluxoid quantization conditions, we can eliminate a degree of freedom from the problem because $\gamma_2 = \gamma_1 + 2\pi f_{\mathrm{x\,s}}$.

Thus, we finally have that the equation of motion for the circuit is

$$\begin{aligned} -\frac{\phi_0}{L_{\mathrm{m}}} \left[\gamma_1 + 2\,\pi \left(f_{\mathrm{x\,s}} + f_{\mathrm{x\,m}}\right)\right] &= I_{\mathrm{m}} \\ &= 2\left[I_{\mathrm{c}} \cos\left(\pi f_{\mathrm{x\,s}}\right) \sin\left(\gamma_1 + \pi f_{\mathrm{x}\,s}\right) + C\,\phi_0\,\ddot{\gamma}_1\right] \end{aligned} \tag{3.28}$$

where we used the current flowing through the DC-SQUID in Eq. (2.35) for the circulating current in the main loop I_{m}.

After a few manipulations, the Hamiltonian can then be written as

$$\hat{H}_{\mathrm{cjj}} \approx \frac{E_{\mathrm{C}}}{\hbar^2}\,\hat{p}_1^2 - 2E_{\mathrm{J}}\cos\left(\pi f_{\mathrm{x\,s}}\right)\,\cos\left(\hat{\gamma}_1 + \pi f_{\mathrm{x\,s}}\right) + \frac{E_{\mathrm{L}}}{2}\left[\hat{\gamma}_1 + 2\pi\left(f_{\mathrm{x\,s}} + f_{\mathrm{x\,m}}\right)\right]^2, \tag{3.29}$$

with $E_{\mathrm{L}} = \frac{\phi_0^2}{L_{\mathrm{m}}}$ the inductive energy and $E_{\mathrm{J}} = \phi_0\, I_{\mathrm{c}}$ the base Josephson energy.

We can now discuss the behavior of this circuit as a 2-qubit coupler, as discussed above for the single-junction rf-SQUID. Following the steps outlined above to determine the effective coupling mediated by the rf-SQUID for the circuit in figure 3.4, we find a similar expression for the compound-junction coupler with an additional parameter dependence, the external flux threading the small loop[3]. The mediated interactions will depend on the following

$$L_{\mathrm{eff}}^{-1} \equiv \frac{1}{\phi_0^2}\,\frac{\mathrm{d}^2}{\mathrm{d}f_{\mathrm{x\,2m}}^2} E_{\mathrm{c}}^{(0)}\left(f_{\mathrm{x\,2m}},\, f_{\mathrm{x\,2s}}\right) \tag{3.30}$$

and

$$\left\langle \hat{I}_{\mathrm{c}} \right\rangle \equiv \frac{1}{\phi_0}\,\frac{\mathrm{d}}{\mathrm{d}f_{\mathrm{x\,2m}}} E_{\mathrm{c}}^{(0)}\left(f_{\mathrm{x\,2m}},\, f_{\mathrm{x\,2s}}\right), \tag{3.31}$$

where $E_{\mathrm{c}}^{(0)}\left(f_{\mathrm{x\,2m}},\, f_{\mathrm{x\,2s}}\right)$ is the ground-state energy of the coupler circuit in figure 3.4, dependent on the external frustration in the two loops of the coupler circuit $f_{\mathrm{x\,2m}}$ and $f_{\mathrm{x\,2s}}$.

The additional control parameter makes it possible to operate the coupler in such a way that the expectation value of the current circulating in the large loop is zero (at $f_{\mathrm{x\,2m}} = 0$ and at $f_{\mathrm{x\,2m}} = 0.5$) as in figure 3.2.2. This minimizes the cross-talk effect of the coupler offset flux into the qubits due to terms proportional to (3.31). Furthermore, the coupling strength mediated by this coupler is tunable in sign and magnitude by threading flux into the small loop and keeping the flux in the large loop at one of the two points mentioned above, see figure 3.2.2 where we see the slope of the current-flux trace change sign and go through zero at the $f_{\mathrm{x\,2m}} = 0.5$ flux point. Additionally, due to the control over the critical current in this circuit, this coupler can cancel its mediated interaction (coupling strength cannot be tuned to zero) when $\beta > 1$ by changing the flux in the small DC-SQUID loop. This point makes this circuit robust to fabrication variations in the junction sizes (the junction size controls the critical current of the junction)[105].

---

[3] We do not, however, take the perturbative expansion with respect to this additional parameter. The perturbative expansion is done with respect to the qubit offset fluxes threading the large loop.

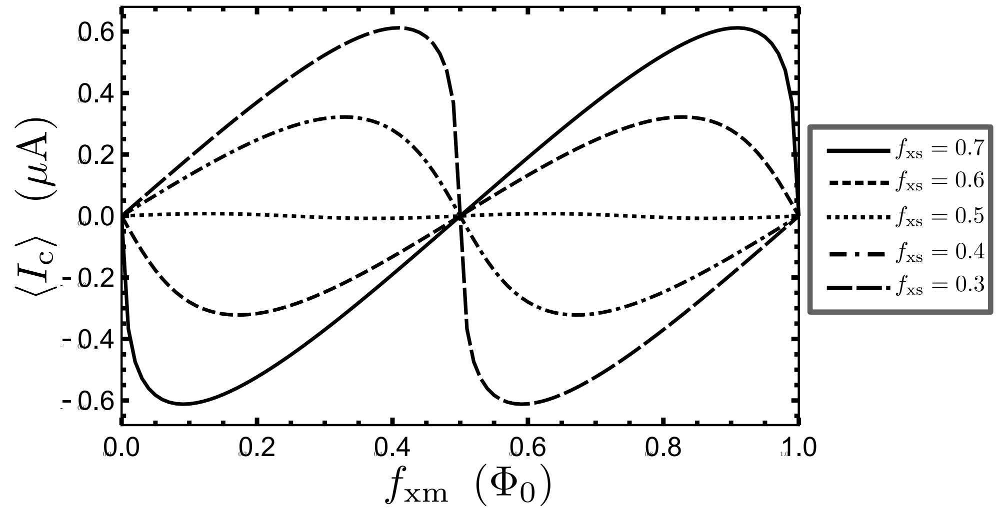

Figure 3.5: The expectation value of the circulating current in the loop of a compound-junction RF-SQUID-type coupler with respect to the external flux threading its large loop, at various values of the external flux threading its small loop. The parameters of the SQUID are $E_{\rm L} = 467.0$ GHz, $E_{\rm J} = 208.6$ GHz and $E_{\rm C} = 18.4$ GHz; the change in the flux in the small loop effectively changes the non-linearity parameter β.

3.3 Born-Oppenheimer Inversion Method for Extracting Coupling Strength

The derivation of the effective Hamiltonian of a coupler circuit can be simplified further and generalized. To achieve this, we approximate the qubits as a classical spin. In this case, the circulating current operator of the qubits becomes

$$\hat{I}_{{\rm cir}\,i} \approx |I_{\rm p}|\,\hat{\sigma}_{{\rm z}\,i}\,, \tag{3.32}$$

with $|I_{\rm p}|$ the persistent current of the qubit.

This simplification means that in the expansion (3.18), the terms proportional to even powers of $\hat{I}_{{\rm cir}\,i}$ will simplify to identity, while the odd powers will simplify to single qubit or 2-qubit coupling terms. We are thus left with an expansion of the form

$$\hat{E}_{\rm c}^{(0)}\left(\hat{f}_{\rm c}\right) = E_0\,\hat{\mathbf{I}} + h_1\,\hat{\sigma}_{{\rm z}\,1} + h_2\,\hat{\sigma}_{{\rm z}\,2} + J_{12}\,\hat{\sigma}_{{\rm z}\,1}\hat{\sigma}_{{\rm z}\,2}\,, \tag{3.33}$$

where E_0, h_i and J_{12} are the energy offset, the energy bias and the 2-qubit coupling strength, respectively, mediated by the coupler circuit.

This simple formula can be used to numerically determine the coupling coefficients in a computationally efficient manner. We take the qubit-dependent coupler Hamiltonian and replace the qubit operators by the eigenvalues of the operator (3.32), that is $(-1)\,|I_{\mathrm{p}\,i}|$ or $(1)\,|I_{\mathrm{p}\,i}|$. By mapping the ground state energy of the coupler Hamiltonian for all 4 spin configurations to the coupling coefficients, one has

$$\begin{bmatrix} E_{\mathrm{c}}^{(0)}(\ \ 1,\ \ \ 1) \\ E_{\mathrm{c}}^{(0)}(\ \ 1,-1) \\ E_{\mathrm{c}}^{(0)}(-1,\ \ \ 1) \\ E_{\mathrm{c}}^{(0)}(-1,-1) \end{bmatrix} = \mathcal{S} \begin{bmatrix} E_0 \\ h_1 \\ h_2 \\ J_{1\,2} \end{bmatrix} \tag{3.34}$$

with[4]

$$\mathcal{S} = [1, i, j, i\,j\,] \rightarrow \begin{bmatrix} \{i = \ \ 1,\, j = \ \ 1\} \\ \{i = -1,\, j = \ \ 1\} \\ \{i = \ \ 1,\, j = -1\} \\ \{i = -1,\, j = -1\} \end{bmatrix} \tag{3.35}$$

$$= \begin{bmatrix} 1 & 1 & 1 & 1 \\ 1 & -1 & 1 & -1 \\ 1 & 1 & -1 & -1 \\ 1 & -1 & -1 & 1 \end{bmatrix}. \tag{3.36}$$

The coupling coefficients are found by inverting the set of equations (3.34). We note that this method to extract the coupling coefficients is different than the on used in Ref. [115], where they analyze the spectrum of the full qubit subspace instead of the coupler ground state. Our method is a numerically efficient way to extract the coupling strength of complex qubit-coupler circuits, without the need to diagonalize the entire coupled system.

The 2-qubit coupling strength mediated by a compound-junction rf-SQUID coupler, extracted by the inversion method just described, is displayed in figure 3.3. In figure 3.3, we see the sign and magnitude tunability of the coupling strength while changing both fluxes in the coupler.

To summarize, the derivation of the effective mediated interactions by using the BO approximation can be simplified to the following steps:

- Write the qubit-dependent coupler Hamiltonian while keeping the qubit Hamiltonian bare.

---

[4] We note in passing that matrix (3.35) is the 4 × 4 Hadamard matrix [115].

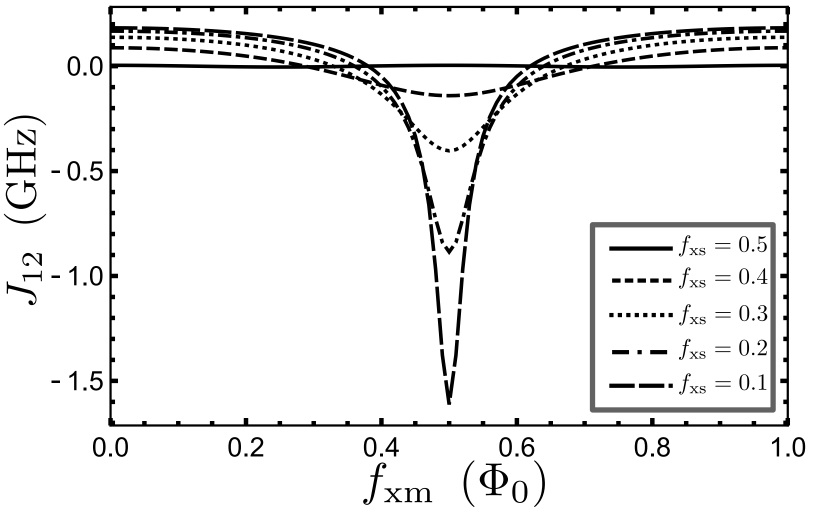

Figure 3.6: The 2-qubit coupling strength mediated by a compound-junction RF-SQUID coupler, with $E_{\mathrm{L}} = 467.0$ GHz, $E_{\mathrm{J}} = 208.6$ GHz and $E_{\mathrm{C}} = 18.4$ GHz, versus the flux threading the large loop, at various values of the flux threading the small loop.

- Take the Born-Oppenheimer approximation and assume that the coupler stays in the ground state. Replace the qubit-dependent coupler Hamiltonian by its ground state energy.
- Numerically diagonalize the qubit-dependent coupler Hamiltonian by treating the qubit operators as binary offset flux parameters.
- Map the ground state energy of the coupler Hamiltonian for all qubit offset flux configurations to the coupling coefficients.
- Solve the set of equations to determine the coupling coefficients.

This general method can be adapted to extract the coupling strength of any coupler circuit, for which the interaction is diagonal in the computational basis, that can be described by the Born-Oppenheimer approximation, and for which the effect of the qubits on the coupler can be approximated by binary variables. That is, the coupler must have an excitation energy much larger than that of the qubits and the qubit spectrum must be sufficiently anharmonic to justify the definition of two well-defined computational states corresponding to the circulating current. This method could also be expanded to charge qubits, but this is beyond the scope of this thesis.

Chapter 4

Three-body Inductive Coupler for Quantum Annealing

The mediated interactions that we investigated in the last chapter were all two-body interactions. However, many-body interactions can arise as mediated interactions from fundamental two-body couplings in various physical systems [116, 117]. As mentioned in the introductory chapter, in quantum information, many-body interactions are relevant for quantum error correction [39, 40], complexity theory [118], quantum thermodynamics [119], quantum chemistry [120], and quantum simulations [41, 42]. The implementation of suitable high-order many-body interactions for quantum information comes with unique challenges, due to the fact that these interactions have to be of comparable strength with and controlled independently from lower-order interactions.

The implementation of many-body interactions has been considered in various physical systems for quantum information including ion traps [121], atoms in optical lattices [122, 123], and cold polar molecules [124]. In superconducting circuits, high-order effective interactions between qubits can be made strong, due to the fact that the underlying two-body interactions are strong. High-order interactions have been analyzed for several types of superconducting qubits and coupler circuits [125, 108, 126, 127]. Recently, there has been increased interest in many-qubit couplers for quantum annealers based on superconducting qubits. Proposals for engineered couplers for superconducting qubits suitable for quantum annealing include a three-body coupler circuit based on galvanic coupling [128] and four-body coupler circuits based on a single-loop interferometer device [57] or a more complex circuit with a symmetric susceptibility used to cancel effectively lower-order interactions [129]. Other proposals rely on the use of ancilla qubits to reproduce the low-energy spectrum of many-body interactions, in the regime where the qubits have a

Hamiltonian with negligible transverse terms in the basis of the interaction [43]. However, designing circuits that implement many-body interactions and have other desirable features, including large tunable interaction strength, independence of the biasing conditions for the coupled qubits, cancellation of lower-order interactions, low design complexity, and robustness to noise and parameter variations, is a challenging problem.

We propose and analyze a superconducting quantum circuit used to implement a three-body interaction between three superconducting flux qubits. Flux-type qubits are promising candidates for both quantum annealing [29, 51] and gate-based quantum computing [74]. The three-body coupler design that we propose is a relatively low-complexity circuit that combines strong tunable interactions of the order of 1 GHz, comparable to the qubit energy scales, effective cancellation of two-body terms, and robustness to noise and parameter variations.

4.1 Coupling circuit

Our proposed coupler device consists of two superconducting Josephson circuits, labeled "c1" and "c2" (see Fig. 4.1). Each of these circuits has a main superconducting loop, interrupted by two Josephson junctions, which form a secondary loop. This circuit is referred to in other contexts as a tunable rf-SQUID [113] or a compound Josephson junction rf-SQUID [109]. The tunable rf-SQUID has the important property that the susceptibility, which is the relative change in current in the main loop due to a change in flux, can be controlled, in both sign and magnitude, by the magnetic fluxes applied to its two loops. In chapter 3, we analyzed the properties of this circuit as a two-qubit tunable coupler and have seen that it can be operated either in the monostable [105, 28] or quantum bistable (where the quantum fluctuations from tunneling through a small barrier in a quartic potential) [51] regimes, while mediating a tunable interaction between two flux qubits.

To achieve a strong three-body interaction, we employ the tunable rf-SQUID in the following way. We make the interaction between two qubits, each coupled to the rf-SQUID main loop, dependent on the state of a third qubit, coupled to the secondary loop, thereby generating an effective three-qubit interaction. However, in this coupler circuit based on only one tunable rf-SQUID, two-body interactions cannot be canceled or generally controlled independently from three-body interactions. To cancel the two-body interactions between qubits 1 and 2, we combine two rf-SQUIDs (circuits "c1" and "c2" in Fig. 4.1) in such a way that the sign of the flux coming from "q1" in the main loop of "c1" is of opposite sign from the one in "c2", by adding a twist in the main loop of "c2". To cancel the two-body interactions between qubits 1 and 3, and 2 and 3, we bias "c1" and "c2"

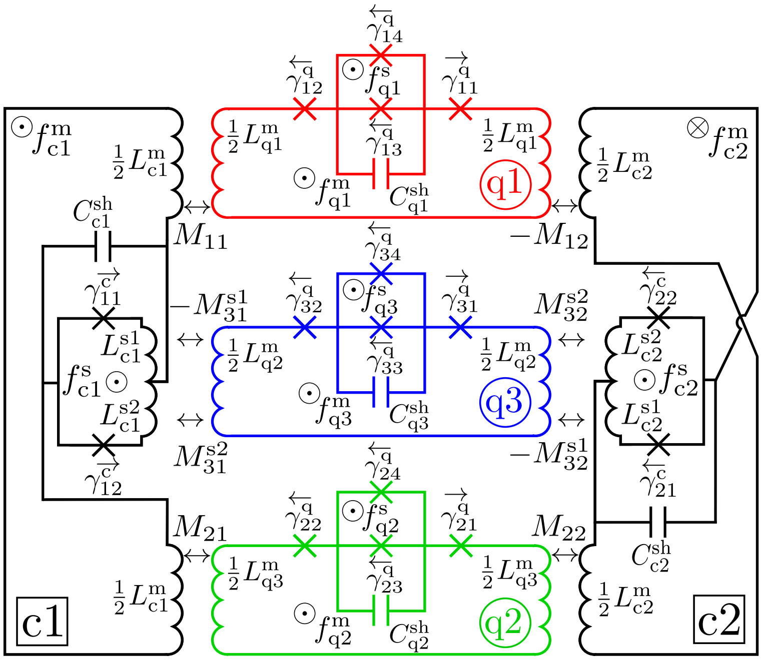

Figure 4.1: Circuit schematic of the coupler - qubits system. The two tunable rf-SQUID circuits forming the coupler ("c1" and "c2") are coupled to the three tunable capacitively shunted flux qubits ("q1", "q2", and "q3") by mutual inductances. Each loop of these circuits is subjected to a flux bias, as indicated. Josephson junctions are indicated by crosses; arrows indicate the orientation of the relative phase. Capacitances and inductances of the secondary loops of the qubits are not shown. See text for additional details.

at their main loop symmetry point, where the susceptibility to flux in the secondary loop is suppressed. Thus, the sum of the two-body interactions vanishes due to symmetry of the coupling and susceptibilities, with the susceptibilities controlled by the flux biasing conditions.

We next consider the full circuit representation of the coupler device and the qubits. In what follows, we consider the case of a tunable rf-SQUID with significant inductance in the secondary loop, as opposed to the treatment in the last chapter. Additionally, we assume a symmetrical tunable rf-SQUID circuit, this means that both Josephson junctions are identical, both branches of the secondary loop are identical. Finally, we consider the case of a non-negligible shunting capacitance across the terminals of the secondary loop coming from realistic stray capacitance between the long wires of the device (see appendix B.1 for derivation of un-shunted case, for symmetric and asymmetric parameters).

For the qubit circuit, we use capacitively shunted flux qubits (CSFQ) [74], which are considered in recent efforts related to coherent quantum annealing [51]. However, the analysis applies straightforwardly to other flux qubit variants. Quantizing the qubit circuit in Fig.4.1, we find that the Hamiltonian of the tunable capacitively shunted flux qubit is

$$H_{\mathrm{q}i} = T_{\mathrm{q}\,i}\left(\{p^{\mathrm{q}}_{i\,k}\}_{k\in\left\{\overline{1,5}\right\}}\right) + U^{\mathrm{J}}_{\mathrm{q}\,i}\left(\{\gamma^{\mathrm{q}}_{i\,k}\}_{k\in\left\{\overline{1,5}\right\}}\right) + U^{\mathrm{L}}_{\mathrm{q}\,i}\left(\{\gamma^{\mathrm{q}}_{i\,k}\}_{k\in\left\{\overline{1,5}\right\}}\right), \tag{4.1}$$

where $\gamma^{\mathrm{q}}_{i\,k}$ and for $k \in \left\{\overline{1,5}\right\}$ are the phase degrees of freedom. These represent the phase across junction k for $k \in \left\{\overline{1,4}\right\}$ and the phase across the main loop inductance of the qubit for $k = 5$. The conjugate momenta to these degrees of freedom are the $p^{\mathrm{q}}_{i\,k}$ for $k \in \left\{\overline{1,5}\right\}$. The kinetic energy in the qubit is

$$T_{\mathrm{q}\,i}\left(\{p^{\mathrm{q}}_{i\,k}\}_{k\in\left\{\overline{1,5}\right\}}\right) = \frac{1}{2\phi_0^2\,\alpha C_{\mathrm{q}}}\,\mathbf{p}_i^{\mathrm{q}\mathrm{T}}\,\mathbf{C}_{\mathrm{q}}^{-1}\,\mathbf{p}_i^{\mathrm{q}}, \tag{4.2}$$

where $\mathbf{p}_i^{\mathrm{q}\mathrm{T}} = [p^{\mathrm{q}}_{i\,1},\, p^{\mathrm{q}}_{i\,2},\, p^{\mathrm{q}}_{i\,3},\, p^{\mathrm{q}}_{i\,4},\, p^{\mathrm{q}}_{i\,5}]$ and where $\mathbf{C}_{\mathrm{q}}$ is the capacitance matrix for the qubit, written as

$$\mathbf{C}_{\mathrm{q}} = \begin{bmatrix} \frac{1}{\alpha} & 0 & 0 & 0 & 0 \\ 0 & \frac{1}{\alpha} & 0 & 0 & 0 \\ 0 & 0 & 1+\frac{C^{\mathrm{sh}}_{\mathrm{q}}}{\alpha C_{\mathrm{q}}} & 0 & \frac{C^{\mathrm{sh}}_{\mathrm{q}}}{\alpha C_{\mathrm{q}}} \\ 0 & 0 & 0 & 1 & 0 \\ 0 & 0 & \frac{C^{\mathrm{sh}}_{\mathrm{q}}}{\alpha C_{\mathrm{q}}} & 0 & \frac{C^{\mathrm{sh}}_{\mathrm{q}}}{\alpha C_{\mathrm{q}}}. \end{bmatrix} \tag{4.3}$$

In Eqs. (4.2) and (4.3), C_{q} is the junction capacitance of the two large junctions (1 and 2 in this case), $\alpha < 1$ is the dimensionless ratio of the junction areas of the small (junctions 3 and 4 in this case) and large junctions and $C^{\mathrm{sh}}_{\mathrm{q}}$ is the shunting capacitance of the qubits. The Josephson potential energy is

$$U^{\mathrm{J}}_{\mathrm{q}\,i}\left(\{\gamma^{\mathrm{q}}_{i\,k}\}_{k\in\left\{\overline{1,5}\right\}}\right) = -\phi_0 I^{\mathrm{J}}_{\mathrm{q}}\left(\cos\gamma^{\mathrm{q}}_{i\,1} + \cos\gamma^{\mathrm{q}}_{i\,2} + \alpha\cos\gamma^{\mathrm{q}}_{i\,3} + \alpha\cos\gamma^{\mathrm{q}}_{i\,4}\right), \tag{4.4}$$

where $I^{\mathrm{J}}_{\mathrm{q}}$ is the critical current of the large junctions of the qubit (junction 1 and 2). The inductive potential energy is

$$U^{\mathrm{L}}_{\mathrm{q}\,i}\left(\{\gamma^{\mathrm{q}}_{i\,k}\}_{k\in\left\{\overline{1,5}\right\}}\right) = \frac{\phi_0^2}{2L^{\mathrm{s}}_{\mathrm{q}}}\,\boldsymbol{\gamma}_i^{\mathrm{q}\mathrm{T}}\,\mathbf{L}_{\mathrm{q}}^{-1}\,\boldsymbol{\gamma}_i^{\mathrm{q}}, \tag{4.5}$$

where

$$\mathbf{L}_{\mathrm{q}} = \begin{bmatrix} \frac{L^{\mathrm{m}}_{\mathrm{q}}}{L^{\mathrm{s}}_{\mathrm{q}}} & 0 & 0 \\ 0 & \frac{1}{2} & 0 \\ 0 & 0 & \frac{1}{2} \end{bmatrix}, \tag{4.6}$$

is the inductive matrix of the qubits, with $L_{\mathrm{q}}^{\mathrm{m}}$ the main loop inductance and $L_{\mathrm{q}}^{\mathrm{s}} = L_{\mathrm{q}}^{\mathrm{s1}} + L_{\mathrm{q}}^{\mathrm{s2}}$ is the secondary loop inductance, with $L_{\mathrm{q}}^{\mathrm{s1}} = L_{\mathrm{q}}^{\mathrm{s2}} = L_{\mathrm{q}}^{\mathrm{s}}/2$ the inductance of each branch of the secondary loop. Finally,

$$\boldsymbol{\gamma}_i^{\mathrm{q}} = \begin{bmatrix} \gamma_{i\,5}^{\mathrm{q}} \\ \gamma_{i\,1}^{\mathrm{q}} - \gamma_{i\,2}^{\mathrm{q}} - \gamma_{i\,4}^{\mathrm{q}} - \gamma_{i\,5}^{\mathrm{q}} - 2\pi f_{\mathrm{q}\,i}^{\mathrm{m}} - \pi f_{\mathrm{q}\,i}^{\mathrm{s}} \\ \gamma_{i\,1}^{\mathrm{q}} - \gamma_{i\,2}^{\mathrm{q}} - \gamma_{i\,3}^{\mathrm{q}} - \gamma_{i\,5}^{\mathrm{q}} - 2\pi f_{\mathrm{q}\,i}^{\mathrm{m}} + \pi f_{\mathrm{q}\,i}^{\mathrm{s}} \end{bmatrix}, \tag{4.7}$$

is the vector of phases across each inductance of the circuit, after accounting for the fluxoid quantization conditions, with, $f_{\mathrm{q}i}^{\mathrm{m}}$ and $f_{\mathrm{q}i}^{\mathrm{s}}$ the external flux biases in the main and the secondary loop, respectively.

From the quantization of the coupler circuit in Fig. 4.1, we readily find that the Hamiltonian of the symmetric tunable-rf-SQUID with capacitive shunting is

$$H_{\mathrm{c}i} = T_{\mathrm{c}i}\left(p_{i1}^{\mathrm{c}}, p_{i2}^{\mathrm{c}}, p_{i3}^{\mathrm{c}}\right) + U_{\mathrm{c}i}^{\mathrm{J}}\left(\gamma_{i1}^{\mathrm{c}}, \gamma_{i2}^{\mathrm{c}}\right) + U_{\mathrm{c}i}^{\mathrm{L}}\left(\gamma_{i1}^{\mathrm{c}}, \gamma_{i2}^{\mathrm{c}}, \gamma_{i3}^{\mathrm{c}}\right), \tag{4.8}$$

where the degrees of freedom are the γ_{ij}^{c} for $j \in \{1, 2, 3\}$ representing the phase across junction j for $j \in \{1, 2\}$ and the phase across the main loop inductance for $j = 3$. The p_{ij}^{c} represent the canonical conjugate momenta to the degrees of freedom γ_{ij}^{c} for $j \in \{1, 2, 3\}$. In Eq. (4.8), the kinetic energy is

$$T_{\mathrm{c}\,i}\left(p_{i1}^{\mathrm{c}}, p_{i2}^{\mathrm{c}}, p_{i3}^{\mathrm{c}}\right) = \frac{1}{2\phi_0^2\, C_{\mathrm{c}}}\, \mathbf{p}_i^{\mathrm{c}\mathrm{T}}\, \mathbf{C}_{\mathrm{c}}^{-1}\, \mathbf{p}_i^{\mathrm{c}}, \tag{4.9}$$

where $\mathbf{p}_i^{\mathrm{c}\mathrm{T}} = [p_{i\,1}^{\mathrm{c}},\ p_{i\,2}^{\mathrm{c}},\ p_{i\,3}^{\mathrm{c}}]$ and where $\mathbf{C}_{\mathrm{c}}$ is the capacitance matrix for the qubit, written as

$$\mathbf{C}_{\mathrm{c}} = \begin{bmatrix} 1 + \frac{C_{\mathrm{c}}^{\mathrm{sh}}}{C_{\mathrm{c}}} & 0 & \frac{C_{\mathrm{c}}^{\mathrm{sh}}}{C_{\mathrm{c}}} \\ 0 & 1 & 0 \\ \frac{C_{\mathrm{c}}^{\mathrm{sh}}}{C_{\mathrm{c}}} & 0 & \frac{C_{\mathrm{c}}^{\mathrm{sh}}}{C_{\mathrm{c}}}, \end{bmatrix} \tag{4.10}$$

with C_{c} the junction capacitance of the two coupler junctions and $C_{\mathrm{c}}^{\mathrm{sh}}$ is the shunting capacitance of the couplers. The Josephson potential is

$$U_{\mathrm{c}\,i}^{\mathrm{J}}\left(\gamma_{i1}^{\mathrm{c}}, \gamma_{i2}^{\mathrm{c}}\right) = -\phi_0 I_{\mathrm{c}}^{\mathrm{J}}\left(\cos\gamma_{i\,1}^{\mathrm{c}} + \cos\gamma_{i\,2}^{\mathrm{c}}\right), \tag{4.11}$$

where $I_{\mathrm{c}}^{\mathrm{J}}$ is the critical current of the junctions of the coupler. The inductive potential is

$$U_{\mathrm{c}\,i}^{\mathrm{L}}\left(\gamma_{i1}^{\mathrm{c}}, \gamma_{i2}^{\mathrm{c}}, \gamma_{i3}^{\mathrm{c}}\right) = \frac{\phi_0^2}{2L_{\mathrm{c}}^{\mathrm{s}}}\, \boldsymbol{\gamma}_i^{\mathrm{c}\mathrm{T}}\, \mathbf{L}_{\mathrm{c}}^{-1}\, \boldsymbol{\gamma}_i^{\mathrm{c}}, \tag{4.12}$$

where

$$\mathbf{L}_{\mathrm{c}} = \begin{bmatrix} \frac{L_{\mathrm{c}}^{\mathrm{m}}}{L_{\mathrm{c}}^{\mathrm{s}}} & 0 & 0 \\ 0 & \frac{1}{2} & 0 \\ 0 & 0 & \frac{1}{2} \end{bmatrix}, \tag{4.13}$$

is the inductive matrix of the couplers, with $L_{\mathrm{c}}^{\mathrm{m}}$ the main loop inductance and $L_{\mathrm{c}}^{\mathrm{s}} = L_{\mathrm{c}}^{\mathrm{s1}} + L_{\mathrm{c}}^{\mathrm{s2}}$ is the secondary loop inductance, with $L_{\mathrm{c}}^{\mathrm{s1}} = L_{\mathrm{c}}^{\mathrm{s2}} = L_{\mathrm{c}}^{\mathrm{s}}/2$ the inductance of each branch of the secondary loop. Finally,

$$\boldsymbol{\gamma}_i^{\mathrm{c}} = \begin{bmatrix} \gamma_{i\,3}^{\mathrm{q}} \\ -\gamma_{i\,1}^{\mathrm{c}} - \gamma_{i\,3}^{\mathrm{c}} - 2\pi f_{\mathrm{c}\,i}^{\mathrm{m}} + \pi f_{\mathrm{c}\,i}^{\mathrm{s}} \\ -\gamma_{i\,2}^{\mathrm{c}} - \gamma_{i\,3}^{\mathrm{c}} - 2\pi f_{\mathrm{c}\,i}^{\mathrm{m}} - \pi f_{\mathrm{c}\,i}^{\mathrm{s}} \end{bmatrix}, \tag{4.14}$$

is the vector of phases across each inductance of the circuit, after accounting for the fluxoid quantization conditions, with, $f_{\mathrm{c}\,i}^{\mathrm{m}}$ and $f_{\mathrm{c}\,i}^{\mathrm{s}}$ the external flux biases in the main and the secondary loop, respectively.

With this, the complete Hamiltonian of the qubits and coupler system is

$$H = \sum_{i=1}^{3} H_{\mathrm{q}\,i} + \sum_{j=1}^{2} H_{\mathrm{c}\,j} + H_{\mathrm{int}}, \tag{4.15}$$

where the inductive interaction Hamiltonian is

$$H_{\mathrm{int}} = \frac{\phi_0^2}{2L_{\mathrm{q}}^{\mathrm{s}}} \boldsymbol{\gamma}^{\mathrm{T}} \left(\mathbf{L}^{-1} - \mathbf{L}_0^{-1} \right) \boldsymbol{\gamma}, \tag{4.16}$$

where $\mathbf{L}$ is the full inductance matrix of the system, including all the mutual inductances, $\mathbf{L}_0$ is the inductance matrix of the uncoupled system and $\boldsymbol{\gamma}$ is a vector formed of the phases across all self-inductances in the system.

Finally, in what follows, we take identical qubits and identical rf-SQUIDs with the following values of the circuit parameters: for qubits i ($i \in \{1,2,3\}$), $I_{\mathrm{q}}^{\mathrm{J}} = 221.0$ nA and $C^{\mathrm{q}} = 4.5$ fF, $\alpha = 0.46$, $C_{\mathrm{q}i}^{\mathrm{sh}} = 40.0$ fF, $L_{\mathrm{q}\,i}^{\mathrm{m}} = 250.0$ pH, $L_{\mathrm{q}\,i}^{\mathrm{s1}} = L_{\mathrm{q}\,i}^{\mathrm{s2}} = 10.0$ pH, and for coupler j ($j \in \{1,2\}$) $I_{\mathrm{c}}^{\mathrm{J}} = 600.0$ nA and $C^{\mathrm{c}} = 12.0$ fF, $C_{\mathrm{c}j}^{\mathrm{sh}} = 10.0$ fF, $L_{\mathrm{c}\,i}^{\mathrm{m}} = 550.0$ pH, $L_{\mathrm{c}\,i}^{\mathrm{s1}} = L_{\mathrm{c}\,i}^{\mathrm{s2}} = 85.0$ pH, and mutual inductances of $M_{i\,j} = -50.0$ pH for $i, j \in \{1,2\}$ and $M_{3\,j}^{\mathrm{s1}} = M_{3\,j}^{\mathrm{s2}} = -25.0$ pH for $j \in \{1,2\}$.

4.2 Born-Oppenheimer approximation analysis

We first discuss the properties of the coupler using the Born-Oppenheimer approximation, which validates the intuitive picture for the three-body coupler based on rf-SQUID susceptibility. Since the tunable rf-SQUID circuits are designed to have a significantly larger energy gap between the ground and excited states (typical gap of 15 GHz) than the qubits (typical gap of 4 GHz), it is reasonable to apply the Born-Oppenheimer approximation [111, 105, 108]. This is done by replacing H with the effective qubit Hamiltonian

$$H_{\mathrm{eff}} \approx \sum_{i=1}^{3} H_{\mathrm{q}\,i} + \widetilde{E}_{\mathrm{c}}^{(0)}\left(\left\{f_{\mathrm{c}\,j}^{\beta} + \delta f_{\mathrm{q}}^{\beta}\right\}_{\substack{\beta\in\{\mathrm{m,s}\}\\ j\in\{1,2\}}}\right), \tag{4.17}$$

where $\widetilde{E}_{\mathrm{c}}^{(0)}$ is the quantum ground state energy of

$$\widetilde{H}_{\mathrm{c}} = \sum_{j=1}^{2} H_{\mathrm{c}\,j} + H_{\mathrm{int}}. \tag{4.18}$$

Here, $\widetilde{E}_{\mathrm{c}}^{(0)}$ is an operator, dependent on the effective qubit flux shifts $\delta f_{\mathrm{q}}^{\mathrm{m}} = \sum_{i=1}^{2} I_i\, M_{i\,j}$ and $\delta f_{\mathrm{q}}^{\mathrm{s}} = I_3\, M_{3\,j}$, with $I_i = \varphi_{\mathrm{q}\,i}^{\mathrm{m}}/L_{\mathrm{q}\,i}^{\mathrm{m}}\,\phi_0$ the circulating current operator of qubit i, $L_{\mathrm{q}\,i}^{\mathrm{m}}$ the self-inductance of the main loop of qubit i and $M_{i\,j}$ the mutual inductance between qubit i and coupler j, for $j \in \{1, 2\}$.

The analysis of the Born-Oppenheimer approximation is simplified if we project $\widetilde{E}_{\mathrm{c}}^{(0)}$ onto the subspace formed by the two lowest energy states of each qubit, which is appropriate because of the large anharmonicity in the spectrum of the CSFQ [74, 51]. The state of each qubit i is represented by the binary current variable $\widetilde{I}_i = I_{\mathrm{p}\,i}\, s_i$, where $s_i = \pm 1$ and $I_{\mathrm{p}\,i}$ is the persistent current of qubit i. The persistent current is the average of the magnitudes of the eigenvalues of the current operator represented in the basis of the two lowest energy states of each qubit. In terms of the binary qubit parameters, the energy is written as

$$\widetilde{E}_{\mathrm{c}}^{(0)}(s_1, s_2, s_3) = \widetilde{A}_0 + \sum_{i=1}^{3} \tilde{h}_i\, s_i + \sum_{\substack{i,\,j=1\\ i\neq j}}^{3} \widetilde{J}_{ij}\, s_i s_j + \widetilde{J}_{123}\, s_1 s_2 s_3, \tag{4.19}$$

where $\widetilde{A}_0$ is an energy offset, $\tilde{h}_i$ are single qubit biases arising from screening currents in the coupler, $\widetilde{J}_{ij}$ are two-body interactions, and $\widetilde{J}_{123}$ is the 3-local coupling strength. We determine these coefficients by solving the linear system of equations given by

$$\begin{bmatrix} \tilde{E}_{\mathrm{c}}^{(0)}(-1,-1,-1) \\ \tilde{E}_{\mathrm{c}}^{(0)}(-1,-1,\ \ 1) \\ \tilde{E}_{\mathrm{c}}^{(0)}(-1,\ \ 1,-1) \\ \tilde{E}_{\mathrm{c}}^{(0)}(-1,\ \ 1,\ \ 1) \\ \tilde{E}_{\mathrm{c}}^{(0)}(\ \ 1,-1,-1) \\ \tilde{E}_{\mathrm{c}}^{(0)}(\ \ 1,-1,\ \ 1) \\ \tilde{E}_{\mathrm{c}}^{(0)}(\ \ 1,\ \ 1,-1) \\ \tilde{E}_{\mathrm{c}}^{(0)}(\ \ 1,\ \ 1,\ \ 1) \end{bmatrix} = \mathcal{S} \begin{bmatrix} \tilde{A}_0 \\ \tilde{h}_1 \\ \tilde{h}_2 \\ \tilde{h}_3 \\ \tilde{J}_{1\,2} \\ \tilde{J}_{1\,3} \\ \tilde{J}_{2\,3} \\ \tilde{J}_{123} \end{bmatrix}, \tag{4.20}$$

with

$$\mathcal{S} = \begin{bmatrix} 1 & -1 & -1 & -1 & 1 & 1 & 1 & -1 \\ 1 & -1 & -1 & 1 & 1 & -1 & -1 & 1 \\ 1 & -1 & 1 & -1 & -1 & 1 & -1 & 1 \\ 1 & -1 & 1 & 1 & -1 & -1 & 1 & -1 \\ 1 & 1 & -1 & -1 & -1 & -1 & 1 & 1 \\ 1 & 1 & -1 & 1 & -1 & 1 & -1 & -1 \\ 1 & 1 & 1 & -1 & 1 & -1 & -1 & -1 \\ 1 & 1 & 1 & 1 & 1 & 1 & 1 & 1 \end{bmatrix}. \tag{4.21}$$

Coefficients $\tilde{A}_0$, $\tilde{h}_i$, $\tilde{J}_{ij}$, and $\tilde{J}_{123}$ are found by inverting the system of equations (4.20). To calculate $\widetilde{E}_{\mathrm{c}}^{(0)}(s_1, s_2, s_3)$ for each triplet of $s_i = \pm 1$, we numerically diagonalize $\widetilde{H}_{\mathrm{c}}$, using a representation in terms of the harmonic oscillator states for the quadratic part of the Hamiltonian.

The three-body coupling strength $\widetilde{J}_{123}$ is shown in Fig. 4.2 versus $f^{\mathrm{s}}_{\mathrm{c}\,1}$, with $f^{\mathrm{s}}_{\mathrm{c}\,1} = -f^{\mathrm{s}}_{\mathrm{c}\,2}$. With this biasing condition, all two-body terms cancel, in agreement with the qualitative picture presented above.

4.3 Spin model analysis

We discuss next a useful model for the coupler, in which each of the two tunable rf-SQUIDS is modeled as a two-level system (see Fig. 4.3). The two-level approximation is reasonable due to the large energy gap between the first and second excited states. This model, in which both qubits and the coupling circuits are treated as spins, allows to obtain

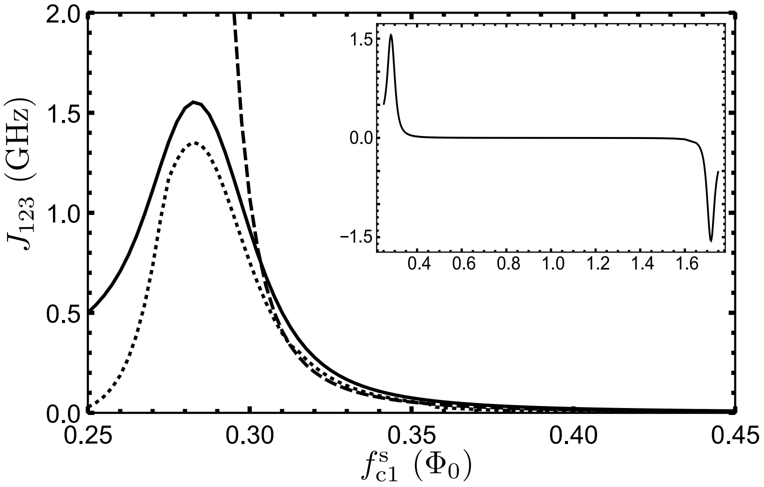

Figure 4.2: Three-body coupling strength extracted by Born-Oppenheimer method in the circuit model (solid line), perturbation theory in the spin model (dashed line), and numerical calculations of the full circuit (dotted line) versus the external magnetic flux threading loop $c1\,s$. The inset shows a wider scan of the magnetic flux, where the three-body coupling is extracted by the Born-Oppenheimer method only. The flux biases are $f^{\mathrm{m}}_{\mathrm{c}\,1} = f^{\mathrm{m}}_{\mathrm{c}\,2} = 1/2$, $f^{\mathrm{s}}_{\mathrm{c}\,1} = -f^{\mathrm{s}}_{\mathrm{c}\,2}$, $f^{\mathrm{m}}_{\mathrm{q}\,i} = 1/2$ and $f^{\mathrm{s}}_{\mathrm{q}\,i} = 0$ for $i \in \{1, 2, 3\}$.

perturbative analytical expressions for the effective mediated interactions, giving additional insight into the valid parameter range of the coupler and on the required conditions for cancellation of two-body interactions.

In this spin model, the full Hamiltonian is

$$\bar{H} = \bar{H}_{\mathrm{Q}} + \bar{H}_{\mathrm{C}} + \bar{H}_{\mathrm{int}}, \tag{4.22}$$

where

$$\bar{H}_{\mathrm{Q}} = \sum_{i=1}^{3} \left[\frac{\bar{\Delta}_{\mathrm{Q},i}}{2}\, \sigma^{x}_{\mathrm{Q},i} + \frac{\bar{\epsilon}_{\mathrm{Q},i}}{2}\, \sigma^{z}_{\mathrm{Q},i} \right], \tag{4.23}$$

$$\bar{H}_{\mathrm{C}} = \sum_{j=1}^{2} \left[\frac{\bar{\Delta}_{\mathrm{C},j}}{2}\, \sigma^{x}_{\mathrm{C},j} + \frac{\bar{\epsilon}_{\mathrm{C},j}}{2}\, \sigma^{z}_{\mathrm{C},j} \right] \tag{4.24}$$

and

$$\bar{H}_{\mathrm{int}} = \sum_{i=1}^{2} \sum_{j=1}^{2} \bar{J}_{i,\mathrm{C}j}\, \sigma^{z}_{\mathrm{Q},i}\, \sigma^{z}_{\mathrm{C},j} + \sum_{j=1}^{2} \bar{J}_{3,\mathrm{C}j}\, \sigma^{z}_{\mathrm{Q},3}\, \sigma^{x}_{\mathrm{C},j} \tag{4.25}$$

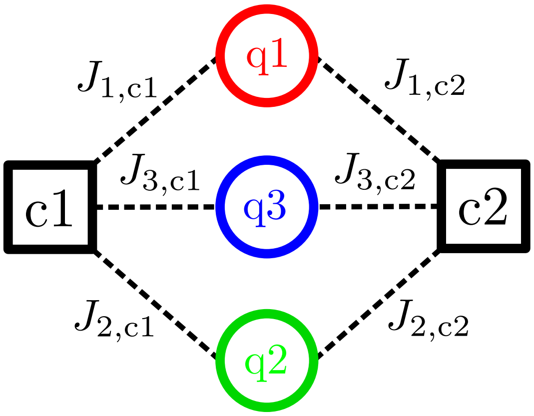

Figure 4.3: Spin-model schematic of the coupler plus qubits system. The circles and squares represent the qubit and coupler spins, respectively. The dashed lines represent bare two-body interactions.

are the Hamiltonians for the qubits, coupler, and the interaction between them, respectively. Note that we use capital letters Q and C to denote qubits and coupling circuits in the spin model and spin model parameters are differentiated from the rest by an over-bar. Here $\bar{\Delta}$ and $\bar{\epsilon}$ are the tunneling and bias of the respective device, and the coupling between the i^{th} qubit and the j^{th} coupler is denoted by $\bar{J}_{i,\mathrm{C}j} = M_{ij}\, I_{\mathrm{p}\,i}\, I_{\mathrm{p}\,j}$. We determine the relevant model parameters $\bar{\epsilon}_{\alpha i}$ and $\bar{\Delta}_{\alpha i}$ for $\alpha \in \{\mathrm{Q}, \mathrm{C}\}$, based on the properties of the lowest two energy eigenstates of each qubit/coupler unit.

To obtain the correspondence between the circuit parameters and the spin parameters, we numerically diagonalize the circuit Hamiltonian of each isolated qubit or coupler at each bias point. Then, we take the two lowest energy states as the spin subspace of each device.

The excitation energy at each bias point is defined as the difference between the ground state energy and the first excited state energy, written as

$$E^{01}_{\alpha\, i}\,(f^{\mathrm{m}}_{\alpha i},\, f^{\mathrm{s}}_{\alpha\, i}) = E^{1}_{\alpha\, i}\,(f^{\mathrm{m}}_{\alpha i},\, f^{\mathrm{s}}_{\alpha\, i}) - E^{0}_{\alpha\, i}\,(f^{\mathrm{m}}_{\alpha i},\, f^{\mathrm{s}}_{\alpha\, i})\,. \tag{4.26}$$

For any qubit or coupler, the energy bias spin parameter $\bar{\epsilon}_{\alpha\, i}$, is taken to be

$$\bar{\epsilon}_{\alpha\, i} = \sqrt{E^{01}_{\alpha\, i}\,(f^{\mathrm{m}}_{\alpha i},\, f^{\mathrm{s}}_{\alpha\, i})^2 - \bar{\Delta}_{\alpha\, i}\,(f^{\mathrm{m}}_{\alpha i},\, f^{\mathrm{s}}_{\alpha\, i})^2}. \tag{4.27}$$

For any qubit or coupler, the transverse field spin parameter $\bar{\Delta}_{\alpha\, i}$ is taken to be

$$\bar{\Delta}_{\alpha\, i} = E^{01}_{\alpha\, i}\,(f^{\mathrm{s}}_{\alpha\, i},\, 0.5)\,. \tag{4.28}$$

For any qubit - coupler pair, the direct 2-body interaction strength spin parameter $\bar{J}_{i\,\alpha\,j}$ is

$$\bar{J}_{i\,\alpha\,j} = M_{i\,\alpha\,j}\, I^{\mathrm{q}}_{\mathrm{p}\,i}\left(f^{\mathrm{m}}_{\mathrm{q}\,i},\, f^{\mathrm{s}}_{\mathrm{q}\,i}\right) I^{\mathrm{c}}_{\mathrm{p}\,j}\left(f^{\mathrm{m}}_{\mathrm{c}\,j},\, f^{\mathrm{s}}_{\mathrm{c}\,j}\right). \tag{4.29}$$

The persistent current in the devices, $I^{\alpha}_{\mathrm{p}\,i}$, is defined as

$$I^{\alpha}_{\mathrm{p}\,i} = \frac{1}{2}\left|I^{\alpha}_{0\,i}\left(f^{\mathrm{m}}_{\alpha\,i},\, f^{\mathrm{s}}_{\alpha\,i}\right)\right| + \left|I^{\alpha}_{1\,i}\left(f^{\mathrm{m}}_{\alpha\,i},\, f^{\mathrm{s}}_{\alpha\,i}\right)\right|, \tag{4.30}$$

where $I^{\alpha}_{n\,i}$ for $n \in \{0,\, 1\}$ are the eigenvalues of the current operator of the device in the energy basis of the ground and first excited states of the device.

The derivation of an effective Hamiltonian begins with the assumption of weak interaction; specifically, we assume $\langle 0|\, \bar{H}_{\mathrm{int}}\, |0\rangle_{\mathrm{c}} / \omega_{0,1} \ll 1$, where $\omega_{0,1}$ is the coupler excitation energy and $|0\rangle_{\mathrm{c}}$ represents the ground state of the coupler. The time evolution operator in the interaction picture is

$$\bar{U}(t,0) = T \exp\left[\frac{-\mathrm{i}}{\hbar}\int_0^t \bar{H}_{\mathrm{int}}\left(t'\right) \mathrm{d}t'\right], \tag{4.31}$$

where T specifies the time ordering. The effective coupling between the qubits can be found by projecting the full time evolution operator onto the ground state of the coupler, $|0\rangle_{\mathrm{c}}$. The effective propagator is given by

$$\begin{aligned}\bar{U}_{\mathrm{eff}}(t,0) &\equiv \langle 0|\, \bar{U}(t,0)\, |0\rangle_{\mathrm{c}} \\ &= T \exp\left[\frac{-\mathrm{i}}{\hbar}\int_0^t \bar{H}_{\mathrm{eff}}\left(t'\right) \mathrm{d}t'\right].\end{aligned} \tag{4.32}$$

The effective qubit Hamiltonian is found by expanding $\bar{U}_{\mathrm{eff}}(t,0)$ perturbatively up to third order [99].

$$\begin{aligned}\bar{H}_{\mathrm{eff}} \approx \sum_i \frac{1}{2}&\left[\left(\bar{\Delta}_{\mathrm{Q},i} + \bar{\Delta}'_{\mathrm{Q},i}\right)\sigma^x_{\mathrm{Q},i} + \left(\bar{\epsilon}_{\mathrm{Q},i} + \bar{\epsilon}'_{\mathrm{Q},i}\right)\sigma^z_{\mathrm{Q},i}\right] \\ &+ \bar{J}_{12}\,\sigma^z_{\mathrm{Q},1}\,\sigma^z_{\mathrm{Q},2} + \bar{J}_{13}\,\sigma^z_{\mathrm{Q},1}\,\sigma^z_{\mathrm{Q},3} + \bar{J}_{23}\,\sigma^z_{\mathrm{Q},2}\,\sigma^z_{\mathrm{Q},3} \\ &\quad + \bar{J}_{123}\,\sigma^z_{\mathrm{Q},1}\,\sigma^z_{\mathrm{Q},2}\,\sigma^z_{\mathrm{Q},3}.\end{aligned} \tag{4.33}$$

In Eq. (4.33),

$$\bar{\epsilon}'_{\mathrm{Q},1} = \sum_{j}^{2} \bar{J}_{1,\mathrm{C}j} \left\langle 0 \right| \sigma^z_{\mathrm{C},j} \left| 0 \right\rangle_{\mathrm{c}}, \tag{4.34}$$

$$\bar{\epsilon}'_{\mathrm{Q},2} = \sum_{j}^{2} \bar{J}_{2,\mathrm{C}j} \left\langle 0 \right| \sigma^z_{\mathrm{C},j} \left| 0 \right\rangle_{\mathrm{c}}, \tag{4.35}$$

$$\bar{\epsilon}'_{\mathrm{Q},3} = \sum_{j}^{2} \bar{J}_{3,\mathrm{C}j} \left\langle 0 \right| \sigma^x_{\mathrm{C},j} \left| 0 \right\rangle_{\mathrm{c}} \tag{4.36}$$

are the qubit bias corrections induced by the coupler,

$$\bar{\Delta}'_{\mathrm{Q},1} = -\frac{\bar{\Delta}_{\mathrm{Q1}}\, \bar{J}_{1,\mathrm{C1}}\, \bar{J}_{1,\mathrm{C2}}}{2} \sum_{n} \frac{\left\langle 0 \right| \sigma^z_{\mathrm{C1}} \left| n \right\rangle_{\mathrm{c}} \left\langle n \right| \sigma^z_{\mathrm{C2}} \left| 0 \right\rangle_{\mathrm{c}}}{\omega^2_{0,n}}, \tag{4.37}$$

$$\bar{\Delta}'_{\mathrm{Q},2} = -\frac{\bar{\Delta}_{\mathrm{Q2}}\, \bar{J}_{2,\mathrm{C1}}\, \bar{J}_{2,\mathrm{C2}}}{2} \sum_{n} \frac{\left\langle 0 \right| \sigma^z_{\mathrm{C1}} \left| n \right\rangle_{\mathrm{c}} \left\langle n \right| \sigma^z_{\mathrm{C2}} \left| 0 \right\rangle_{\mathrm{c}}}{\omega^2_{0,n}}, \tag{4.38}$$

$$\bar{\Delta}'_{\mathrm{Q},3} = -\frac{\bar{\Delta}_{\mathrm{Q3}}\, \bar{J}_{3,\mathrm{C1}}\, \bar{J}_{3,\mathrm{C2}}}{2} \sum_{n} \frac{\left\langle 0 \right| \sigma^x_{\mathrm{C1}} \left| n \right\rangle_{\mathrm{c}} \left\langle n \right| \sigma^x_{\mathrm{C2}} \left| 0 \right\rangle_{\mathrm{c}}}{\omega^2_{0,n}}, \tag{4.39}$$

represent the qubit detuning shifts induced by the coupler,

$$\bar{J}_{12} = -\sum_{n} \frac{\left\langle 0 \right| \sigma^z_{\mathrm{C1}} \left| n \right\rangle_{\mathrm{c}} \left\langle n \right| \sigma^z_{\mathrm{C2}} \left| 0 \right\rangle_{\mathrm{c}}}{\omega_{n,0}} \left(\bar{J}_{1,\mathrm{C1}}\, \bar{J}_{2,\mathrm{C2}} + \bar{J}_{2,\mathrm{C1}}\, \bar{J}_{1,\mathrm{C2}} \right), \tag{4.40}$$

$$\bar{J}_{13} = -\bar{J}_{1,\mathrm{C1}}\, \bar{J}_{3,\mathrm{C2}} \sum_{n} \frac{\left\langle 0 \right| \sigma^z_{\mathrm{C1}} \left| n \right\rangle_{\mathrm{c}} \left\langle n \right| \sigma^x_{\mathrm{C2}} \left| 0 \right\rangle_{\mathrm{c}}}{\omega_{n,0}} - \bar{J}_{3,\mathrm{C1}}\, \bar{J}_{1,\mathrm{C2}} \sum_{n} \frac{\left\langle 0 \right| \sigma^x_{\mathrm{C1}} \left| n \right\rangle_{\mathrm{c}} \left\langle n \right| \sigma^z_{\mathrm{C2}} \left| 0 \right\rangle_{\mathrm{c}}}{\omega_{n,0}}, \tag{4.41}$$

$$\bar{J}_{23} = -\bar{J}_{2,\mathrm{C1}}\, \bar{J}_{3,\mathrm{C2}} \sum_{n} \frac{\left\langle 0 \right| \sigma^z_{\mathrm{C1}} \left| n \right\rangle_{\mathrm{c}} \left\langle n \right| \sigma^x_{\mathrm{C2}} \left| 0 \right\rangle_{\mathrm{c}}}{\omega_{n,0}} - \bar{J}_{3,\mathrm{C1}}\, \bar{J}_{2,\mathrm{C2}} \sum_{n} \frac{\left\langle 0 \right| \sigma^x_{\mathrm{C1}} \left| n \right\rangle_{\mathrm{c}} \left\langle n \right| \sigma^z_{\mathrm{C2}} \left| 0 \right\rangle_{\mathrm{c}}}{\omega_{n,0}}, \tag{4.42}$$

are the effective two-qubit interactions mediated by the coupler, here, $\left| 0 \right\rangle_{\mathrm{c}}$ and $\left| n \right\rangle_{\mathrm{c}}$ are coupler energy eigenstates, and finally

$$\bar{J}_{123} = \sum_{i=1}^{2} \sum_{j=1}^{2} \sum_{k=1}^{2} \bar{J}_{1,\mathrm{C}i}\, \bar{J}_{2,\mathrm{C}j}\, \bar{J}_{3,\mathrm{C}k} \sum_{n} \sum_{m} \frac{\left\langle 0 \right| \sigma^z_{\mathrm{C},i} \left| n \right\rangle_{\mathrm{c}} \left\langle n \right| \sigma^z_{\mathrm{C},j} \left| m \right\rangle_{\mathrm{c}} \left\langle m \right| \sigma^x_{\mathrm{C},k} \left| 0 \right\rangle_{\mathrm{c}}}{\omega_{0,n}\, \omega_{0,m}}, \tag{4.43}$$

is the effective three-qubit interaction mediated by the coupler. Figure 4.2 shows $\bar{J}_{123}$ versus $f^{\mathrm{s}}_{\mathrm{c}\,j}$. The spin model predicts the cancellation of the two-body term $\bar{J}_{12}$, and similarly of the other two-body interactions, for correct choice of bias conditions. These cancellation conditions are in agreement with our intuitive picture based on symmetries of coupling and susceptibilities.

4.4 Full numerical analysis

To validate the above approximate treatments, we numerically compute the eigenstates of the complete Hamiltonian (4.15). We represent each non-periodic (periodic) degree of freedom of the Hamiltonian in a basis formed of harmonic oscillator (Fourier) states (see appendix A). Due to the complexity of the complete circuit, we proceed hierarchically by first diagonalizing each device separately. Then, keeping only the low-energy eigenstates of each device, we introduce the coupling between all devices and diagonalize the combined system in this low-energy basis to calculate the energy spectrum [130]. The two-body and three-body interactions are determined based on energy gaps at anti-crossing in the numerically calculated spectrum.

To determine the strength of the three-body interaction mediated by the coupler based on circuit simulations, the following approach is used. Qubit flux biasing parameters are chosen to have $\bar{\Delta}_{\mathrm{Q1}} = \bar{\Delta}_{\mathrm{Q2}}$ and $\bar{\Delta}_{\mathrm{Q3}} = \bar{\Delta}_{\mathrm{Q1}} + \bar{\Delta}_{\mathrm{Q2}}$. For this bias condition, the spectrum of the complete circuit Hamiltonian Eq. (4.15) has an avoided-level crossing between the 4^{th} and 5^{th} energy levels, $|\uparrow\uparrow\downarrow\rangle$ and $|\downarrow\downarrow\uparrow\rangle$ where the ↑ or ↓ refers to the current state of one of the three qubits. The avoided level crossing arises due to the ZZZ interaction. This coupling results in a mutual repulsion between the levels. Calculating the minimum spacing between these two avoided levels gives $2\,|J_{123}|$. Figure 4.4 illustrates this procedure.

An alternative method to calculate the coupling relies on choosing biasing conditions for the qubits such that $\bar{\Delta}_{\mathrm{Q1}} = \bar{\Delta}_{\mathrm{Q2}} = \bar{\Delta}_{\mathrm{Q3}}$ and $\bar{\epsilon}_{\mathrm{Q1}} = \bar{\epsilon}_{\mathrm{Q2}} = \bar{\epsilon}_{\mathrm{Q3}} = 0$. If the coupler is biased such that it is mediating a pure three-body interaction, that is $\bar{\epsilon}'_{\mathrm{Q}i} = 0$ and $\bar{J}_{ij} = 0$, the 8-lowest energy levels of the circuit will form two four-fold degenerate subspaces. These two subspacces correspond to even and odd parity of the qubit currents states, i.e. the even states are $|\uparrow\uparrow\uparrow\rangle$, $|\uparrow\downarrow\downarrow\rangle$, $|\downarrow\downarrow\uparrow\rangle$ and $|\downarrow\uparrow\downarrow\rangle$ and the odd states are $|\downarrow\downarrow\downarrow\rangle$, $|\uparrow\uparrow\downarrow\rangle$, $|\downarrow\uparrow\uparrow\rangle$ and $|\uparrow\downarrow\uparrow\rangle$. These two subspaces are coupled by the ZZZ operator. Calculating the energy separation between these two subspaces gives $2\,|J_{123}|$. This method was used to extract the coupling strength in Fig. 2 in the main text.

The three-body interaction strength $\bar{J}_{123}$ calculated based on the spin model is in excellent agreement with numerical results for the full circuit model for $|f^{\mathrm{s}}_{\mathrm{c}\,j}| > 0.31$, as

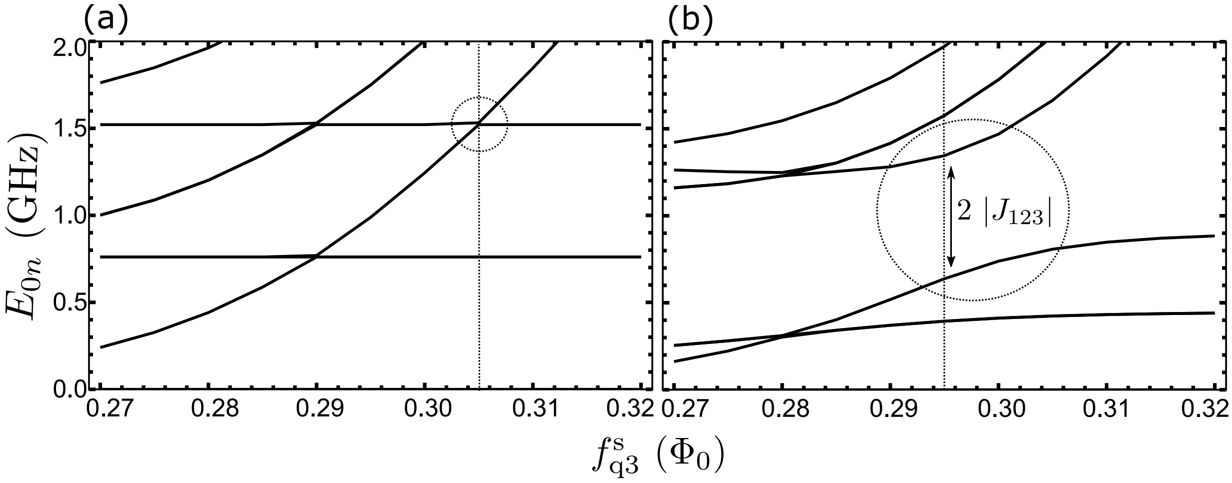

Figure 4.4: Energy spectrum of the complete circuit Hamiltonian, relative to the ground state energy. (a) When the three-body coupling is turned on, an avoided level crossing between level 4 and 5 corresponding to $2\,|J_{123}|$ appears around $\Delta_{\mathrm{Q3}} \approx \Delta_{\mathrm{Q1}} + \Delta_{\mathrm{Q2}}$ (dotted line and circle). (b) When the three-body coupling is turned off, levels 4 and 5 simply cross each other around $\Delta_{\mathrm{Q3}} \approx \Delta_{\mathrm{Q1}} + \Delta_{\mathrm{Q2}}$ (dotted line and circle). The conditions of $\Delta_{\mathrm{Q3}} \approx \Delta_{\mathrm{Q1}} + \Delta_{\mathrm{Q2}}$ happen at different flux values with and without coupling because of a re-normalization of the qubit energy levels due to the coupling.

shown in Fig. 4.2. The disagreement for small values of $|f^{\mathrm{s}}_{\mathrm{c}\,j}|$ is due to the increase in the ratio $\bar{J}_{i,\mathrm{C}j}/\omega_{0,1}$, arising from both a decreasing energy gap of the rf-squids and the increase in the qubit-rf-SQUID coupling. We also find good qualitative agreement between the Born-Oppenheimer method and the numerical calculations. However, the pronounced quantitative disagreement for $|f^{\mathrm{s}}_{\mathrm{c}\,j}| < 0.31$ between the two methods can be attributed to the breakdown of the Born-Oppenheimer approximation in the region of decreasing energy gap of the rf-SQUID [108]. In the region of $|f^{\mathrm{s}}_{\mathrm{c}\,j}| > 0.31$, the disagreement may be explained by the treatment of the qubits as classical variables.

4.5 Robustness of the coupler to noise and fabrication variations

An important feature for a superconducting coupler is robustness to low-frequency flux noise [83]. To analyze the coupler's sensitivity to flux noise, we simulate a noisy environment. We assume Gaussian flux noise with the power spectral density $A^{\beta}_{\mathrm{c}\,i}/\omega^{\gamma}$ [81], where ω is the angular frequency. We use parameters $A^{\mathrm{m}}_{\mathrm{c}\,j} = 14.57\ \mu\Phi_0/\sqrt{\mathrm{Hz}}$, $A^{\mathrm{s}}_{\mathrm{c}\,j} = 8.15\ \mu\Phi_0/\sqrt{\mathrm{Hz}}$, and $\gamma = 0.9$ is an exponent derived from experiments [84, 74, 51]. The simulated flux noise environment for loop β in device $\alpha\, i$ induces fluctuations in flux bias with a normal distribution with variance given by

$$\delta\Phi^{\beta}_{\alpha\, i} = \int_{\omega_{\mathrm{lo}}}^{\omega_{\mathrm{hi}}} \mathrm{d}\omega\, \frac{A^{\beta}_{\alpha\, i}}{\omega^{0.9}}, \tag{4.44}$$

where $\omega_{\mathrm{hi}} = 10$ GHz is the high-frequency cut-off, $\omega_{\mathrm{lo}} = 2\pi/T_{\mathrm{f}}$ is the low-frequency cut-off, where T_{f} is the total experiment time which we have taken to be 1 μs. We have determined the value of the $A^{\beta}_{\alpha\, i}$ by measuring the width-over-length ratio of the superconducting wires making up realistic computer assisted designs of the devices, and scaling this ratio with respect to established experimental values [74, 51, 84]. We impose this noisy flux environment on the coupler flux biases at the bias point where we get large three-body coupling and a cancellation of all two-body couplings ($f^{\mathrm{m}}_{\mathrm{c}\,1} = f^{\mathrm{m}}_{\mathrm{c}\,2} = 0.5$ and $f^{\mathrm{s}}_{\mathrm{c}\,1} = -f^{\mathrm{s}}_{\mathrm{c}\,2} = 0.3$) and observe a standard deviation in $\widetilde{J}_{123}$ of at most 0.002 GHz around the nominal value of 1 GHz as well as a standard deviation of at most 0.007 GHz around the nominal cancellation point for $\widetilde{J}_{12}$, $\widetilde{J}_{13}$ and $\widetilde{J}_{23}$ (see SI for full table, including all coefficients). The spread in single qubit energy bias terms $\tilde{h}_i$ induced by the coupler circulating currents is comparable with fluctuations induced by flux noise intrinsic to the qubit loops. As a result, we do not expect the coupler to induce significant dephasing of the qubit. These small uncertainties in the couplings correspond to a high precision of parameters in a quantum annealing Hamiltonian, ensuring that the correct solution is found at the end of the computation [131].

We determine the variations in the coupling and bias parameters induced by flux noise in the coupler loops. We model the spread in coupling and bias parameters when the system is subjected to this realistic noisy environment. The standard deviation of the parameter due to noise on the 4 loops of the coupling circuit and the qubit loops are reported in table 4.1.

Table 4.1: Annealing parameter standard deviations due to uncorrelated flux noise in all coupler loops.

Parameter	Nominal value (GHz)	Standard deviation (GHz)
$\tilde{h}1$	0.000	0.102
$\tilde{h}2$	0.000	0.092
$\tilde{h}3$	0.000	0.007
$\tilde{J}12$	0.000	0.012
$\tilde{J}13$	0.000	0.014
$\tilde{J}23$	0.000	0.016
$\tilde{J}123$	0.915	0.003

Besides robustness to flux noise, the coupler should be functional when variations in fabrication parameters are taken into account. To validate robustness to errors, we analyze the effect on the coupling strength and on the ability to cancel the two-body interactions when introducing variations in the mutual inductances between the coupler and the qubits, the self inductances of the coupler and the Josephson junctions in the coupler circuit (see appendix B.2).

The mutual inductances between the qubits and SQUIDs and the self-inductances of the SQUIDs were sampled randomly from a normal distribution with a 95% confidence interval within 3% of their nominal value. The coupling strengths J_{ij} and J_{123} were calculated with the Born-Oppenheimer method at the same bias point ($f^{\mathrm{m}}_{\mathrm{c}\,1} = f^{\mathrm{m}}_{\mathrm{c}\,2} = 0.5$ and $f^{\mathrm{s}}_{\mathrm{c}\,1} = -f^{\mathrm{s}}_{\mathrm{c}\,2} = 0.3$) for all random instances. This was repeated for 100 random instances.

All the Josephson junction critical currents in the rf-SQUIDs were sampled randomly from a normal distribution with a 95% confidence interval within 3% of their nominal value. For each random instance, the coupling strengths J_{ij} and J_{123} were calculated with the Born-Oppenheimer method at the same bias point ($f^{\mathrm{m}}_{\mathrm{c}\,1} = f^{\mathrm{m}}_{\mathrm{c}\,2} = 0.5$ and $f^{\mathrm{s}}_{\mathrm{c}\,1} = -f^{\mathrm{s}}_{\mathrm{c}\,2} = 0.3$). The asymmetry in the junctions affects the cancellation of the two-body interactions. New bias conditions where all two-body interactions are suppressed to within 10 MHz and where the three-body interaction is tunable were found by local optimization by rejection sampling around the nominal bias point.

We extracted the effective qubit Hamiltonian over a normal distribution of parameter variations, with standard deviation of 3% of the nominal values. We find that inductance variations in the secondary loop have a negligible effect on the two- and three- body coupling strengths. On the other hand, main loop self inductance and junction asymmetry significantly affects the values of the $\widetilde{J}_{ij}$. However, cancellation conditions for two-body terms, to within 10 MHz, can be recovered by suitable compensations of the bias fluxes.

4.6 Quantum annealing simulations

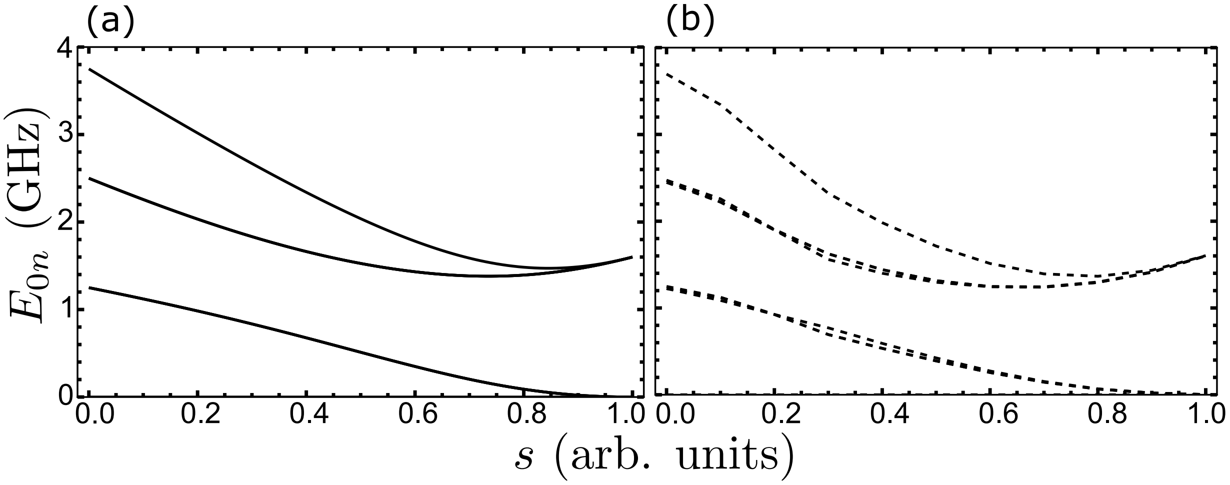

Figure 4.5: Low-energy spectrum versus annealing parameter s. (a) Spectrum of the 8 levels of an ideal 3-spin Hamiltonian implementing Eq. (4.45). (b) Spectrum of the lowest 8 qubit-like levels of the circuit Hamiltonian (4.15) when biased to implement a linear annealing schedule as in (4.45).

When implementing this coupler in a quantum annealing context, an important metric is the extent to which the coupler emulates the spectrum of an ideal spin Hamiltonian. In quantum annealing [18], one seeks to prepare the ground state of a Hamiltonian that encodes the solution to a computational problem. The solution is found by initializing the computation in the ground state of a trivial Hamiltonian, then adiabatically deforming to the Hamiltonian of interest. We consider an annealing schedule with an initial Hamiltonian given by the standard transverse field Hamiltonian and a final Hamiltonian given by a three-body interaction:

$$H_{\mathrm{anneal}}(s) = (1-s)\sum_{i}^{3} \frac{\Delta_i}{2}\,\sigma_i^x + s\,J_{123}\,\sigma_1^z\sigma_2^z\sigma_3^z, \tag{4.45}$$

where s is the annealing parameter, changing from 0 to 1.

The full circuit annealing simulation is done in the following way. We start by diagonalizing the individual qubits to determine the relation between $f^{\mathrm{s}}_{\mathrm{q}\,i}$ and $f^{\mathrm{s}}_{\mathrm{c}\,i}$, and $(1-s)\,\Delta_i$ in the annealing Hamiltonian. To account for the effect of the coupler on the qubits, we re-normalize the qubit inductance with a term proportional to the coupler susceptibility, as is discussed for the two-qubit coupler case in section 3.2 and in Refs. [105, 109, 51]. This re-normalization is

$$L^{\mathrm{m}}_{\mathrm{q}\,i} \to L^{\mathrm{m}}_{\mathrm{q}\,i} - \sum_{j=1}^{2} M_{ij}^2\,\frac{\partial \langle 0_{\mathrm{c}}|\, I_i\, |0_{\mathrm{c}}\rangle}{\partial f^{\mathrm{m}}_{\mathrm{c}\,j}}, \tag{4.46}$$

for $i \in \{1,2\}$, and

$$L^{\mathrm{m}}_{\mathrm{q}\,3} \to L^{\mathrm{m}}_{\mathrm{q}\,3} - \sum_{j=1}^{2} M_{3j}^2\,\frac{\partial \langle 0_{\mathrm{c}}|\, I_3\, |0_{\mathrm{c}}\rangle}{\partial f^{\mathrm{s}}_{\mathrm{c}\,j}}. \tag{4.47}$$

We next determine the persistent current of these re-normalized qubits. These persistent currents are then used to determine the relation between $f^{\mathrm{s}}_{\mathrm{q}\,i}$ and $f^{\mathrm{s}}_{\mathrm{c}\,i}$, and $s\,J_{123}$ in the annealing Hamiltonian. We use the Born-Oppenheimer method described in Eq. (6) in the main text, with the qubit persistent currents just calculated. This procedure is then repeated for all values of s.

Figure 4.5 shows the energy levels of the Hamiltonian (4.45) and of the complete circuit, including the three body coupler, where we have used $\Delta_i = 1.22$ GHz and $J_{123} = 0.8$ GHz. We find excellent agreement between the energy spectra in the two cases, and in particular the physical system correctly preserves the degeneracy of the ideal spin Hamiltonian. We also have that the lowest 8 qubit-like energy levels of the complete circuit are well separated from the higher levels (gap of approximately 8 GHz).

4.7 Extension to more qubits

We now briefly discuss the application of our proposed coupler to the situation of more than three qubits. When building a quantum annealer with this coupler, one needs to decide on the fundamental architecture or graph of the device. This means that one must decide how many of these three-body couplers are to be included in the annealer and how they will be connected to the qubits. we include here a brief discussion on how this coupler could be included in an annealer.

It is important to mention that it is possible to propagate flux signals from qubits through intermediate flux transformers or couplers [133]. This concept could be used to connect many qubits to a single three-body coupler and thus control which qubit would interact with the three-body coupler by using the intermediate flux transformers as switches. To visualize this, let us first simplify the proposed coupler circuit in the form of Fig. 4.6a, where the circuits are replaced by boxes or circles and the direct inductive connections are indicated by straight lines. The extension of this coupler to more qubits is pictured in Fig. 4.6b, where 6 qubits are coupled to one three-qubit coupler in such a way that one can have more flexible coupling between the qubits by turning off the tree-couplers connecting the qubits that are to be left out of the interaction. One can just as easily extend this scheme further with more three-body couplers and more qubits, all that is needed is to add a tree-coupler as a switch in between the three-body coupler and the qubits.

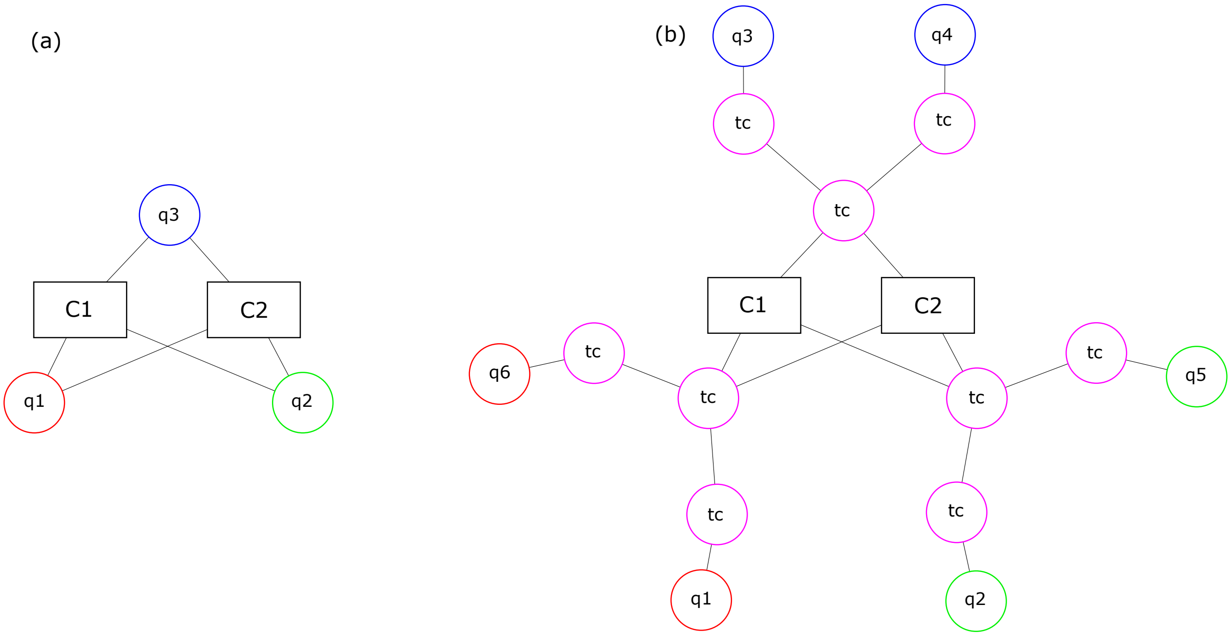

Figure 4.6: (a) Simplified coupler schematic. The circles represent the qubits ("q1", "q2", "q3"), the rectangular boxes represent the couplers ("C1", "C2") and the straight lines indicate the direct inductive coupling. (b) Extension of proposed three-body coupler to many qubits. The introduction of circular tree-couplers ("tc") make the connection and switching between other qubits possible.

Chapter 5

Conclusion

When starting this research project, we had as a goal to develop a superconducting circuit capable of mediating three-body interactions between flux qubits. In this thesis, we have proposed and analyzed such a circuit based on a rf-SQUID. We have seen that our proposed circuit is capable of mediating strong and tunable in sign and magnitude three-qubit interaction between three capacitively shunted flux qubits. The analysis in this thesis has shown that this interaction is of the ZZZ form and has a strength of the same order as the qubit energies, of order 1 GHz. Furthermore, this coupling is symmetrically tunable from negative to positive through zero coupling, that is, both signs have equal maximum coupling magnitude. The symmetric sign of the coupling is a useful property that is absent in the standard tunable rf-SQUID two-qubit couplers used in quantum annealing. Additionally, the circuit developed is also capable of being operated as a tunable three-qubit coupler while in the regime where all two-body interactions vanish. This last condition is very important for practical implementation because it minimizes the need for additional compensatory circuitry to be included on chip. Being able to operate the coupling circuit in this regime enabled us to readily reproduce the low-energy spectrum of quantum annealing Hamiltonian with three body interactions and zero two-body interactions. Finally, we determined that this circuit was also robust to realistic flux noise and can be readily compensated to adapt to realistic fabrication variations.

The methods used in this work, analytical derivation of circuit Hamiltonians using standard circuit quantization, the Born-Oppenheimer approximation, the spin model and the full numerical simulations, enabled us to properly analyze and optimize the coupling circuit. The development of an efficient method to extract the coupling coefficient based on the Born-Oppenheimer approximation proved to be a great approximation to the circuit as well as a very useful treatment for computationally efficient results. The spin model also proved to be a good approximation in the regime of weak coupling and developed our understanding of the conditions of cancellation of the two-body terms. In the regime of strong coupling, strong non-linearity and small coupler energy gap, however, full numerical simulations, with hierarchical diagonalization, were important for the most accurate picture of the interaction.

The analysis presented in this work will be relevant in designing the next generation of quantum annealing hardware, which will have increased embedding efficiency for hard problems that include multi-body terms, quantum annealing error correction and that will have capabilities to simulate increasingly complex quantum systems.

References

[1] G. Moore, “Cramming more components onto integrated circuits,” *Electronics Magazine*, vol. 38, no. 8, 1965.

[2] J. Hromkovič, “A Guide to Solving Hard Problems,” in *Algorithmics for Hard Problems: Introduction to Combinatorial Optimization, Randomization, Approximation, and Heuristics*, pp. 461–501, Berlin, Heidelberg: Springer Berlin Heidelberg, 2004.

[3] G. J. Woeginger, “Exact Algorithms for NP-Hard Problems: A Survey,” in *Combinatorial Optimization — Eureka, You Shrink!: Papers Dedicated to Jack Edmonds 5th International Workshop Aussois, France, March 5–9, 2001 Revised Papers* (M. Jünger, G. Reinelt, and G. Rinaldi, eds.), pp. 185–207, Berlin, Heidelberg: Springer Berlin Heidelberg, 2003.

[4] S. Aaronson, “A linear-optical proof that the permanent is #¡b¿p¡/b¿-hard,” *Proceedings of the Royal Society A: Mathematical, Physical and Engineering Sciences*, vol. 467, no. 2136, pp. 3393–3405, 2011.

[5] L. Eeckhout, “Is moores law slowing down? whats next?,” *IEEE Micro*, vol. 37, no. 4, pp. 4–5, 2017.

[6] R. P. Feynman, “Simulating physics with computers,” *International Journal of Theoretical Physics*, vol. 21, no. 6, pp. 467–488, 1982.

[7] P. Benioff, “Quantum mechanical models of turing machines that dissipate no energy,” *Phys. Rev. Lett.*, vol. 48, pp. 1581–1585, 1982.

[8] S. Lloyd, “Universal Quantum Simulators,” *Science*, vol. 273, no. 5278, pp. 1073–1078, 1996.

[9] I. Buluta and F. Nori, “Quantum Simulators,” *Science*, vol. 326, no. 5949, pp. 108–111, 2009.

[10] D. E. Deutsch and R. Penrose, "Quantum computational networks," *Proceedings of the Royal Society of London. A. Mathematical and Physical Sciences*, vol. 425, no. 1868, pp. 73–90, 1989.

[11] P. Shor, "Polynomial-time algorithms for prime factorization and discrete logarithms on a quantum computer," *SIAM Journal on Computing*, vol. 26, no. 5, pp. 1484–1509, 1997.

[12] L. K. Grover, "A fast quantum mechanical algorithm for database search," in *Proceedings of the Twenty-eighth Annual ACM Symposium on Theory of Computing*, STOC '96, (New York, NY, USA), pp. 212–219, ACM, 1996.

[13] D. P. DiVincenzo, "The physical implementation of quantum computation," *Fortschritte der Physik*, vol. 48, no. 911, pp. 771–783, 2000.

[14] M. A. Nielsen and I. L. Chuang, *Quantum Computation and Quantum Information: 10th Anniversary Edition*. New York, NY, USA: Cambridge University Press, 10th ed., 2011.

[15] B. Apolloni, C. Carvalho, and D. de Falco, "Quantum stochastic optimization," *Stochastic Processes and their Applications*, vol. 33, no. 2, pp. 233–244, 1989.

[16] T. Kadowaki and H. Nishimori, "Quantum annealing in the transverse Ising model," *Physical Review E*, vol. 58, no. 5, pp. 5355–5363, 1998.

[17] E. Farhi, J. Goldstone, S. Gutmann, and M. Sipser, "Quantum computation by adiabatic evolution," *arXiv:0001106*, 2000.

[18] T. Albash and D. A. Lidar, "Adiabatic quantum computation," *Reviews of Modern Physics*, vol. 90, no. 1, p. 015002, 2018.

[19] D. Aharonov, W. van Dam, J. Kempe, Z. Landau, S. Lloyd, and O. Regev, "Adiabatic quantum computation is equivalent to standard quantum computation," *SIAM Review*, vol. 50, no. 4, pp. 755–787, 2008.

[20] T. D. Ladd, F. Jelezko, R. Laflamme, Y. Nakamura, C. Monroe, and J. L. OBrien, "Quantum computers," *Nature*, vol. 464, p. 45, 2010.

[21] I. Ames, "An overview of materials and process aspects of josephson integrated circuit fabrication," *IBM Journal of Research and Development*, vol. 24, no. 2, pp. 188–194, 1980.

[22] T. van Duzer, “Superconductor electronics, 1986-1996,” *IEEE Transactions on Applied Superconductivity*, vol. 7, no. 2, pp. 98–111, 1997.

[23] W. D. Oliver and P. B. Welander, “Materials in superconducting quantum bits,” *MRS Bulletin*, vol. 38, no. 10, p. 816825, 2013.

[24] S. K. Tolpygo, “Superconductor digital electronics: Scalability and energy efficiency issues (review article),” *Low Temperature Physics*, vol. 42, no. 5, pp. 361–379, 2016.

[25] G. Wendin, “Quantum information processing with superconducting circuits: a review,” *Reports on Progress in Physics*, vol. 80, no. 10, p. 106001, 2017.

[26] A. Lucas, “Ising formulations of many np problems,” *Frontiers in Physics*, vol. 2, p. 5, 2014.

[27] S. H. W. van der Ploeg, A. Izmalkov, M. Grajcar, U. Hubner, S. Linzen, S. Uchaikin, T. Wagner, A. Y. Smirnov, A. M. van den Brink, M. H. S. Amin, A. M. Zagoskin, E. Il’ichev, and H. . Meyer, “Adiabatic quantum computation with flux qubits, first experimental results,” *IEEE Transactions on Applied Superconductivity*, vol. 17, no. 2, pp. 113–119, 2007.

[28] R. Harris, A. J. Berkley, M. W. Johnson, P. Bunyk, S. Govorkov, M. C. Thom, S. Uchaikin, A. B. Wilson, J. Chung, E. Holtham, J. D. Biamonte, A. Y. Smirnov, M. H. S. Amin, and A. Maassen van den Brink, “Sign- and Magnitude-Tunable Coupler for Superconducting Flux Qubits,” *Physical Review Letters*, vol. 98, no. 17, p. 177001, 2007.

[29] R. Harris, J. Johansson, A. J. Berkley, M. W. Johnson, T. Lanting, S. Han, P. Bunyk, E. Ladizinsky, T. Oh, I. Perminov, E. Tolkacheva, S. Uchaikin, E. M. Chapple, C. Enderud, C. Rich, M. Thom, J. Wang, B. Wilson, and G. Rose, “Experimental demonstration of a robust and scalable flux qubit,” *Physical Review B*, vol. 81, no. 13, p. 134510, 2010.

[30] R. Harris, M. W. Johnson, T. Lanting, A. J. Berkley, J. Johansson, P. Bunyk, E. Tolkacheva, E. Ladizinsky, N. Ladizinsky, T. Oh, F. Cioata, I. Perminov, P. Spear, C. Enderud, C. Rich, S. Uchaikin, M. C. Thom, E. M. Chapple, J. Wang, B. Wilson, M. H. S. Amin, N. Dickson, K. Karimi, B. Macready, C. J. S. Truncik, and G. Rose, “Experimental investigation of an eight-qubit unit cell in a superconducting optimization processor,” *Phys. Rev. B*, vol. 82, p. 024511, 2010.

[31] M. W. Johnson, M. H. S. Amin, S. Gildert, T. Lanting, F. Hamze, N. Dickson, R. Harris, A. J. Berkley, J. Johansson, P. Bunyk, E. M. Chapple, C. Enderud, J. P. Hilton, K. Karimi, E. Ladizinsky, N. Ladizinsky, T. Oh, I. Perminov, C. Rich, M. C. Thom, E. Tolkacheva, C. J. S. Truncik, S. Uchaikin, J. Wang, B. Wilson, and G. Rose, "Quantum annealing with manufactured spins," *Nature*, vol. 473, pp. 194–198, 2011.

[32] J. King, S. Yarkoni, J. Raymond, I. O. dan, A. D. King, M. M. Nevisi, J. P. Hilton, and C. C. McGeoch, "Quantum annealing amid local ruggedness and global frustration," *arXiv:1701.04579*, 2017.

[33] C. C. McGeoch, "Benchmarking d-wave quantum annealing systems: some challenges," in *Electro-Optical and Infrared Systems: Technology and Applications XII; and Quantum Information Science and Technology*, vol. 9648, p. 964815, International Society for Optics and Photonics, 2015.

[34] E. Gibney, "D-wave upgrade: How scientists are using the worlds most controversial quantum computer," *Nature News*, vol. 541, no. 7638, p. 447, 2017.

[35] V. S. Denchev, S. Boixo, S. V. Isakov, N. Ding, R. Babbush, V. Smelyanskiy, J. Martinis, and H. Neven, "What is the Computational Value of Finite-Range Tunneling?," *Physical Review X*, vol. 6, no. 3, p. 031015, 2016.

[36] T. Albash and D. A. Lidar, "Demonstration of a scaling advantage for a quantum annealer over simulated annealing," *Phys. Rev. X*, vol. 8, p. 031016, 2018.

[37] V. Choi, "Minor-embedding in adiabatic quantum computation: I. the parameter setting problem," *Quantum Information Processing*, vol. 7, no. 5, pp. 193–209, 2008.

[38] V. Choi, "Minor-embedding in adiabatic quantum computation: Ii. minor-universal graph design," *Quantum Information Processing*, vol. 10, no. 3, pp. 343–353, 2011.

[39] A. Kitaev, "Fault-tolerant quantum computation by anyons," *Annals of Physics*, vol. 303, no. 1, pp. 2 – 30, 2003.

[40] Z. Jiang and E. G. Rieffel, "Non-commuting two-local Hamiltonians for quantum error suppression," *Quantum Information Processing*, vol. 16, no. 4, p. 89, 2017.

[41] X. Peng, J. Zhang, J. Du, and D. Suter, "Quantum simulation of a system with competing two- and three-body interactions," *Phys. Rev. Lett.*, vol. 103, p. 140501, 2009.

[42] D. Porras and J. I Cirac, "Effective quantum spin systems with trapped ions," *Physical review letters*, vol. 92, p. 207901, 2004.

[43] N. Chancellor, S. Zohren, and P. A. Warburton, "Circuit design for multi-body interactions in superconducting quantum annealing systems with applications to a scalable architecture," *npj Quantum Information*, vol. 3, no. 1, p. 21, 2017.

[44] S. Jiang, K. A. Britt, A. J. McCaskey, T. S. Humble, and S. Kais, "Quantum Annealing for Prime Factorization.," *Scientific Reports*, vol. 8, no. 1, pp. 17667–17667, 2018.

[45] J. R. A. R. Kelly Boothby, Paul Bunyk, "Next-generation topology of d-wave quantum processors," 2019. www.dwavesys.com.

[46] W. Vinci and D. A. Lidar, "Non-stoquastic Hamiltonians in quantum annealing via geometric phases," *npj Quantum Information*, vol. 3, 2017.

[47] H. Nishimori and K. Takada, "Exponential enhancement of the efficiency of quantum annealing by non-stoquastic hamiltonians," *Frontiers in ICT*, vol. 4, p. 2, 2017.

[48] A. J. Kerman, "Superconducting qubit circuit emulation of a vector spin-1/2," *arXiv:1810.01352*, 2018.

[49] I. Ozfidan, C. Deng, A. Y. Smirnov, T. Lanting, R. Harris, L. Swenson, J. Whittaker, F. Altomare, M. Babcock, C. Baron, A. J. Berkley, K. Boothby, H. Christiani, P. Bunyk, C. Enderud, B. Evert, M. Hager, A. Hajda, J. Hilton, S. Huang, E. Hoskinson, M. W. Johnson, K. Jooya, E. Ladizinsky, N. Ladizinsky, R. Li, A. MacDonald, D. Marsden, G. Marsden, T. Medina, R. Molavi, R. Neufeld, M. Nissen, M. Norouzpour, T. Oh, I. Pavlov, I. Perminov, G. Poulin-Lamarre, M. Reis, T. Prescott, C. Rich, Y. Sato, G. Sterling, N. Tsai, M. Volkmann, W. Wilkinson, J. Yao, and M. H. Amin, "Demonstration of nonstoquastic Hamiltonian in coupled superconducting flux qubits," *arXiv:1903.06139*, 2019.

[50] K. L. Pudenz, T. Albash, and D. A. Lidar, "Error-corrected quantum annealing with hundreds of qubits," *Nature Communications*, vol. 5, p. ncomms4243, 2014.

[51] S. J. Weber, G. O. Samach, D. Hover, S. Gustavsson, D. K. Kim, A. Melville, D. Rosenberg, A. P. Sears, F. Yan, J. L. Yoder, W. D. Oliver, and A. J. Kerman, "Coherent coupled qubits for quantum annealing," *Physical Review Applied*, vol. 8, p. 014004, 2017.

[52] R. Harris, "Improved coherence leads to gains in quantum annealing performance," 2019. www.dwavesys.com.

[53] L. S. Theis, P. K. Schuhmacher, M. Marthaler, and F. K. Wilhelm, "Gap-independent cooling and hybrid quantum-classical annealing," *arXiv:1808.09873*, 2018.

[54] A. T. Rezakhani, W.-J. Kuo, A. Hamma, D. A. Lidar, and P. Zanardi, "Quantum Adiabatic Brachistochrone," *Physical Review Letters*, vol. 103, no. 8, p. 080502, 2009.

[55] R. D. Wilson, A. M. Zagoskin, S. Savel'ev, M. J. Everitt, and F. Nori, "Feedback-controlled adiabatic quantum computation," *Physical Review A*, vol. 86, no. 5, p. 052306, 2012.

[56] Y. Susa, Y. Yamashiro, M. Yamamoto, and H. Nishimori, "Exponential speedup of quantum annealing by inhomogeneous driving of the transverse field," *Journal of the Physical Society of Japan*, vol. 87, no. 2, p. 023002, 2018.

[57] M. Schöndorf and F. K. Wilhelm, "Four-local interactions in a superconducting qubit architecture without ancilla qubits," *arXiv:1811.07683*, 2018.

[58] K. Gavroglu, H. Onnes, and Y. Goudaroulis, *Through Measurement to Knowledge: The Selected Papers of Heike Kamerlingh Onnes 1853–1926*. Boston Studies in the Philosophy and History of Science, Springer Netherlands, 2012.

[59] F. London, H. London, and F. A. Lindemann, "The electromagnetic equations of the supraconductor," *Proceedings of the Royal Society of London. Series A - Mathematical and Physical Sciences*, vol. 149, no. 866, pp. 71–88, 1935.

[60] V. L. Ginzburg and L. D. Landau, "On the theory of superconductivity," *Zh. Eksp. Teor. Fiz.*, vol. 20, pp. 1064–1082, 1950.

[61] J. Bardeen, L. N. Cooper, and J. R. Schrieffer, "Theory of superconductivity," *Phys. Rev.*, vol. 108, pp. 1175–1204, 1957.

[62] B. Josephson, "Possible new effects in superconductive tunnelling," *Physics Letters*, vol. 1, no. 7, pp. 251 – 253, 1962.

[63] M. H. Devoret and R. J. Schoelkopf, "Superconducting circuits for quantum information: An outlook," *Science*, vol. 339, no. 6124, pp. 1169–1174, 2013.

[64] W. Meissner and R. Ochsenfeld, "Ein neuer effekt bei eintritt der supraleitfähigkeit," *Naturwissenschaften*, vol. 21, no. 44, pp. 787–788, 1933.

[65] M. Tinkham, *Introduction to superconductivity.* McGraw-Hill and Dover Books, 2nd ed., 1996.

[66] U. Vool and M. Devoret, “Introduction to quantum electromagnetic circuits,” *International Journal of Circuit Theory and Applications*, vol. 45, no. 7, pp. 897–934, 2017.

[67] M. H. Devoret, A. Wallraff, and J. M. Martinis, “Superconducting Qubits: A Short Review,” *arXiv:0411174*, 2004.

[68] J. M. Martinis, “Course 13 - Superconducting Qubits and the Physics of Josephson Junctions,” in *Quantum Entanglement and Information Processing* (D. Estve, J.-M. Raimond, and J. Dalibard, eds.), vol. 79 of *Les Houches*, pp. 487–520, Elsevier, 2004. ISSN: 0924-8099.

[69] P. W. Anderson and J. M. Rowell, “Probable observation of the josephson superconducting tunneling effect,” *Phys. Rev. Lett.*, vol. 10, pp. 230–232, 1963.

[70] A. Barone and G. Paternò, *Physics and Applications of the Josephson Effect.* John Wiley & Sons, Ltd, 1982.

[71] J. R. Friedman, V. Patel, W. Chen, S. K. Tolpygo, and J. E. Lukens, *Macroscopic Quantum Coherence in an Rf-SQUID*, pp. 7–16. Boston, MA: Springer US, 2001.

[72] T. P. Orlando, J. E. Mooij, L. Tian, C. H. van der Wal, L. S. Levitov, S. Lloyd, and J. J. Mazo, “Superconducting persistent-current qubit,” *Physical Review B*, vol. 60, no. 22, pp. 15398–15413, 1999.

[73] Chiorescu, I. et al., “Coherent quantum dynamics of a superconducting flux qubit,” *Science*, vol. 299, pp. 1869–1871, 2003.

[74] F. Yan, S. Gustavsson, A. Kamal, J. Birenbaum, A. P. Sears, D. Hover, T. J. Gudmundsen, D. Rosenberg, G. Samach, S. Weber, J. L. Yoder, T. P. Orlando, J. Clarke, A. J. Kerman, and W. D. Oliver, “The flux qubit revisited to enhance coherence and reproducibility,” *Nature Communications*, vol. 7, p. ncomms12964, 2016.

[75] W. H. Zurek, *Decoherence and the Transition from Quantum to Classical — Revisited*, pp. 1–31. Birkhäuser Basel, 2007.

[76] Bylander, J. et al., “Noise spectroscopy through dynamical decoupling with a superconducting flux qubit,” *Nature Physics*, vol. 7, p. nphys1994, 2011.

[77] Ithier, G. et al., "Decoherence in a superconducting quantum bit circuit," *Physical Review B*, vol. 72, 2005.

[78] J. M. Martinis, K. B. Cooper, R. McDermott, M. Steffen, M. Ansmann, K. D. Osborn, K. Cicak, S. Oh, D. P. Pappas, R. W. Simmonds, and C. C. Yu, "Decoherence in josephson qubits from dielectric loss," *Phys. Rev. Lett.*, vol. 95, p. 210503, 2005.

[79] J. M. Martinis, M. Ansmann, and J. Aumentado, "Energy decay in superconducting josephson-junction qubits from nonequilibrium quasiparticle excitations," *Phys. Rev. Lett.*, vol. 103, p. 097002, 2009.

[80] Koch, J. et al., "Charge-insensitive qubit design derived from the Cooper pair box," *Phys. Rev. A*, vol. 76, p. 042319, 2007.

[81] R. H. Koch, D. P. DiVincenzo, and J. Clarke, "Model for $1/f$ Flux Noise in SQUIDs and Qubits," *Physical Review Letters*, vol. 98, no. 26, p. 267003, 2007.

[82] R. McDermott, "Materials origins of decoherence in superconducting qubits," *IEEE Transactions on Applied Superconductivity*, vol. 19, no. 1, pp. 2–13, 2009.

[83] F. Yoshihara, K. Harrabi, A. O. Niskanen, Y. Nakamura, and J. S. Tsai, "Decoherence of Flux Qubits due to $1/f$ Flux Noise," *Physical Review Letters*, vol. 97, no. 16, p. 167001, 2006.

[84] R. C. Bialczak, R. McDermott, M. Ansmann, M. Hofheinz, N. Katz, E. Lucero, M. Neeley, A. D. OConnell, H. Wang, A. N. Cleland, and J. M. Martinis, "$1/f$ Flux Noise in Josephson Phase Qubits," *Physical Review Letters*, vol. 99, no. 18, p. 187006, 2007.

[85] T. Lanting, A. J. Berkley, B. Bumble, P. Bunyk, A. Fung, J. Johansson, A. Kaul, A. Kleinsasser, E. Ladizinsky, F. Maibaum, R. Harris, M. W. Johnson, E. Tolkacheva, and M. H. S. Amin, "Geometrical dependence of the low-frequency noise in superconducting flux qubits," *Physical Review B*, vol. 79, no. 6, p. 060509, 2009.

[86] S. Sendelbach, D. Hover, M. Mück, and R. McDermott, "Complex inductance, excess noise, and surface magnetism in dc squids," *Phys. Rev. Lett.*, vol. 103, p. 117001, 2009.

[87] S. Gustavsson, J. Bylander, F. Yan, W. D. Oliver, F. Yoshihara, and Y. Nakamura, "Noise correlations in a flux qubit with tunable tunnel coupling," *Phys. Rev. B*, vol. 84, p. 014525, 2011.

[88] S. M. Anton, J. S. Birenbaum, S. R. O'Kelley, V. Bolkhovsky, D. A. Braje, G. Fitch, M. Neeley, G. C. Hilton, H.-M. Cho, K. D. Irwin, F. C. Wellstood, W. D. Oliver, A. Shnirman, and J. Clarke, "Magnetic flux noise in dc squids: Temperature and geometry dependence," *Phys. Rev. Lett.*, vol. 110, p. 147002, 2013.

[89] N. F. Ramsey, "Electron coupled interactions between nuclear spins in molecules," *Phys. Rev.*, vol. 91, pp. 303–307, Jul 1953.

[90] M. A. Ruderman and C. Kittel, "Indirect exchange coupling of nuclear magnetic moments by conduction electrons," *Phys. Rev.*, vol. 96, pp. 99–102, 1954.

[91] S. Ashhab, A. O. Niskanen, K. Harrabi, Y. Nakamura, T. Picot, P. C. de Groot, C. J. P. M. Harmans, J. E. Mooij, and F. Nori, "Interqubit coupling mediated by a high-excitation-energy quantum object," *Physical Review B*, vol. 77, no. 1, p. 014510, 2008.

[92] S. Bose, "Quantum communication through an unmodulated spin chain," *Phys. Rev. Lett.*, vol. 91, p. 207901, 2003.

[93] L. Trifunovic, F. L. Pedrocchi, and D. Loss, "Long-distance entanglement of spin qubits via ferromagnet," *Phys. Rev. X*, vol. 3, p. 041023, 2013.

[94] A. Blais, R.-S. Huang, A. Wallraff, S. M. Girvin, and R. J. Schoelkopf, "Cavity quantum electrodynamics for superconducting electrical circuits: An architecture for quantum computation," *Phys. Rev. A*, vol. 69, p. 062320, Jun 2004.

[95] J. Majer, J. M. Chow, J. M. Gambetta, J. Koch, B. R. Johnson, J. A. Schreier, L. Frunzio, D. I. Schuster, A. A. Houck, A. Wallraff, A. Blais, M. H. Devoret, S. M. Girvin, and R. J. Schoelkopf, "Coupling superconducting qubits via a cavity bus," *Nature*, vol. 449, no. 7161, pp. 443–447, 2007.

[96] Y. Makhlin, G. Schn, and A. Shnirman, "Josephson-junction qubits with controlled couplings," *Nature*, vol. 398, no. 6725, p. 305, 1999.

[97] H. Xu, F. W. Strauch, S. K. Dutta, P. R. Johnson, R. C. Ramos, A. J. Berkley, H. Paik, J. R. Anderson, A. J. Dragt, C. J. Lobb, and F. C. Wellstood, "Spectroscopy of three-particle entanglement in a macroscopic superconducting circuit," *Phys. Rev. Lett.*, vol. 94, p. 027003, 2005.

[98] A. Blais, A. M. van den Brink, and A. M. Zagoskin, "Tunable coupling of superconducting qubits," *Phys. Rev. Lett.*, vol. 90, p. 127901, 2003.

[99] C. Hutter, A. Shnirman, Y. Makhlin, and G. Schön, “Tunable coupling of qubits: Nonadiabatic corrections,” *Europhysics Letters (EPL)*, vol. 74, no. 6, pp. 1088–1094, 2006.

[100] R. C. Bialczak, M. Ansmann, M. Hofheinz, M. Lenander, E. Lucero, M. Neeley, A. D. OConnell, D. Sank, H. Wang, M. Weides, J. Wenner, T. Yamamoto, A. N. Cleland, and J. M. Martinis, “Fast Tunable Coupler for Superconducting Qubits,” *Physical Review Letters*, vol. 106, no. 6, p. 060501, 2011.

[101] A. O. Niskanen, Y. Nakamura, and J.-S. Tsai, “Tunable coupling scheme for flux qubits at the optimal point,” *Physical Review B*, vol. 73, no. 9, p. 094506, 2006.

[102] A. O. Niskanen, K. Harrabi, F. Yoshihara, Y. Nakamura, S. Lloyd, and J. S. Tsai, “Quantum Coherent Tunable Coupling of Superconducting Qubits,” *Science*, vol. 316, no. 5825, pp. 723–726, 2007.

[103] B. L. T. Plourde, J. Zhang, K. B. Whaley, F. K. Wilhelm, T. L. Robertson, T. Hime, S. Linzen, P. A. Reichardt, C.-E. Wu, and J. Clarke, “Entangling flux qubits with a bipolar dynamic inductance,” *Physical Review B*, vol. 70, no. 14, p. 140501, 2004. 00095.

[104] M. D. Kim and J. Hong, “Coupling of Josephson current qubits using a connecting loop,” *Physical Review B*, vol. 70, no. 18, p. 184525, 2004.

[105] A. M. van den Brink, A. J. Berkley, and M. Yalowsky, “Mediated tunable coupling of flux qubits,” *New Journal of Physics*, vol. 7, no. 1, p. 230, 2005. 00055.

[106] M. D. Kim, “Controllable coupling in phase-coupled flux qubits,” *Physical Review B*, vol. 74, no. 18, p. 184501, 2006.

[107] S. H. W. van der Ploeg, A. Izmalkov, A. M. van den Brink, U. Hbner, M. Grajcar, E. Ilichev, H.-G. Meyer, and A. M. Zagoskin, “Controllable Coupling of Superconducting Flux Qubits,” *Physical Review Letters*, vol. 98, no. 5, p. 057004, 2007. 00138.

[108] D. Kafri, C. Quintana, Y. Chen, A. Shabani, J. M. Martinis, and H. Neven, “Tunable inductive coupling of superconducting qubits in the strongly nonlinear regime,” *Physical Review A*, vol. 95, no. 5, p. 052333, 2017.

[109] R. Harris, T. Lanting, A. J. Berkley, J. Johansson, M. W. Johnson, P. Bunyk, E. Ladizinsky, N. Ladizinsky, T. Oh, and S. Han, “Compound Josephson-junction coupler for flux qubits with minimal crosstalk,” *Physical Review B*, vol. 80, no. 5, p. 052506, 2009.

[110] M. Born and R. Oppenheimer, “Zur quantentheorie der molekeln,” *Annalen der Physik*, vol. 389, no. 20, pp. 457–484, 1927.

[111] H. S. W. Massey, “Collisions between atoms and molecules at ordinary temperatures,” *Reports on Progress in Physics*, vol. 12, no. 1, pp. 248–269, 1949.

[112] T. Duty, G. Johansson, K. Bladh, D. Gunnarsson, C. Wilson, and P. Delsing, “Observation of quantum capacitance in the cooper-pair transistor,” *Phys. Rev. Lett.*, vol. 95, p. 206807, 2005.

[113] S. Poletto, F. Chiarello, M. G. Castellano, J. Lisenfeld, A. Lukashenko, P. Carelli, and A. V. Ustinov, “A tunable rf SQUID manipulated as flux and phase qubits,” *Physica Scripta*, vol. T137, p. 014011, 2009.

[114] T. Hime, P. A. Reichardt, B. L. T. Plourde, T. L. Robertson, C.-E. Wu, A. V. Ustinov, and J. Clarke, “Solid-State Qubits with Current-Controlled Coupling,” *Science*, vol. 314, no. 5804, 2006.

[115] C. H. Tseng, S. Somaroo, Y. Sharf, E. Knill, R. Laflamme, T. F. Havel, and D. G. Cory, “Quantum simulation of a three-body-interaction hamiltonian on an nmr quantum computer,” *Phys. Rev. A*, vol. 61, p. 012302, 1999.

[116] P. Navrátil and W. E. Ormand, “Ab initio shell model with a genuine three-nucleon force for the p-shell nuclei,” *Phys. Rev. C*, vol. 68, p. 034305, 2003.

[117] J. von Stecher, “Five- and six-body resonances tied to an efimov trimer,” *Phys. Rev. Lett.*, vol. 107, p. 200402, 2011.

[118] J. Kempe, A. Kitaev, and O. Regev, “The complexity of the local hamiltonian problem,” in *FSTTCS 2004: Foundations of Software Technology and Theoretical Computer Science* (K. Lodaya and M. Mahajan, eds.), (Berlin, Heidelberg), pp. 372–383, Springer Berlin Heidelberg, 2005.

[119] N. Linden, S. Popescu, and P. Skrzypczyk, “How small can thermal machines be? the smallest possible refrigerator,” *Phys. Rev. Lett.*, vol. 105, p. 130401, 2010.

[120] R. Babbush, P. Love, and A. Aspuru-Guzik, “Adiabatic quantum simulation of quantum chemistry,” *Scientific Reports*, vol. 4, p. 6603 EP, 2014.

[121] A. Bermudez, D. Porras, and M. A. Martin-Delgado, “Competing many-body interactions in systems of trapped ions,” *Phys. Rev. A*, vol. 79, p. 060303, 2009.

[122] J. K. Pachos and E. Rico, "Effective three-body interactions in triangular optical lattices," *Phys. Rev. A*, vol. 70, p. 053620, 2004.

[123] F. L. Semião and M. Paternostro, "Quantum circuits for spin and flavor degrees of freedom of quarks forming nucleons," *Quantum Information Processing*, vol. 11, no. 1, pp. 67–75, 2012.

[124] H. P. Büchler, A. Micheli, and P. Zoller, "Three-body interactions with cold polar molecules," *Nature Physics*, vol. 3, no. 10, pp. 726–731, 2007.

[125] Y.-X. Chen and S.-W. Li, "Quantum refrigerator driven by current noise," *EPL (Europhysics Letters)*, vol. 97, no. 4, p. 40003, 2012.

[126] S. Y. Cho and M. D. Kim, "Macroscopic many-qubit interactions in superconducting flux qubits," *Physical Review B*, vol. 77, no. 21, p. 212506, 2008.

[127] M. Sameti, A. Potočnik, D. E. Browne, A. Wallraff, and M. J. Hartmann, "Superconducting quantum simulator for topological order and the toric code," *Physical Review A*, vol. 95, no. 4, p. 042330, 2017.

[128] J. Strand, A. Przybysz, D. Ferguson, and K. Zick, "Zzz coupler for native embedding of max-3sat problem instances in quantum annealing hardware," in *American Physical Society, March Meeting, Abstract: B51.00009*, 2017.

[129] A. J. Kerman, "Design and simulation of complex superconducting circuits for advanced quantum annealing hardware," in *American Physical Society, March Meeting, Abstract: C26.00001*, 2018.

[130] A. J. Kerman. In preparation.

[131] A. Perdomo-Ortiz, B. OGorman, J. Fluegemann, R. Biswas, and V. N. Smelyanskiy, "Determination and correction of persistent biases in quantum annealers," *Scientific Reports*, vol. 6, p. srep18628, 2016.

[132] A. J. Kerman, "Overview of the iarpa quantum enhanced optimization (qeo) study," in *Adiabatic Quantum Computing, Zurich*, 2015.

[133] A. J. Kerman, "Paramagnetic tree coupling of spin qubits," 2017.

[134] S. A. Cook, "The complexity of theorem-proving procedures," in *Proceedings of the Third Annual ACM Symposium on Theory of Computing*, STOC '71, (New York, NY, USA), pp. 151–158, ACM, 1971.

[135] W. Lechner, P. Hauke, and P. Zoller, "A quantum annealing architecture with all-to-all connectivity from local interactions," *Science Advances*, vol. 1, no. 9, p. e1500838, 2015.

[136] S. P. Jordan, E. Farhi, and P. W. Shor, "Error-correcting codes for adiabatic quantum computation," *Physical Review A*, vol. 74, no. 5, p. 052322, 2006.

[137] I. Marvian and D. A. Lidar, "Quantum Error Suppression with Commuting Hamiltonians: Two Local is Too Local," *Physical Review Letters*, vol. 113, no. 26, p. 260504, 2014.

[138] J. R.Reimers, L. K.McKemmish, R. H.McKenzie, and N. S.Hush, "Non-adiabatic effects in thermochemistry, spectroscopy and kinetics: the general importance of all three BornOppenheimer breakdown corrections," *Physical Chemistry Chemical Physics*, vol. 17, no. 38, pp. 24641–24665, 2015.

[139] D. Debroy, M. Li, M. Newman, and K. R. Brown, "Stabilizer Slicing: Coherent Error Cancellations in LDPC Codes," *arXiv:1810.01040*, 2018.

[140] S. B. Prasad and A. M. Martin, "Effective Three-Body Interactions in Jaynes-Cummings-Hubbard Systems," *arXiv:1710.02424*, 2017.

[141] N. R. Cooper, "Exact Ground States of Rotating Bose Gases Close to a Feshbach Resonance," *Physical Review Letters*, vol. 92, no. 22, p. 220405, 2004.

[142] M. Leib, P. Zoller, and W. Lechner, "A transmon quantum annealer: decomposing many-body Ising constraints into pair interactions," *Quantum Science and Technology*, vol. 1, no. 1, p. 015008, 2016.

[143] M. Neeley, R. C. Bialczak, M. Lenander, E. Lucero, M. Mariantoni, A. D. OConnell, D. Sank, H. Wang, M. Weides, J. Wenner, Y. Yin, T. Yamamoto, A. N. Cleland, and J. M. Martinis, "Generation of three-qubit entangled states using superconducting phase qubits," *Nature*, vol. 467, no. 7315, pp. 570–573, 2010.

[144] J. D. Biamonte, "Nonperturbative k-body to two-body commuting conversion Hamiltonians and embedding problem instances into Ising spins," *Physical Review A*, vol. 77, no. 5, p. 052331, 2008.

[145] P. Silvi, E. Rico, T. Calarco, and S. Montangero, "Lattice gauge tensor networks," *New Journal of Physics*, vol. 16, no. 10, p. 103015, 2014.

[146] R. Schmied, J. H. Wesenberg, and D. Leibfried, “Quantum simulation of the hexagonal kitaev model with trapped ions,” *New Journal of Physics*, vol. 13, no. 11, p. 115011, 2011.

[147] D. Lu, B. Xu, N. Xu, Z. Li, H. Chen, X. Peng, R. Xu, and J. Du, “Quantum chemistry simulation on quantum computers: theories and experiments,” *Phys. Chem. Chem. Phys.*, vol. 14, pp. 9411–9420, 2012.

[148] I. S. Gradshteyn and I. M. Ryzhik, *Table of Integrals, Series, and Products.* Academic Press, seventh ed., 2007.

APPENDICES

Appendix A

Numerical Diagonalization

In order to find the eigenvalues of a Hamiltonian numerically, we need to write it in terms of a known basis. It is convenient to use the harmonic oscillator basis in situations where the potential is non periodic and to use the Fourier basis for periodic potentials. We chose a distinct basis for each degree of freedom in the problem.

A.1 Non-periodic potential

As a simple example of a non-periodic potential and of the harmonic oscillator basis, let us use the Hamiltonian of the rf-SQUID, Eq. 2.31. Collecting the harmonic oscillator like terms together, we construct creation and annihilation operators. The Hamiltonian can be rewritten as

$$\hat{\mathcal{H}} = \hat{H}_{\mathrm{ho}} + \hat{H}_{\mathrm{l}} + \hat{H}_{\mathrm{nl}}, \tag{A.1}$$

where

$$\begin{aligned} \hat{H}_{\mathrm{ho}} &= \frac{E_{\mathrm{C}}}{2}\left(\frac{\hat{p}}{\hbar}\right)^2 + \frac{E_{\mathrm{L}}}{2}\hat{\gamma}^2 && \text{(A.2)} \\ &= \sqrt{E_{\mathrm{C}}E_{\mathrm{L}}}\left(\hat{a}^\dagger\hat{a} + \frac{1}{2}\right), && \text{(A.3)} \end{aligned}$$

$$\begin{aligned} \hat{H}_{\mathrm{l}} &= \frac{E_{\mathrm{L}}}{2}\left(4\pi^2 f_{\mathrm{x}}^2 - 4\pi f_{\mathrm{x}}\,\hat{\gamma}\right) && \text{(A.4)} \\ &= -\sqrt{2}\pi E_{\mathrm{C}}^{\frac{1}{4}} E_{\mathrm{L}}^{\frac{3}{4}}(a^\dagger + a) f_{\mathrm{x}} + 2\pi^2 E_{\mathrm{L}} f_{\mathrm{x}}^2 && \text{(A.5)} \end{aligned}$$

and

$$\hat{H}_{\mathrm{nl}} = -E_{\mathrm{J}} \cos \hat{\gamma} \tag{A.6}$$

$$= -E_{\mathrm{J}} \cos\left(\frac{1}{\sqrt{2}}\left(\frac{E_{\mathrm{C}}}{E_{\mathrm{L}}}\right)^{\frac{1}{4}}\left[a^{\dagger}+a\right]\right), \tag{A.7}$$

and finally we have defined

$$\hat{\gamma} = \frac{1}{\sqrt{2}}\left(\frac{E_{\mathrm{C}}}{E_{\mathrm{L}}}\right)^{\frac{1}{4}}\left(\hat{a}^{\dagger}+\hat{a}\right) \tag{A.8}$$

$$\hat{p} = \frac{\mathrm{i}\hbar}{\sqrt{2}}\left(\frac{E_{\mathrm{L}}}{E_{\mathrm{C}}}\right)^{\frac{1}{4}}\left(\hat{a}^{\dagger}-\hat{a}\right) \tag{A.9}$$

We can now replace the creation and annihilation operators with their matrix representations, truncated to a maximal number of states N_{ho}, and diagonalize the Hamiltonian. The matrix representation for these operators is

$$\hat{a} = \begin{bmatrix} 0 & \sqrt{1} & & & & \\ & 0 & \sqrt{2} & & & \\ & & 0 & \sqrt{3} & & \\ & & & \cdots & \cdots & \\ & & & & 0 & \sqrt{N_{\mathrm{ho}}-1} \\ & & & & & 0 \end{bmatrix} \tag{A.10}$$

and

$$\hat{a}^{\dagger}\hat{a} = \begin{bmatrix} 1 & & & & \\ & 2 & & & \\ & & 3 & & \\ & & & \cdots & \\ & & & & N_{\mathrm{ho}}-1 \end{bmatrix} \tag{A.11}$$

and we can write the non-linear terms in a complex exponential form and use the following identity [148]

$$\langle i|\,\mathrm{e}^{\mathrm{i}r\left(\hat{a}^{\dagger}+\hat{a}\right)}\,|j\rangle = \frac{\mathrm{e}^{\frac{-r^2}{2}}}{\sqrt{i!j!}} \sum_{m=0}^{\mathrm{Min}[i,j]} \binom{i}{m}\binom{j}{m} m!\,(\mathrm{i}r)^{i+j-2m} \tag{A.12}$$

A.2 Periodic potential

As a simple example of a periodic potential and the Fourier or charge basis, let us use the Hamiltonian of the Josephson junction, Eq. 2.26. Writing this Hamiltonian in the charge basis we get

$$H_{\mathrm{J}} = \frac{E_{\mathrm{C}}}{2}\hat{n}^2 - \frac{E_{\mathrm{J}}}{2}\left(\mathrm{e}^{\mathrm{i}\hat{\gamma}} + \mathrm{e}^{-\mathrm{i}\hat{\gamma}}\right). \tag{A.13}$$

Using the following basis transformation

$$|\gamma\rangle_{\mathrm{ph}} = \frac{1}{\sqrt{2\pi}}\sum_n \mathrm{e}^{-\mathrm{i}n\gamma}\,|n\rangle_{\mathrm{ch}}\,, \tag{A.14}$$

where $|\gamma\rangle_{\mathrm{ph}}$ and $|n\rangle_{\mathrm{ch}}$ are phase and charge states, respectively, we can find the matrix representation, truncated to a maximal number of states N_{ch}, of the diagonal charge operator

$$\hat{n} = \begin{bmatrix} -N_{\mathrm{ch}} & & & & & & \\ & -\left(N_{\mathrm{ch}}-1\right) & & & & & \\ & & \cdots & & & & \\ & & & 0 & & & \\ & & & & \cdots & & \\ & & & & & N_{\mathrm{ch}}-1 & \\ & & & & & & N_{\mathrm{ch}} \end{bmatrix}, \tag{A.15}$$

and the off-diagonal shift operator

$$\mathrm{e}^{\mathrm{i}\hat{\gamma}} = \begin{bmatrix} 0 & & & & & \\ 1 & 0 & & & & \\ & 1 & 0 & & & \\ & & \cdots & \cdots & & \\ & & & 1 & 0 & \\ & & & & 1 & 0 \end{bmatrix}. \tag{A.16}$$

Appendix B

Derivation of tunable rf-SQUID Hamiltonian

B.1 Symmetric case

The total flux threading the tunable rf-SQUID circuit, as in Fig. 4.1, along the contour comprised of the main loop and the right part of the secondary loop (identified with the index 1) is

$$\Phi_{\mathrm{ms1}} = \frac{L_{\mathrm{s}}}{2} I_1 + L_{\mathrm{m}} I_3 + \Phi_{\mathrm{m}}^{\mathrm{x}} + \frac{\Phi_{\mathrm{s}}^{\mathrm{x}}}{2}, \tag{B.1}$$

the total flux threading the contour comprised of the main loop and the left part of the secondary loop (identified with the index 2) is

$$\Phi_{\mathrm{ms2}} = \frac{L_{\mathrm{s}}}{2} I_2 + L_{\mathrm{m}} I_3 + \Phi_{\mathrm{m}}^{\mathrm{x}} - \frac{\Phi_{\mathrm{s}}^{\mathrm{x}}}{2}, \tag{B.2}$$

and the total flux threading the contour comprised of both parts of the secondary loop is

$$\Phi_{\mathrm{s}} = \frac{L_{\mathrm{s}}}{2} (I_1 - I_2) + \Phi_{\mathrm{s}}^{\mathrm{x}}, \tag{B.3}$$

where $\Phi_{\mathrm{m}}^{\mathrm{x}}$ is the external flux treading the main loop and $\Phi_{\mathrm{s}}^{\mathrm{x}}$ is the external flux threading the secondary loop, L_{s} is the geometrical inductance of the secondary loop and L_{m} is the total inductance of the main loop. Finally, the I_i for $i \in \{1, 2, 3\}$ are the currents flowing through each branch.

In Eqs. (B.1–B.3), it is clear that we have only two independent contours in this circuit, we have that $\Phi_{\mathrm{ms1}} - \Phi_{\mathrm{ms2}} = \Phi_{\mathrm{s}}$. Because of this, we only have two independent external fluxes to consider, $\Phi_{\mathrm{m}}^{\mathrm{x}} + \Phi_{\mathrm{s}}^{\mathrm{x}}/2$ and $\Phi_{\mathrm{m}}^{\mathrm{x}} - \Phi_{\mathrm{s}}^{\mathrm{x}}/2$.

The currents in the three branches are related to each other by the Kirchoff current law that reads $I_3 = I_1 + I_2$. This last current conservation relation can be inserted into Eq. (B.1) and Eq. (B.2) to give

$$\Phi_{\mathrm{ms1}} = \frac{L_{\mathrm{s}}}{2} I_1 + L_{\mathrm{m}} (I_1 + I_2) + \Phi_{\mathrm{m}}^{\mathrm{x}} + \frac{\Phi_{\mathrm{s}}^{\mathrm{x}}}{2} \tag{B.4}$$

and

$$\Phi_{\mathrm{ms2}} = \frac{L_{\mathrm{s}}}{2} I_2 + L_{\mathrm{m}} (I_1 + I_2) + \Phi_{\mathrm{m}}^{\mathrm{x}} - \frac{\Phi_{\mathrm{s}}^{\mathrm{x}}}{2}. \tag{B.5}$$

The fluxoid quantization in a superconductor further constrains the problem such that the total phase along each contour (loop) is equal to an integer number, which we take to be zero. Thus, we have

$$\gamma_1 = -\frac{2\pi\, \Phi_{\mathrm{ms1}}}{\Phi_0} \tag{B.6}$$

and

$$\gamma_2 = -\frac{2\pi\, \Phi_{\mathrm{ms2}}}{\Phi_0}, \tag{B.7}$$

with γ_i the superconducting phase difference across Josephson junction i. These two fluxoid conditions can be written as

$$\gamma_1 = -\left[\frac{I_1 L_{\mathrm{s}}}{2\phi_0} + \frac{(I_1 + I_2) L_{\mathrm{m}}}{\phi_0} + 2\pi f_{\mathrm{m}}^{\mathrm{x}} + \pi f_{\mathrm{s}}^{\mathrm{x}}\right] \tag{B.8}$$

and

$$\gamma_2 = -\left[\frac{I_2 L_{\mathrm{s}}}{2\phi_0} + \frac{(I_1 + I_2) L_{\mathrm{m}}}{\phi_0} + 2\pi f_{\mathrm{m}}^{\mathrm{x}} - \pi f_{\mathrm{s}}^{\mathrm{x}}\right], \tag{B.9}$$

were we defined the external magnetic flux in units of the reduced magnetic flux quantum $2\pi f_{\alpha}^{\mathrm{x}} = \Phi_{\alpha}^{\mathrm{x}}/\phi_0$ for $\alpha \in \{\mathrm{s}, \mathrm{m}\}$.

Equations (B.1–B.9) enable us to reduce the number of degrees of freedom of the problem to two and to write the currents running along branch 1 and 2 in terms of the junction phases only

$$I_1 = \frac{-\phi_0}{L_{\mathrm{s}} \left(L_{\mathrm{m}} + \frac{L_{\mathrm{s}}}{4}\right)} \left[L_{\mathrm{m}} (\gamma_1 - \gamma_2 + 2\pi f_{\mathrm{s}}^{\mathrm{x}}) + \frac{L_{\mathrm{s}}}{2} (\gamma_1 + 2\pi f_{\mathrm{m}}^{\mathrm{x}} + \pi f_{\mathrm{s}}^{\mathrm{x}})\right] \tag{B.10}$$

and

$$I_2 = \frac{-\phi_0}{L_\mathrm{s}\left(L_\mathrm{m} + \frac{L_\mathrm{s}}{4}\right)}\left[-L_\mathrm{m}\left(\gamma_1 - \gamma_2 + 2\pi f_\mathrm{s}^\mathrm{x}\right) + \frac{L_\mathrm{s}}{2}\left(\gamma_2 + 2\pi f_\mathrm{m}^\mathrm{x} - \pi f_\mathrm{s}^\mathrm{x}\right)\right]. \tag{B.11}$$

The current in branch 1 and 2 is also limited by the standard equation of motion for each Josephson junction. This means that the total current flowing through the branches is also

$$I_1 = I_\mathrm{c}\sin\gamma_1 + \phi_0 C\,\ddot{\gamma}_1 \tag{B.12}$$

and

$$I_2 = I_\mathrm{c}\sin\gamma_2 + \phi_0 C\,\ddot{\gamma}_2, \tag{B.13}$$

where I_c and C are the critical current and the capacitance of junction each junction, respectively. We can then write the complete equations of motion for branch 1 and 2 as

$$I_\mathrm{c}\sin\gamma_1 + \phi_0 C\,\ddot{\gamma}_1 = \frac{-\phi_0}{L_\mathrm{s}L_{\mathrm{m}'}}\left[L_\mathrm{m}\left(\gamma_1 - \gamma_2 + 2\pi f_\mathrm{s}^\mathrm{x}\right) + \frac{L_\mathrm{s}}{2}\left(\gamma_1 + 2\pi f_\mathrm{m}^\mathrm{x} + \pi f_\mathrm{s}^\mathrm{x}\right)\right] \tag{B.14}$$

and

$$I_\mathrm{c}\sin\gamma_2 + \phi_0 C\,\ddot{\gamma}_2 = \frac{-\phi_0}{L_\mathrm{s}L_{\mathrm{m}'}}\left[-L_\mathrm{m}\left(\gamma_1 - \gamma_2 + 2\pi f_\mathrm{s}^\mathrm{x}\right) + \frac{L_\mathrm{s}}{2}\left(\gamma_2 + 2\pi f_\mathrm{m}^\mathrm{x} - \pi f_\mathrm{s}^\mathrm{x}\right)\right], \tag{B.15}$$

where we have defined the effective main loop inductance $L_{\mathrm{m}'} = L_\mathrm{m} + L_\mathrm{s}/4$.

It will be more convenient to transform these equations of motion for branch 1 and 2 into the equations of motion for the loops in the circuit. By taking the sum of Eqs. (B.14–B.15), we get

$$I_\mathrm{c}\left(\sin\gamma_1 + \sin\gamma_2\right) + \phi_0 C\left(\ddot{\gamma}_1 + \ddot{\gamma}_2\right) = \frac{-\phi_0}{2L_{\mathrm{m}'}}\left(\gamma_1 + \gamma_2 + 4\pi f_\mathrm{m}^\mathrm{x}\right), \tag{B.16}$$

and taking the difference we get

$$I_\mathrm{c}\left(\sin\gamma_1 - \sin\gamma_2\right) + \phi_0 C\left(\ddot{\gamma}_1 - \ddot{\gamma}_2\right) = \frac{-2\phi_0}{L_\mathrm{s}}\left(\gamma_1 - \gamma_2 + 2\pi f_\mathrm{s}^\mathrm{x}\right). \tag{B.17}$$

We readily find that the Hamiltonian of the symmetric tunable-rf-SQUID is

$$H = T\left(p_1, p_2\right) + U_\mathrm{J}\left(\gamma_1, \gamma_2\right) + U_\mathrm{L}\left(\gamma_1, \gamma_2\right), \tag{B.18}$$

with the kinetic energy, written in terms of the canonical conjugate momenta p_i for $i \in \{1, 2\}$,

$$T\left(p_1, p_2\right) = \frac{1}{2\phi_0^2 C}\left(p_1^2 + p_2^2\right), \tag{B.19}$$

the Josephson potential

$$U_{\mathrm{J}}\left(\gamma_1, \gamma_2\right) = -\phi_0 I_{\mathrm{c}}\left(\cos\gamma_1 + \cos\gamma_2\right), \tag{B.20}$$

and the inductive potential

$$U_{\mathrm{L}}\left(\gamma_1, \gamma_2\right) = \frac{\phi_0^2}{2L_{\mathrm{s}}}\left(\gamma_1 - \gamma_2 + 2\pi f_{\mathrm{s}}^{\mathrm{x}}\right)^2 + \frac{\phi_0^2}{8L_{\mathrm{m'}}}\left(\gamma_1 + \gamma_2 + 4\pi f_{\mathrm{m}}^{\mathrm{x}}\right)^2. \tag{B.21}$$

B.2 Asymmetric case

Following a similar derivation as for the symmetric case, we now introduce asymmetry coefficients for the circuit parameters. The various parameters are defined as follows

$$\begin{aligned} \alpha &= \frac{I_{\mathrm{c1}} - I_{\mathrm{c2}}}{I_{\mathrm{c1}} + I_{\mathrm{c2}}} \\ &= \frac{I_{\mathrm{c1}} - I_{\mathrm{c2}}}{I_{\mathrm{c}}}, \end{aligned} \tag{B.22}$$

$$\begin{aligned} \mu &= \frac{C_1 - C_2}{C_1 - C_2} \\ &= \frac{C_1 - C_2}{C}, \end{aligned} \tag{B.23}$$

$$\begin{aligned} \delta &= \frac{f_{\mathrm{s1}}^{\mathrm{x}} - f_{\mathrm{s2}}^{\mathrm{x}}}{f_{\mathrm{s1}}^{\mathrm{x}} + f_{\mathrm{s2}}^{\mathrm{x}}} \\ &= \frac{f_{\mathrm{s1}}^{\mathrm{x}} - f_{\mathrm{s2}}^{\mathrm{x}}}{f_{\mathrm{s}}^{\mathrm{x}}}, \end{aligned} \tag{B.24}$$

and

$$\begin{aligned} \eta &= \frac{L_{\mathrm{s1}} - L_{\mathrm{s2}}}{L_{\mathrm{s1}} + L_{\mathrm{s2}}} \\ &= \frac{L_{\mathrm{s1}} - L_{\mathrm{s2}}}{L_{\mathrm{s}}}. \end{aligned} \tag{B.25}$$

In typical circuit designs, these asymmetry coefficients are made to be as small as possible. In what follows, we will take the assumption that the coefficients in Eqs. (B.22–B.25) represent a small perturbation to the energy scales and therefore will only keep terms up to first order in these coefficients. With these new definitions, the equations of motion are

$$\begin{aligned}&I_{\mathrm{c}}\left[(1+\alpha)\sin\gamma_1+(1-\alpha)\sin\gamma_2\right]\\&\quad+\phi_0 C\left[(1+\mu)\ddot{\gamma}_1+(1-\mu)\ddot{\gamma}_2\right]=\frac{-\phi_0}{L_{\mathrm{m}'}}\left[\gamma_1+\gamma_2+2\pi\left(2f_{\mathrm{m}}^{\mathrm{x}}+\delta f_{\mathrm{s}}^{\mathrm{x}}\right)\right]\\&\qquad\qquad-\frac{\eta\phi_0}{L_{\mathrm{m}'}}\left(\gamma_1-\gamma_2+2\pi f_{\mathrm{s}}^{\mathrm{x}}\right),\end{aligned}\tag{B.26}$$

and

$$\begin{aligned}&I_{\mathrm{c}}\left[(1+\alpha)\sin\gamma_1-(1-\alpha)\sin\gamma_2\right]\\&\quad+\phi_0 C\left[(1+\mu)\ddot{\gamma}_1-(1-\mu)\ddot{\gamma}_2\right]=\frac{-4\phi_0}{L_{\mathrm{s}}}\left(\gamma_1-\gamma_2+2\pi f_{\mathrm{s}}^{\mathrm{x}}\right)\\&\qquad\qquad+\frac{\eta\phi_0}{L_{\mathrm{m}'}}\left(\gamma_1+\gamma_2+4\pi f_{\mathrm{m}}^{\mathrm{x}}\right).\end{aligned}\tag{B.27}$$

We can then readily find that the Hamiltonian for the asymmetric tunable rf-SQUID is

$$H=T\left(p_1,p_2\right)+U_{\mathrm{J}}\left(\gamma_1,\gamma_2\right)+U_{\mathrm{L}}\left(\gamma_1,\gamma_2\right),\tag{B.28}$$

with the kinetic energy, written in terms of the canonical conjugate momenta $p_i=\partial\mathcal{L}/\partial\dot{\gamma}_i$ for $i\in\{1,2\}$, written as

$$T\left(p_1,p_2\right)=\frac{1}{2\phi_0^2 C}\left[p_1^2(1-\mu)+p_2^2(1+\mu)\right],\tag{B.29}$$

the Josephson potential

$$U_{\mathrm{J}}\left(\gamma_1,\gamma_2\right)=-\phi_0 I_{\mathrm{c}}\left[(1+\alpha)\cos\gamma_1+(1-\alpha)\cos\gamma_2\right],\tag{B.30}$$

and the inductive potential

$$\begin{aligned}U_{\mathrm{L}}\left(\gamma_1,\gamma_2\right)=&\frac{\phi_0^2}{L_{\mathrm{s}}}\left(\gamma_1-\gamma_2+2\pi f_{\mathrm{s}}^{\mathrm{x}}\right)^2+\frac{\phi_0^2}{4L_{\mathrm{m}'}}\left[\gamma_1+\gamma_2+2\pi\left(2f_{\mathrm{m}}^{\mathrm{x}}+\delta f_{\mathrm{s}}^{\mathrm{x}}\right)\right]^2\\&+\frac{\eta\phi_0^2}{4L_{\mathrm{m}'}}\left(\gamma_1+\gamma_2+4\pi f_{\mathrm{m}}^{\mathrm{x}}\right)\left(\gamma_1-\gamma_2+2\pi f_{\mathrm{s}}^{\mathrm{x}}\right).\end{aligned}\tag{B.31}$$